

University of Alberta

Studying the Collapse of Photoresist Patterns during Photolithography Process

by

Seyed Farshid Chini



A thesis submitted to the Faculty of Graduate Studies and Research
in partial fulfillment of the requirements for the degree of Master of Science

Department of Mechanical Engineering

Edmonton, Alberta
Spring 2008



Library and
Archives Canada

Published Heritage
Branch

395 Wellington Street
Ottawa ON K1A 0N4
Canada

Bibliothèque et
Archives Canada

Direction du
Patrimoine de l'édition

395, rue Wellington
Ottawa ON K1A 0N4
Canada

Your file Votre référence
ISBN: 978-0-494-45793-1
Our file Notre référence
ISBN: 978-0-494-45793-1

NOTICE:

The author has granted a non-exclusive license allowing Library and Archives Canada to reproduce, publish, archive, preserve, conserve, communicate to the public by telecommunication or on the Internet, loan, distribute and sell theses worldwide, for commercial or non-commercial purposes, in microform, paper, electronic and/or any other formats.

The author retains copyright ownership and moral rights in this thesis. Neither the thesis nor substantial extracts from it may be printed or otherwise reproduced without the author's permission.

AVIS:

L'auteur a accordé une licence non exclusive permettant à la Bibliothèque et Archives Canada de reproduire, publier, archiver, sauvegarder, conserver, transmettre au public par télécommunication ou par l'Internet, prêter, distribuer et vendre des thèses partout dans le monde, à des fins commerciales ou autres, sur support microforme, papier, électronique et/ou autres formats.

L'auteur conserve la propriété du droit d'auteur et des droits moraux qui protègent cette thèse. Ni la thèse ni des extraits substantiels de celle-ci ne doivent être imprimés ou autrement reproduits sans son autorisation.

In compliance with the Canadian Privacy Act some supporting forms may have been removed from this thesis.

Conformément à la loi canadienne sur la protection de la vie privée, quelques formulaires secondaires ont été enlevés de cette thèse.

While these forms may be included in the document page count, their removal does not represent any loss of content from the thesis.

Bien que ces formulaires aient inclus dans la pagination, il n'y aura aucun contenu manquant.

■ ■ ■
Canada

Abstract

Photolithography is the most widely used mass nano-production process. Technology requirements demand smaller nano-devices. However, smaller features risk collapse during the drying of rinse liquid.

Studies identified Laplace pressure as the cause of the collapse. Based on these studies, an analytical model was developed for predicting patterns collapse. However, the analytical models lacked in three major aspects: (i) inclusion of another contributor to capillary force, *i.e.* surface tension force (STF) on the three-phase line, (ii) prediction of non-cylindrical rinse interface shapes, and (iii) consideration of complex geometries such as L-shaped patterns.

To address the shortcomings, an improved analytical model was developed which included the STF. However, it did not satisfy the last two shortcomings. A more complex (*i.e.* a Finite Element, FE) model was developed using ANSYS and Surface Evolver. The FE model not only addressed all three above shortcomings but also considered lateral deformation and force rotation during pattern deformation.

Dedication

This thesis is dedicated to my parents. They introduced me to the joy of reading, which enabled me to do this study. I would also like to express a special word of thanks to my supervisor Dr. Amirfazli who tirelessly listened to my ideas and offered encouragements when they were most needed. Without his patience, understanding and support the completion of this work would have been impossible. I also extend my thanks to all those who generously contributed to the completion of this thesis.

Acknowledgement

I would like to thank my supervisor, Dr. Amirfazli, for his support and kind advice and Dr. Grundke, in the Leipzig Institute for polymer research in Dresden, Germany, who gave me the chance to visualize my rinse interface shape simulations while at the institute. This study was improved by the contributions of Ms. Nicole Petong and Mr. Goldwin McEwen. Ms. Petong helped with setting up experiments, and Mr. McEwen helped with valuable comments and discussion during the writing of my thesis. Financial support was provided by National Sciences and Engineering Research Council of Canada (NSERC) and Canada Research Chair (CRC) program.

Table of Content

CHAPTER 1 – INTRODUCTION	1
1-1 NANO-MANUFACTURING METHODS.....	1
1-2 PHOTOLITHOGRAPHY	2
1-3 MANUFACTURING LIMITATIONS DURING PHOTOLITHOGRAPHY	5
1-3.1 OPTICAL LIMITATION.....	5
1-3.2 MOSFET DESIGN LIMITATION	6
1-3.3 PATTERN COLLAPSE LIMITATION.....	7
1-3.3.1 <i>Intrusion</i>	8
1-3.3.2 <i>Swelling</i>	8
1-3.3.3 <i>Laplace Pressure</i>	9
1-4 PATTERN COLLAPSE PROBLEM RESOLUTIONS BASED ON TANAKA’S BEAM BENDING MODEL.....	14
1-4.1 PATTERN STIFFNESS INCREASE	14
1-4.2 LAPLACE PRESSURE DECREASE	15
1-4.2.1 <i>Surface Tension Decrease</i>	15
1-4.2.2 <i>Contact Angle Increase</i>	18
1-5 SHORTCOMINGS OF TANAKA’S BEAM BENDING MODELS	19
1-5.1 INCLUSION OF SURFACE TENSION FORCE	19
1-5.2 SHORT LENGTH TWO-LINE PARALLEL PATTERNS	21
1-5.3 BOX- AND L-SHAPED PATTERNS.....	22
1-6 THESIS OUTLINE.....	22
FIGURES.....	24
REFERENCES.....	25

CHAPTER 2 - ANALYTICAL STUDY OF THE PATTERN COLLAPSE IN	
PHOTOLITHOGRAPHY PROCESS USING MODIFIED CAPILLARY FORCES.....28	
2-1	INTRODUCTION.....28
2-2	PATTERN COLLAPSE MODELING.....33
2-3	PATTERN DEFORMATION MODEL WITH INCLUSION OF STF35
2-3.1	ANALYTICAL MODEL FOR CALCULATION OF δ_236
2-3.2	ANALYTICAL MODEL FOR CALCULATION OF δ_138
2-4	RESULTS FROM THE NEW ANALYTICAL PATTERN DEFORMATION MODEL41
2-5	NON-CYLINDRICAL RINSE INTERFACE SHAPE42
2-5.1	RINSE INTERFACE INSIDE TWO-LINE PARALLEL AND BOX-SHAPED PATTERNS44
2-5.2	RESULTS FROM NON-CYLINDRICAL RINSE INTERFACE SHAPE46
2-6	CONCLUSIONS47
TABLES.....49	
FIGURES.....54	
REFERENCES.....60	
CHAPTER 3 - A FINITE ELEMENT MODEL FOR PREDICTING COLLAPSE FOR DIFFERENT	
PATTERN SHAPES DURING DRYING PROCESS IN PHOTOLITHOGRAPHY.....63	
3-1	INTRODUCTION.....63
3-2	FE MODEL FOR FINDING PATTERN DEFORMATION66
3-2.1	CAPILLARY FORCES IN FE MODEL.....67
3-2.2	FINITE ELEMENT METHOD FOR FINDING PATTERN DEFORMATION.....69
3-3	VALIDATION OF FE MODEL FOR FINDING PATTERN DEFORMATION70
3-4	PATTERN DEFORMATION USING FE71

3-4.1	TWO-LINE PARALLEL PATTERNS WITH SHORT LENGTH	72
3-4.2	OPEN END L-SHAPED PATTERNS.....	73
3-4.3	BOX-SHAPED AND CLOSE END L-SHAPED PATTERNS.....	76
3-5	CONCLUSION.....	77
	FIGURES.....	80
	REFERENCES.....	91
	CHAPTER 4 - CONCLUSION.....	93
4-1	DRIVING FORCES OF PATTERN COLLAPSE.....	93
4-2	ANALYTICAL MODEL TO PREDICT COLLAPSE OF TWO-LINE PARALLEL PATTERNS	93
4-2.1	BOUNDS OF APPLICABILITY FOR ANALYTICAL MODEL FOR TWO-LINE PARALLEL PATTERNS.....	94
4-3	FE MODEL TO PREDICT COLLAPSE OF DIFFERENT PATTERN SHAPES.....	95
4-4	FUTURE WORKS.....	97
	REFERENCES.....	99
	APPENDIX A – ANSYS CODES	100
	APPENDIX B – METHODOLOGY USED IN SURFACE EVOLVER.....	102
	FIGURES.....	108
	REFERENCES.....	109
	APPENDIX C - RELAXATION OF THE SMALL DEFORMATION ASSUMPTION USED IN TANAKA’S MODEL.....	110
	TABLES.....	112
	REFERENCES.....	113

APPENDIX D - DETAILS OF THE NEW ANALYTICAL BEAM BENDING MODEL..... 114

REFERENCES..... 117

APPENDIX E - REASON OF DEFINING *LAR* 118

FIGURES..... 119

APPENDIX F –DEFINING A BOX-SHAPED PATTERN WITH INFINITE LENGTH IN

SURFACE EVOLVER..... 120

List of Tables

TABLE 2-1 SURFACE TENSIONS AND CONTACT ANGLES OF SURFACTANT SOLUTIONS IN JUNG <i>ET AL.</i> [15] EXPERIMENT ARE PRESENTED. TWO CONTRIBUTORS IN CAPILLARY FORCE (<i>I.E.</i> STF ON THREE PHASE LINE AND LAPLACE PRESSURE) ARE NORMALIZED WITH RESPECT TO THE VALUES FOR WATER, <i>I.E.</i> ΔP_{water} AND $F_x(water)$	49
TABLE 2-2 DEFORMATION AT THREE DIFFERENT TROUGH WIDTHS VALUES IS PRESENTED WITH AND WITHOUT CONSIDERING SURFACE TENSION FORCE ($H=250NM$, $E=5GPA$, $\theta = 45^\circ$, $AR=4$ AND $\gamma = 72mN / m$).	49
TABLE 2-3 DEFORMATION FOR THREE DIFFERENT ELASTICITY MODULUS VALUES IS PRESENTED WITH AND WITHOUT CONSIDERING SURFACE TENSION FORCE ($H=250NM$, $D=104NM$, $\theta = 45^\circ$, $AR=4.5$ AND $\gamma = 72mN / m$).	50
TABLE 2-4 DEFORMATION WITH AND WITHOUT CONSIDERING SURFACE TENSION FORCE AT THREE DIFFERENT PATTERN WIDTHS IS PRESENTED ($AR=3$, $\gamma = 72mN / m$, $D=100NM$, $E=4GP$ AND $\theta = 45^\circ$).	50
TABLE 2-5 DEFORMATION WITH AND WITHOUT CONSIDERING STF AT THREE DIFFERENT PATTERN	51
WIDTHS IS PRESENTED ($AR=3$, $\gamma = 72mN / m$, $E=4GPA$, $\theta = 45^\circ$ AND $D=W$).	51
TABLE 2-6 DEFORMATION WITH AND WITHOUT CONSIDERING STF AT THREE DIFFERENT ARS IS PRESENTED ($H=250NM$, $D=104NM$, $E=5GPA$, $\theta = 45^\circ$ AND $\gamma = 72mN / m$).	51
TABLE 2-7 DEFORMATION WITH AND WITHOUT CONSIDERING SURFACE TENSION FORCE AT THREE DIFFERENT CONTACT ANGLES IS PRESENTED ($H=250NM$, $D=104NM$, $E=5GPA$, $AR=4.5$ AND $\gamma = 72mN / m$).	52
TABLE 2-8 EFFECT OF INCREASING CONTACT ANGLE AND LAR ON CURVATURE FOR TWO-LINE PARALLEL AND BOX-SHAPED PATTERNS IS SUMMARIZED. CURVATURE IS CALCULATED FORM SE.	53
TABLE C1 LAPLACE PRESSURE DEFORMATION WITH AND WITHOUT SMALL DEFORMATION APPROXIMATION ($H=250NM$, $D=104NM$, $E=5GPA$, $AR=4$ AND $\gamma = 72mN / m$).	112
TABLE C2 LAPLACE PRESSURE DEFORMATION WITH AND WITHOUT SMALL DEFORMATION ASSUMPTION ($H=250NM$, $E=5GPA$, $\theta = 45^\circ$, $AR=4$ AND $\gamma = 72mN / m$).	112

TABLE C3 LAPLACE PRESSURE DEFORMATION WITH AND WITHOUT APPROXIMATION. $H=250\text{NM}$, $D=104\text{NM}$,

$E=5\text{GPA}$, $\theta = 45^\circ$ AND $\gamma = 72\text{mN/m}$ 112

List of Figures

FIGURE 1-1 PHOTOLITHOGRAPHY PROCEDURE IS SHOWN. ONE OF THE OBSTACLES OF PHOTOLITHOGRAPHY PROCESS IS COLLAPSE OF PHOTORESISTS DURING DRYING THE RINSE LIQUID.....	24
FIGURE 1-2 SCHEMATIC OF A MOSFET (METAL-OXIDE-SEMICONDUCTOR FIELD-EFFECT-TRANSISTOR) IS SHOWN.....	24
FIGURE 1-3 PATTERN COLLAPSE FOR THE CASE OF A TWO-LINE PARALLEL PATTERN IS SHOWN.....	24
FIGURE 2-1 SCHEMATIC OF AN ISOLATED TWO-LINE PARALLEL PATTERN, AND RINSE LIQUID INTERFACE WITH SURROUNDING AIR.	54
FIGURE 2-2 (A) SURFACE TENSION FORCES AT THREE PHASE LINE ARE SHOWN. HORIZONTAL PROJECTION OF LIQUID-VAPOR PHASE SURFACE TENSION (γ_{LV}) EXERTS A FORCE ON THE PATTERN'S SIDE WALL. (B) CASE OF A FLAT INTERFACE ($\Delta P = 0$) WHERE γ_{LV} EXERTS A FORCE ON THE PATTERN'S SIDE WALL.	54
FIGURE 2-3 SCHEMATIC OF A BEAM SWAY MODEL AND ADDITIVE NATURE OF THE STF AND LAPLACE PRESSURE ON THE PATTERN. SUPERPOSITION ASSUMPTIONS ARE: (I) LOADS REMAINS HORIZONTAL, (II) ELASTIC DEFORMATION (MAXIMUM STRESS IS LESS THAN YIELD STRESS), AND (III) DEFORMATION WITH RESPECT TO HEIGHT IS VERY SMALL [32].	55
FIGURE 2-4 COMPARING RESTORING AND COHESIVE PRESSURES DUE TO LAPLACE PRESSURE BY: (I) TANAKA'S MODEL, AND (II) CURRENT MODEL FOR δ_1 WHICH CONSIDERS THE EFFECT OF STF ON LAPLACE PRESSURE DEFORMATION ($AR=6, H=350\text{NM}, D=150\text{NM}, \theta = 15^\circ, E=5.9\text{GPA}$ AND $\gamma =72\text{MN/M}$). DESPITE TANAKA'S MODEL, JUST BY CONSIDERING δ_1 THE NEW MODEL PREDICTS COLLAPSE.	55
FIGURE 2-5 AT CONSTANT AR , PATTERN DEFORMATION INCREASES BY INCREASING w AND CONSEQUENTLY $H(= AR \times w)$ USING BOTH THE CURRENT MODEL FOR δ_1 AND TANAKA'S MODEL ($D=300\text{NM}, AR=5, E=5.9\text{GPA}, \theta = 15^\circ$ AND $\gamma =72\text{MN/M}$).	56
FIGURE 2-6 THE EFFECT OF CONSIDERING STF IN PREDICTING DEFORMATION VALUE AND COLLAPSE OF FEATURES IS SHOWN AT DIFFERENT CONTACT ANGLES ($H=1000\text{NM}, D=300\text{NM}, AR=6.67, E=5.9\text{GPA}$ AND $\gamma =72\text{MN/M}$).....	56

FIGURE 2-7 SURFACE EVOLVER ($LAR \gg 1$) AND CIM CURVATURE VALUES ARE COMPARED AT DIFFERENT ILH VALUES ($H=250$ NM, $D=104$ NM, $\theta = 5^\circ$ AND WATER INSIDE A TWO-LINE PARALLEL PATTERN). OVERFILLING AND UNDER FILLING EFFECTS ON THE INTERFACE CURVATURE VALUES ARE NOTICEABLE IN SE RESULTS.	57
FIGURE 2-8 SCHEMATIC OF: (A) CYLINDRICAL RINSE INTERFACE SHAPE FOR A PATTERN WITH VERY LARGE LENGTH ($LAR \gg 1$), (B) RINSE INTERFACE SHAPE FOR A CASE WHERE RINSE IS BETWEEN A TWO-LINE PARALLEL PATTERN WITH SMALL LENGTH ($LAR = 5$), AND (C) RINSE INTERFACE SHAPE FOR A CASE WHERE RINSE IS SURROUNDED IN A BOX-SHAPED PATTERN WITH SMALL LENGTH ($LAR = 5$). INTERFACE SHAPES ARE DERIVED USING SURFACE EVOLVER.....	57
FIGURE 2-9 ERROR OF USING CIM TO FIND INTERFACE CURVATURE VALUES, COMPARED TO CURVATURE VALUES FROM SE AT (A) DIFFERENT θ VALUES WITH $LAR=10$, AND (B) DIFFERENT LAR VALUES; FOR TWO-LINE PARALLEL (OPEN-ENDS) AND BOX-SHAPED (CLOSE-ENDS) PATTERNS ($\theta = 5^\circ$, $H=250$ NM, $ILH=110$ NM AND $D=104$ NM).	58
FIGURE 2-10 SE AND CIM CURVATURE VALUES AT DIFFERENT LAR VALUES FOR (A) TWO-LINE PARALLEL, AND (B) BOX-SHAPED PATTERNS ($H=250$ NM, $ILH=110$ NM, $D=104$ NM AND $\theta = 5^\circ$).	58
FIGURE 2-11 SE AND CIM CURVATURE VALUES AT DIFFERENT CONTACT ANGLES FOR (A) TWO-LINE PARALLEL, AND (B) BOX-SHAPED PATTERNS ARE SHOWN ($ILH=110$ NM, $AR=5$, $H=250$ NM AND $D=104$ NM). NEGATIVE CURVATURE VALUE MEANS THAT INTERFACE CURVATURE IS CONVEX AND DEFORMATION DUE TO THE PRESSURE IS IN OUTWARD DIRECTION.	59
FIGURE 3-1 (A) HORIZONTAL PROJECTION OF γ_{LV} IS EXERTING A FORCE ON THE PATTERN WHILE ITS VERTICAL PROJECTION, ACCORDING TO YOUNG EQUATION, IS CANCELED BY TWO OTHER INTERFACIAL TENSIONS, I.E. γ_{SL} AND γ_{SV} . (B) EXTRAND ET AL. [5] EXPERIMENT, I.E. A DROPLET ON A SOFT SUBSTRATE. WHITE CIRCLE SIGNIFIES A RIDGE THAT WAS FORMED AT THE THREE-PHASE LINE ON A SOFT SUBSTRATE. IT SHOWS THAT THE MAGNITUDE OF STF IS SUCH THAT CAN DEFORM A SOFT SUBSTRATE.	80
FIGURE 3-2 LAPLACE PRESSURE, THREE-PHASE LINE AND INTERFACE SHAPES OF A TWO-LINE PARALLEL PATTERN AT DIFFERENT ILH (INITIAL LIQUID HEIGHT) VALUES ARE SHOWN. FOR THE CASE "B" WHICH ILH IS 164 NM, THREE-PHASE LINE IS MOSTLY A STRAIGHT LINE HOWEVER PRESSURE VALUE IS NOT	

INFLUENCED BY THE OVERFILLING EFFECT. NOTE THAT THREE-PHASE LINES ARE THE THICK BLACK LINES IN THE THREE PANELS AND GRAY SHADES SHOW THE INTERFACE. $AR (=H/w)$, SHOWN IN FIG. 3-1) $=3$, $LAR=10$, $D=w=57\text{NM}$ (STATE OF THE ART FOR 2008), $\theta = 5^\circ$, $\gamma = 72.9\text{mN/m}$ AND INTERFACE SHAPES SHOWN IN THE PANELS ARE FOUND USING SURFACE EVOLVER.	81
FIGURE 3-3 (A) LAPLACE PRESSURE, THREE-PHASE LINE AND INTERFACE SHAPE OF AN L-SHAPE PATTERN AS A FUNCTION OF RINSE LIQUID VOLUME IS SHOWN. $AR (H/w) =3$, $LAR=10$, $D=w=57\text{NM}$ (STATE OF THE ART FOR 2008), $\theta = 5^\circ$, $\gamma = 72.9\text{mN/m}$ AND INTERFACE SHAPE IS FOUND USING SURFACE EVOLVER, (B) TOP VIEW OF AN L-SHAPED PATTERN IS SHOWN. THE LENGTH OF TWO LEGS ARE L_1 AND L_2 . PATTERN DIMENSIONS SHOWN ARE MEASURED FROM INSIDE OF THE PATTERN WALL.	82
FIGURE 3-4 PROCEDURE OF CALCULATING PATTERN DEFORMATION USING FE METHOD IS SHOWN.	83
FIGURE 3-5 DEFORMATIONS OF A TWO-LINE PARALLEL PATTERN FROM BEAM BENDING, TANAKA'S BEAM BENDING AND FE MODEL ARE COMPARED AT (A) DIFFERENT CONTACT ANGLES WITH $E=4\text{GPA}$, (B) DIFFERENT ELASTICITY MODULUS (E) VALUES WITH $\theta = 45^\circ$. (IN BOTH CASES $D=w=57\text{NM}$, $AR=3$, $\gamma = 72.9\text{mN/m}$ AND $LAR \rightarrow \infty$; SEE APPENDIX F FOR THE METHOD OF DEFINING AN INFINITE LENGTH FOR THE PATTERN IN SIMULATION).	83
FIGURE 3-6 (A) SLOPE OF THE PATTERN AT ITS TIP, AND (B) DEFORMATION FROM FE MODEL AT DIFFERENT CONTACT ANGLES IS SHOWN FOR DIFFERENT LAR VALUES ($D=w=57\text{NM}$, $AR=3$, $\gamma = 72.9\text{mN/m}$, $E=4\text{GPA}$ AND TWO-LINE PARALLEL PATTERN).	84
FIGURE 3-7 CURVATURE VERSUS LAR VALUES FOR DIFFERENT CONTACT ANGLES ARE SHOWN. FOR SMALL LAR VALUES, CURVATURE IS POSITIVE. POSITIVE CURVATURE MEANS THAT LAPLACE PRESSURE IS PUSHING THE PATTERNS OUTWARD (AGAINST THE SURFACE TENSION FORCE EFFECT). THE NEGATIVE CURVATURE HAS THE OPPOSITE MEANING ($D=w=57\text{NM}$, $E=5.9\text{GPA}$, $AR=3$ AND WATER INSIDE A TWO-LINE PARALLEL PATTERN).	85
FIGURE 3-8 CURVATURE VALUE OF OPEN L-SHAPED PATTERNS. AS LONG AS EQUIVALENT LENGTH (OR SUMMATION OF LEGS) IS CONSTANT, CURVATURE VALUE ONLY SLIGHTLY CHANGES. ALTHOUGH, CHANGE OF CURVATURE BY CHANGING THE EQUIVALENT LENGTH FROM 7 TO 16 IS NOT VERY MUCH BUT	

THIS AMOUNT OF CHANGE CAUSES A PRESSURE CHANGE IN THE ORDER OF 10kPa ($\theta = 5^\circ$ AND $D=1$ MICRON). 86

FIGURE 3-9 (A) LAPLACE PRESSURE OF OPEN END L-SHAPED PATTERNS, (B) LAPLACE PRESSURE OF CLOSE END L-SHAPED PATTERNS, (C) PATTERN DEFORMATION OF OPEN END L-SHAPED PATTERNS AND (D) PATTERN DEFORMATION OF CLOSE END L-SHAPED PATTERNS, AT DIFFERENT CONTACT ANGLES FOR DIFFERENT LEG'S LENGTHS ARE SHOWN. AS LONG AS EQUIVALENT LENGTH IS CONSTANT, LAPLACE PRESSURE IS NOT CHANGING BUT THE DEFORMATION MAY CHANGE AND MINIMUM DEFORMATION IS WHERE LEGS ARE EQUAL ($d_1 = d_2 = w = 57nm$, $L_e = 531nm$, $\gamma = 72.9mN/m$ AND $LAR=10$). 87

FIGURE 3-10 CURVATURE VALUE OF A TWO-PARALLEL LINE PATTERN IS EQUAL TO THAT OF AN OPEN END L-SHAPED PATTERN WITH EQUAL LAR VALUE. CURVATURE VALUE OF A BOX-SHAPED PATTERN IS EQUAL TO THAT OF A CLOSE END L-SHAPED PATTERN WITH EQUAL LAR VALUE ($LAR=6$ AND $d_1 = d_2 = w = 65nm$). 88

FIGURE 3-11 (A) LAPLACE PRESSURE OF OPEN END L-SHAPED PATTERNS, (B) LAPLACE PRESSURE OF CLOSE END L-SHAPED PATTERNS, (C) PATTERN DEFORMATION OF OPEN END L-SHAPED PATTERNS AND (D) PATTERN DEFORMATION OF CLOSE END L-SHAPED PATTERNS, AT DIFFERENT CONTACT ANGLES AND LAR VALUES IS SHOWN. FOR LARGE LAR VALUES DEFORMATION INCREASES ($L_1 - L_2 = 0$, $d_1 = d_2 = w = 57nm$ AND $\gamma = 72.9mN/m$). 89

FIGURE 3-12 (A) "LI" CONFIGURATION WHICH COMPRISES "I" AND "L" SHAPE PARTS AND (B) "LL" CONFIGURATION WHICH COMPRISES TWO "L" SHAPE PARTS ARE SHOWN. AMONG GEOMETRIES WITH EQUAL LAR VALUE "LI" CONFIGURATION AND ESPECIALLY ITS "I" PART HAS THE MAXIMUM DEFORMATION. 90

FIGURE B1 (A) A SURFACE EVOLVER AREA IS SHOWN. AREA IS COMPOSED OF SERIES OF ATTACHED TRIANGLES. (B) REFINEMENT PRODUCES FOUR TRIANGLES INSIDE EACH SINGLE TRIANGLE 108

FIGURE B2 INITIAL SHAPE OF THE RINSE INTERFACE FROM SE AND COORDINATION USED IN SE FOR (A) TWO-LINE PARALLEL PATTERN, (B) BOX-SHAPED AND (C) L-SHAPED PATTERN IS SHOWN. 108

FIGURE E1 RINSE INTERFACE CURVATURE VALUE DECREASES BY INCREASING THE TROUGH WIDTH. RINSE HAS FILLED THE SPACE BETWEEN (A) A TWO-LINE PARALLEL PATTERN AND (B) A BOX-SHAPED PATTERN ($H=250$ nm, $\theta = 5^\circ$ AND $ILH=110$ nm). 119

FIGURE E2 ERROR OF USING CIM COMPARED TO SE FOR FINDING THE RINSE INTERFACE CURVATURE VALUE AT DIFFERENT TROUGH WIDTH IS SHOWN FOR (A) TWO-LINE PARALLEL AND (B) BOX-SHAPED PATTERNS. ERROR DOES NOT CHANGE BY INCREASING D AND L AT THE SAME RATE (OR CONSTANT LAR). $H=250$ nm, $\theta = 5^\circ$ 119

List of Acronyms and Symbols

STF	Surface Tension Force
FE	Finite Element
MOSFET	Metal-Oxide Semiconductor Field-Effect Transistor
ILH	Initial Liquid Height
EMS	Electro Mechanical Systems
IC	Integrated Circuit
EUVL	Extreme Ultra Violet Lithography
UV	Ultra Violet
NIL	Nano Imprint Lithography
HMDS	Hexamethyldisilazan
TMAH	Tetra Methyl Ammonium Hydroxide
DIRE	Deep Reactive Ion Etching
CMC	Critical Micelle Concentration
IPA	Isopropyl Alcohol
MEMS	Micro Electro Mechanical System
NEMS	Nano Electro Mechanical system
CIM	Cylindrical Interface Model
SE	Surface Evolver
F	Minimum Feature Size
N_A	Numerical Aperture of Lens
R_1	Radius of Curvature of Rinse Interface
R_2	Radius of Curvature of Rinse Interface

I	Moment of Inertia for Beam
ΔP	Laplace Pressure
w	Pattern width
H	Height of Patterns
E	Elasticity Modulus of Patterns
AR	Aspect Ratio
LAR	Longitudinal Aspect ratio
d	Trough Width
L	Pattern Length
L_e	Equivalent Length
ϕ	Slope of the pattern at the tip
δ_1	Maximum Pattern Deformation Due to Laplace Pressure
δ_2	Maximum Pattern Deformation due to Surface Tension Force
λ	Wave Length
κ	Rinse Interface Curvature
δ	Maximum Deformation of the Pattern
γ^{LV}	Liquid-Vapor Surface Tension
γ^{SV}	Solid-Vapor Surface Tension
γ^{SL}	Liquid-Solid Surface Tension
θ	Contact Angle

Chapter 1 – Introduction

This Chapter introduces the main obstacle (pattern collapse) during nano-scale manufacturing using photolithography. In this Chapter first, the procedure for photolithography is provided. Then, three of the main obstacles to nano-manufacturing by photolithography are mentioned to show that pattern collapse (the collapse of photoresist patterns during the drying of rinse) is the most limiting. A literature review is included to show how others attempted to resolve the pattern collapse limitation. Various methods to solve the pattern collapse based on analytical models in the literature are listed. Shortcomings of the analytical models in the literature are discussed with the intent of developing new more accurate models. The new models are presented in the second and third Chapters.

1-1 Nano-Manufacturing Methods

Due to the need for fast data processing, the application of devices in small volumes, and the trend towards decreasing energy consumption, manufacturing is beginning to move into a new scale (i.e. the nano-scale). Densely packed nano-scale features are mainly used in electro mechanical systems (EMS), semiconductor industries (e.g. integrated circuits, I.C.), comb-drives, channels used in mammography [1], electrophoresis [2], zone plates for X-ray microscopy [3] and gamma-ray collimator grids. In general, two approaches for nano-scale manufacturing exist *i.e.* bottom-up and top-down. However, the bottom-up (also known as self assembly) method is limited to some specific applications (*e.g.* micro channels). The main top-down methods proposed for manufacturing of small features are:

1. Photolithography (Optical Lithography)
2. Extreme Ultra Violet Lithography (EUVL)
3. Optical and Immersion Lithography
4. Nano Imprint Lithography (NIL)
5. Scanning Probe or Dip Pen Lithography
6. Size Reduction Lithography
7. Electron Beam Lithography

Today, the most applied top-down method for mass production of nano-features is photolithography. Due to the wide usage and high efficiency of photolithography, the following section describes the photolithography procedures used to provide nano-features. This helps one to understand the challenges occur during nano-manufacturing using photolithography.

1-2 Photolithography

Photolithography involves transferring a pattern first to a photomask (or mask), then the pattern is transferred from the photomask to the photoresist (or resist). The photoresist pattern is then transferred into the substrate (see Fig. 1-1).

The photomask is a square fused quartz substrate covered with a layer of chrome. The fused quartz is a type of glass containing silica in amorphous (non-crystalline) form. The chrome is what the mask pattern is etched into using photolithography. The etched area of the chrome allows the light to pass through it to cook the pattern in the photoresist.

However, before this is done there are a few steps to be completed, such as the preparation of the substrate, preparation of the photoresist, and the consideration of the distance between the mask and photoresist. These steps are described below.

The substrate is heated for few minutes to remove the moisture. Then a chemically cleaning process is performed on the substrate. After drying and cleaning the substrate, adhesion liquids such as hexamethyldisilazan (HMDS) are applied to the surface of the substrate to enhance the adhesion of the photoresist to the substrate.

Following the substrate preparation, the photoresist is deposited on the substrate by spin coating. After deposition of the photoresist on the substrate, the combined photoresist and substrate are heated at 100 degrees Celsius in presence of nitrogen for up to 30 minutes depending on the photoresist. This is done to drive off the excessive solvents and is called soft-baking or pre-baking.

The manufacturer needs to consider the distance between the photomask and the photoresist when cooking the pattern. Placing the photomask directly on the photoresist (contact printer) is more accurate but more expensive than allowing a small gap between the photomask and the photoresist (proximity printer). Contact printer is more expensive because contact between the photomask and the photoresist may cause damage to either the photomask and/or the photoresist.

After the preparation of substrate and photoresist is completed, the photoresist will be exposed to the UV light through the patterned photomask, see Fig. 1-1. The parts of the photoresist exposed to the UV (Ultra Violet) light are called cooked parts. Either the cooked or uncooked parts may be dissolved in the developer depending on the photoresist used. In positive photoresists, which are more common, the cooked parts of the photoresists are dissolved. In negative photoresists, the uncooked parts of the photoresists are dissolved. Developer liquid is delivered to the photoresist by a spinner. Today developer liquids are Metal-ion free such as tetra methyl ammonium hydroxide (TMAH).

After being exposed to the developer liquid, the photoresist pattern is baked for 20 to 30 minutes at the temperature of 140 to 180 degrees (hard-baking). When the hard-baking is completed, the photoresist is rinsed with a rinse liquid (normally water) to remove the developer liquid. Before exposing the photoresist and substrate to the etcher, rinse liquid is dried from the photoresist. Heating or shaking are procedures applied to increase the rate of evaporation or decrease the rinse drying time.

Etching is the next and last step to transfer the pattern from the photoresist to the substrate. During the etching process the substrate is etched where no photoresist exists. The two categories of etchers are etching acid (wet) and plasma (dry). In the wet etching process the acid is washed away by a rinse which dissolves the etcher. After rinsing, any remaining photoresist attached to the substrate is removed using photoresist stripper and/or plasma (containing oxygen which oxidizes the attachment area).

The process described above, photolithography process, has some general obstacles such as the substrate needs to be flat and extremely clean. Photolithography also faces some challenges during the manufacturing of nano-scale features, which are reviewed in the following section.

1-3 Manufacturing Limitations during Photolithography

For studying the limitations of photolithography in nano-scale, this section focuses on microprocessor manufacturing limitations because microprocessor manufacturing deals with the smallest dimensions and most complex designs. Three main challenges to the manufacturing of nano-scale features for microprocessors are listed. The most challenging one (collapse of photoresist patterns during drying of the rinse liquid) is the focus of this thesis. The two other obstacles regarding the optical limitation and Metal-Oxide-Semiconductor Field-Effect-Transistor (MOSFET) design are briefly mentioned first for completeness.

1-3.1 Optical Limitation

The optical limitation deals with the exposure light (*i.e.* UV) and the optical devices. Equation 1-1 implies that minimum feature size (F) decreases by either a decrease of the wavelength (λ) of the UV light or an increase of the numerical aperture of the lens (N_A).

$$F = K \frac{\lambda}{N_A} \tag{1-1}$$

where K is a process related factor (approximately 0.5). The wavelength of UV lights is shorter than visible light (380nm) and longer than X-rays (10nm). By noting the range of

λ for UV light, it can be understood that there is a limitation for decrease of λ . The next paragraph shows that there is also a limitation for increase of N_A .

Increasing N_A requires a lens with physically larger dimension. Large lenses have a close proximity or a short depth of focus (DofF, see Eq. 1-2).

$$DofF = 0.6 \frac{\lambda}{N_A^2} \quad (1-2)$$

As such, an increase of N_A restricts the thickness of photoresist by decreasing the depth of focus. However, the thickness of photoresist needs to be thick enough for proper etching. So, there is an upper bound for N_A .

1-3.2 MOSFET Design Limitation

MOSFET design limitations are related to scaling down the MOSFET which acts as a transistor in the microprocessor circuit. Difficulties that occur during shrinking of MOSFET are listed as: sub-threshold conduction, interconnect capacitance, heat production and gate oxide leakage [4]. From these obstacles gate oxide leakage is briefly discussed here as it is the most challenging one.

Applying voltage to one side of the gate oxide layer (insulator) charges the other side and forms an electron channel (see Fig. 1-2). With a wider channel the transistor is more efficient. The width of the channel depends on the voltage difference across the insulator. A method to increase the voltage difference across the insulator (and efficiency of semiconductor consequently) is to decrease the thickness of insulator. The thickness of

insulator layer in the Intel 45nm process is as low as 5 atoms (approximately 1.2nm). However, a decrease of the insulator thickness may form electron tunneling between the gate and channel. The power dissipation due to the electron tunneling leakage will grow to be a significant part of chip consumption (the gate tunneling leakage current increases exponentially with decreasing the insulator thickness [5]). The alternative method for increasing the voltage difference across the insulators is using insulators with dielectric constants larger than that of silicon dioxide (such as Hafnium and Zirconium silicates or oxides). Since late 2007, alternative insulators rather than silicon dioxide have been used to resolve the electron tunneling barrier.

1-3.3 Pattern Collapse Limitation

The collapse of photoresist patterns is colloquially called “Pattern collapse” [6]. Pattern collapse is the permanent deformation of photoresist features (see Fig. 1-3) during or after the development step in the photolithography process [7]. Pattern collapse limits the manufacturing of nano-features. Different scenarios for the collapse mechanism have been reported in the literature. These scenarios are discussed below and the most likely causes for the pattern collapse, based on the literature to date, are identified. It should be mentioned that in this thesis another cause for pattern collapse, which is missing in the literature *i.e.* surface tension force (see section 1-5.1), is presented as well.

1-3.3.1 Intrusion

Kawai [8] reported that the penetration of rinse liquid into the interface of photoresist and substrate weakens the bonding between photoresist and substrate and causes collapse. Sanada *et al.* [9] also assumed that intrusion is the cause of collapse and found that intrusion energy becomes large with increasing the developing time and argued that shortening the development time is effective to resolve the collapse problem. Penetration intensity is inversely proportional to the diffusion coefficient of the rinse liquid. Based on that, Namatsu [10] used carbon dioxide in supercritical state for rinsing. Supercritical carbon dioxide diffusion coefficient value is as large as that of a gas. At low intrusion Namatsu formed slim nano-lines without pattern collapse. However, as will be shown later the reason that carbon dioxide resolved the collapse was most likely not due to the increase of diffusion or decrease of intrusion. The reason is provided in section 1-4.2.1.

1-3.3.2 Swelling

Kim [11] stated that condensation due to humidity causes the collapse. As humidity in the form of water or vapor penetrates into the photoresist, it causes the photoresist to inflate (swell). While the pattern is drying, the surface of the pattern dries faster than its interior. Different volume contractions, between the surface and interior of the pattern, induce internal stress resulting in collapse. Smoothing the pattern surface decreases the pattern area exposed to the liquid and reduces the liquid penetration or swelling. Based on the assumption that swelling scenario is the cause of pattern collapse, to reduce the collapse Inatomi *et al.* [12] proposed a process to smooth the surface of the pattern.

Intrusion and swelling scenarios as the main causes of the pattern collapse might be inaccurate. The effect of swelling and intrusion on collapse is the same for both a single isolated pattern, and that of a two-line parallel pattern. Experiments done by Mori *et al.* [13] showed that no collapse is observed for a single isolated pattern (unless the pattern is very tall and slim). This suggests that the above scenarios (intrusion and swelling) will not provide a complete answer to the question of the main cause of pattern collapse. In other words, if intrusion and swelling are causes for collapse an isolated pattern should collapse as well.

1-3.3.3 Laplace Pressure

Deguchi *et al.* [6] showed that the collapse is mainly caused by adhesion between two adjacent patterns; however, the cause of adhesion was not stated in their research. They simulated the photoresist pattern as a beam and applied the analytical beam bending model to describe the pattern behavior.

Tanaka *et al.* [7] hypothesized that either the centrifugal force or Laplace pressure during unbalanced drying of the rinse liquid, in spaces between neighboring patterns, are the driving forces causing the adhesion or collapse of photoresist features. Centrifugal force is the force due to the swirling flow of the rinse liquid (in the photolithography process rinse is delivered to the photoresist by spinning). Laplace pressure (ΔP) is the pressure difference across the rinse liquid interface or in other words, the pressure difference between the rinse liquid and outside. Laplace pressure is a function of interface curvature and surface tension of the rinse liquid (see Eq. 1-3).

$$\Delta P = \gamma \cdot \kappa \quad (1-3)$$

where γ is the surface tension of the rinse liquid and κ is the curvature of the rinse liquid interface.

It should be mentioned that if centrifugal force was the cause of collapse, two adjacent patterns would collapse in one direction. Tanaka's experiments [7] showed that two adjacent patterns stick to each other at tips (usually) which contradict the centrifugal force effect as the cause of pattern collapse. The other issue undermining the centrifugal force scenario is that if centrifugal force was the driving force for pattern collapse, single isolated pattern of Mori *et al.* [13] experiments would have collapsed as well.

The idea that Laplace pressure or capillary force can be the main cause of the pattern collapse is understood, for example, by the observation that Laplace pressure decreases by increasing the spacing between two adjacent patterns. Tanaka's [7] experimental results showed that pattern deformation decreases by increasing the spacing between two adjacent patterns. Also, Mori *et al.* [13] experiments showed no pattern collapse for the case of single isolated patterns (as a representative for infinity spacing between two adjacent patterns).

For simulating pattern deformation during the collapse, many models have been proposed, and based on them collapse elimination methods have been developed. For example, Lai and Fang [14] developed a lumped model for simulating a microstructure and its liquid film and predicted the dynamic response of the microstructure system. Then

by knowing the dynamic response of the system, they applied harmonic excitation on the microstructures to avoid the collapse.

Tanaka *et al.* [7] calculated the pattern deformation (maximum deflection) by considering Laplace pressure as the driving force for pattern deformation and applying the beam bending model. They assumed pure elastic deformation for the pattern and the cylindrical interface shape for the rinse liquid (rinse liquid interface curvature defines Laplace pressure). Comparison of cohesive and restoring forces was the technique used for calculating the deformation value. Pattern deformation based on Tanaka's model is shown in Eq. 1-4 [7].

$$\delta = \frac{Ew^3d - 4\gamma H^3 \sin \theta - \sqrt{(4\gamma H^3 \sin \theta - Ew^3d)^2 - 24\gamma Ew^3 H^4 \cos \theta}}{4Ew^3} \quad (1-4)$$

where E is the elasticity modulus of the pattern material, d is the trough width, H and w are pattern height and pattern width, and θ is the contact angle between rinse liquid interface and pattern's side wall.

Bohme and Pable [15] stated that Tanaka's beam bending model neglects the effect of lateral expansion or contraction due to a non-zero Poisson's ratio. For addressing that, in [15], the pattern was modeled as a plate and the general solution for a long rectangular plate in elastic region was used to find the pattern deformation. Given that the exact value of Poisson's ratio of photoresist, especially for nano-scale polymers, was not accurately known and the plate models, to solve the problem analytically, is too complicated; researchers have made the compromise of using zero value for Poisson's ratio and neglected the effect of horizontal force on lateral deflection or used the beam bending

model (where Poisson's ratio is zero, the plate model equation simplifies to the beam bending equation).

However, in general the range of Poisson's ratio is known (i.e. the maximum value of Poisson's ratio is 0.5 and the minimum is zero). Negative values have also been reported [16] which means that the pattern expands laterally while exposed to the horizontal tension. Also, recently the narrower range for Poisson's ratio of some photoresists is suggested [17]. In this study inclusion of Poisson's ratio is addressed by using the Finite Element Analysis (see Chapter 3).

Yoshimoto *et al.* [18] improved Tanaka's elastic beam bending model for calculating the pattern deformation to an elasto-plastic beam bending model. They stated that depending on the yield stress of photoresist, elastic, plastic, or elasto-plastic model should be applied to calculate the pattern deformation. However, due to the following reasons plastic analysis is not required. Nevertheless, the elasto-plastic deformation analysis using the Finite Element method is provided in Appendix A.

In most of the cases the pattern is peeled off from its base (where it meets the substrate) instead of plastic deformation (this point is addressed in Chapter 2). Also, if the pattern is not peeled off, for typical polymers at room temperature where deformation is smaller than 4% of the structure height, deformation is in the elastic region (after the drying of rinse liquid, pattern restores its initial state). For example, for a 1:1 line-space pattern with the AR (Aspect Ratio; the ratio of pattern height over its width) of 5, as long as the

pattern's deformation is smaller than 40% of the half of the trough width, deformation is in the elastic region. Also, if the pattern's deformation exceeded the value of 40% of the half of the trough width, as will be shown, the pattern will collapse.

By increasing the pattern deformation, rinse interface curvature value and consequently Laplace pressure increases (see Chapter 2 for more details). On the other hand, by increasing the pattern deformation in the elastic region, restoring force of the pattern which acts against the Laplace pressure, increases linearly (similar to a stretched spring in elastic region, see Chapter 2 for more details). However, in the plastic region for further pattern deformation, restoring force does not increase or even in some cases decrease. So, as soon as the deformation of pattern reached the plastic region (which is the 40% of the half of the trough width for AR of 5) deformation continues till collapse.

As shown before, it is deemed that to date the most proper approach for predicting the pattern deformation, which is widely studied and cited, is Tanaka's analytical model [7]. So, Tanaka's model was used as a departure point and studied for different pattern materials and geometries as well as different rinse liquids to find the optimum values for which pattern deformation is at its minimum value (further details of Tanaka's model are provided in Chapter 2). In this study, after mentioning the collapse solution methods based on Tanaka's model, shortages of Tanaka's model will be addressed to find that whether the collapse solution methods based on Tanaka's model are still useful.

1-4 Pattern Collapse Problem Resolutions Based on Tanaka's Beam Bending Model

In this section, all of the applied approaches to resolve the pattern collapse based on findings from Tanaka's model are listed, described and compared to find the most effective approach. Based on Tanaka's model, pattern deformation decreases by either a pattern stiffness increase (for example by increasing the elasticity modulus of pattern) or a Laplace pressure decrease (for example by increasing the spacing between two parallel patterns or decreasing the surface tension of the rinse liquid).

1-4.1 Pattern Stiffness Increase

Tanaka *et al.* [19] increased the photoresist hardness by flood exposure using a high pressure mercury lamp during rinsing and obtained slimmer patterns. To increase the mechanical strength, Choi and Kim [20] applied a sidewall profile to manufacture tall and slim features without collapse. The method Choi and Kim used is called Deep Reactive Ion Etching (DRIE) fabrication. Olynick *et al.* [3] used the buttress to increase the stability of patterns and obtained dense features. Vora *et al.* [21] increased the overall stiffness of SU-8 (a common photoresist used in photolithography) features by using top-plate support members and prevented collapse. Shibata *et al.* [22] formed a nano-composite photoresist system by mixing unspecified amounts of fullerenes C_{60} and C_{70} into ZEP520 (a positive photoresist). C_{60} Molecules which are tiny particles with the diameter of approximately 0.7nm fill the free space between photoresist molecules and reinforce the mechanical strength of the photoresist.

1-4.2 Laplace Pressure Decrease

To decrease the Laplace pressure the surface tension and/or the curvature value of the rinse liquid interface should be decreased (see Eq. 1-3). Curvature value decreases by increasing the spacing between two adjacent patterns and/or the contact angle. As spacing is related to the design of the device, most of the researchers tried to minimize the deformation by surface tension decrease and/or contact angle increase.

1-4.2.1 Surface Tension Decrease

Adding surfactant to the rinse liquid is an approach to reduce the deformation through decreasing the surface tension. Tanaka *et al.* [23] added additives to DI-water and found when the concentration of additives reached the CMC (critical micelle concentration), surface tension and consequently Laplace pressure decreased drastically. However, this concentration of surfactant is harmful to the pattern and causes defects or melting of the pattern. Junarsa *et al.* [24] found that fluoro-surfactants at concentrations lower than CMC (approximately half) can be useful to decrease the surface tension by 20-30%. The concentration of surfactant was still high enough to damage the pattern. Tanaka *et al.* [23] showed that further decrease of the concentration of surfactant is not useful for decreasing the Laplace pressure. At very low solution concentrations the contact angle drastically decreases (due to the absorption of surfactant to the photoresist's side wall) while the surface tension only slightly decreases causing Laplace pressure to increase overall.

Application of low surface tension liquids instead of water for rinsing was the other method to eliminate the effect of surface tension and resolve the collapse problem. Yamashita [25] suggested Perfluorohexane as a low surface tension (approximately 10mN/m) rinse and obtained a higher aspect ratio (*i.e.* 5) compared to the aspect ratio of 4 when water was used as rinse in 450nm thick ZEP (Nippon Zeon Co.) photoresist. Ohtsu *et al.* [26] also suggested rinsing with Fluorinert as a liquid with low surface tension (13mN/m). Ki-Soo and Lee [27] showed that in-house rinse liquids (HR series) have lower surface tensions (*i.e.* 26mN/m) compared to commercial ones (*i.e.* 45mN/m). However, in-house rinse liquids attacked the photoresist and caused surface damage to the photoresist.

The disadvantage of using the above mentioned liquids is that these liquids are poor solvents for photoresist polymers. Addition of liquids, such as alcohols, to water to lower the surface tension of the rinse is another approach. Reese [28] added Isopropyl alcohol (IPA) to DI-water to resolve the collapse, but found high concentrations of IPA dissolve the pattern. In general, for positive photoresists, the alcohol causes pattern pitting [29].

In the supercritical state there is no liquid-gas interface. Therefore, surface tension vanishes and Laplace pressure becomes zero (see Eq. 1-3). As such, the developing step with supercritical carbon dioxide seems proper for decreasing the pattern deformation as developer dries in a Laplace pressure-free process. The obstacle to developing with carbon dioxide is that carbon dioxide is a very poor solvent for common polymers used as photoresists (most photoresists require water as the developer). To reduce the

possibility of collapse (because of water's high surface tension) after development the water can be replaced with another substance such as supercritical carbon dioxide (*i.e.* rinsing with supercritical carbon dioxide). The challenge was that negligible amounts of water dissolve in the carbon dioxide.

Because water easily dissolves in ethanol and ethanol dissolves in carbon dioxide, Namatsu [30] used ethanol to indirectly dissolve water in carbon dioxide. The above procedure was long and expensive. Also, ethanol was harmful to the pattern. Goldfarb *et al.* [31] replaced ethanol as an intermediate liquid by n-hexane mediated by an organic surfactant. Organic solvents such as n-alkanols and n-alkanes are miscible with supercritical carbon dioxide, if pressure is held above 9.5MPa in the temperature range of 31-45 degrees Celsius. However, maintenance of pressure and temperature in that specific range adds cost to the procedure. Recently, for manufacturing features below 65nm, new photoresist components such as molecular glass, soluble in carbon dioxide, have been applied by Felix *et al.* [32], but application of glass is not common and is expensive. The application of molecular glass may be promising for the future.

Tanaka *et al.* [33] applied a freeze-drying process with tert-butylalcohol to avoid collapse (surface tension of their frozen material was very low). Freeze-drying material must have a melting point close to room temperature. The melting point of tert-butylalcohol is 25.4 degrees Celsius. During freeze drying, rinse liquid significantly expands which may cause damage to the patterns, however.

1-4.2.2 Contact Angle Increase

Lee *et al.* [34] increased the contact angle by changing the shape of the photoresist profile at its top to a round shape rather than a flat top profile. However, manufacturing of patterns with a round top is not easy. Also, as the level of liquid due to the drying goes down, the rounded top of the pattern to increase the contact angle is no longer useful.

Drechsler *et al.* [35] suggested a rinsing process with cationic surfactant as a method to increase the contact angle without changing the surface tension. They showed that at a one-tenth of CMC, contact angle increases by 10 degrees. As the concentration was not very high, damage to the pattern was negligible. Drechsler *et al.* [36] also studied the effect of hydrocarbon chain length of the surfactant on contact angle. They found that by increasing the hydrocarbon chain, the adsorption of surfactant to the pattern surface increased. The adsorption increase raised the contact angle which decreased Laplace pressure. This method is inexpensive, easy and imposes no damage to the pattern. So, based on Tanaka's beam bending model, apparently the most promising and economical method to resolve the pattern collapse problem is adding cationic surfactants (which increases the contact angle in the order of 10 degrees).

In the following section shortcomings of Tanaka's beam bending model are listed and described. By describing the shortcomings the development of a new model for finding the pattern deformation will be started. In Chapters 2 and 3 a new model is fully developed. After the model is developed, the model will be used to determine whether

adding cationic surfactants (to increase contact angle by 10 degrees) is really useful for pattern collapse resolution (see Chapter 2).

1-5 Shortcomings of Tanaka's Beam Bending Models

Tanaka's beam bending model was valid for the case of two-line parallel pattern. Also, the rinse liquid interface was modeled as a part of a cylinder (see Chapter 2).

As will be shown, the effect of surface tension force on the three-phase line is not considered in Tanaka's beam bending model or any other models in the literature. Furthermore, in general for some geometries (e.g. short length two-line parallel patterns, L- and box-shaped patterns) application of beam bending models is invalid. The reason is that for these cases the rinse interface shape is not cylindrical and/or the pattern cannot be modeled as a beam. For these cases a FE (coupled Surface Evolver-ANSYS) model will be developed to model and find the pattern deformation (see Chapter 3). Surface Evolver is a Finite Element based software used to find the rinse liquid interface shape and its curvature value (see Appendix B). ANSYS is a widely known Finite Element package used to simulate the pattern deformation.

1-5.1 Inclusion of Surface Tension Force

To date, the effect of liquid-vapor surface tension, a concentrated force operating on the three-phase line, is not considered in beam bending models. According to Young's equation, parallel to the pattern's side wall projection of the liquid-vapor surface tension

is cancelled by considering liquid-solid and solid-vapor surface tensions. However, the normal to the pattern's side wall projection of the liquid-vapor surface tension is unbalanced. As such, the value of surface tension force (STF) on the three-phase line is equal to the projection of liquid-vapor surface tension normal to the pattern's side wall.

The order of magnitude of the STF is defined by performing a dimensionless analysis and comparing the order of magnitudes of the Laplace pressure to that of the STF. It is found that the order of magnitude of the force due to Laplace pressure to that due to STF is H/d (pattern height over trough width). As in most of the cases pattern trough width is equal to the pattern width, so the order of magnitude of the force due to Laplace pressure to that of STF is in the range of AR (H/w , the ratio of pattern height over pattern width). As H and d are in the same order of magnitude, so Laplace pressure and STF are in the same order of magnitude as well (see Appendix D for more details).

To see the importance of consideration of the STF, a new beam bending model will be developed and its results will be compared with Tanaka's beam bending model (see Chapter 2). The new beam bending model uses superposition principle to calculate the pattern deformation due to both the STF and the Laplace pressure. The new beam bending model uses cylindrical interface shape assumption. As such, the new beam bending model is only valid for two-line parallel patterns with large LAR (the ratio of pattern length over spacing between two lines) values. For these geometries the pattern can be modeled as a beam, and the assumption of cylindrical shape for the interface is satisfactory. But in this thesis, a Finite Element based method is also developed to deal

with cases such as two-line parallel patterns with small LAR values, box-shaped and L-shaped patterns.

1-5.2 Short Length Two-line parallel Patterns

To date, similar to Tanaka's model, other literatures have assumed cylindrical shape for the interface of the rinse liquid between the two-line parallel patterns (e.g. Kotera and Ochiai [37]). Despite other assumptions used in Tanaka's model (such as the elastic deformation assumption) which were criticized by other researchers, the cylindrical shape assumption for the rinse interface has remained, and there has been no attempt to improve it. Only Stoykovich *et al.*[38] constrained the size of test feature structures to have LAR values greater than 15. They stated that for their specific experimental case where LAR value is larger than 15, the interface shape is almost cylindrical. It should be noted that in their research there was no comparison of the interface shape or curvature value from the experiment to the cylindrical model to prove their statement.

For the two-line parallel pattern, the curvature value from Surface Evolver will be compared to that from the cylindrical model at different LAR values. This will be done to find how large LAR values should be in order to assume that the rinse interface shape is cylindrical and the new beam bending model is valid.

1-5.3 Box- and L-Shaped Patterns

For other pattern configurations such as box- and L-shaped patterns [39], the interface shape is not cylindrical and the pattern cannot be modeled as a beam. For such configurations the rinse interface curvature is calculated by Surface Evolver. Subsequently, the Finite Element method using ANSYS is applied to calculate the pattern deformation value (see Chapter 3).

1-6 Thesis Outline

Chapter 1 is the introduction which includes the background and purpose and research behind the thesis.

Chapter 2 of this thesis discusses the effect of the inclusion of STF in the beam bending model. The purpose at this stage is to develop a new analytical beam bending model for finding the pattern deformation of a two-line parallel pattern with a very long length. In Chapter 2, infinite length is assumed for the pattern so one may ensure that the interface shape is cylindrical. For the case of a two-line parallel pattern, curvature values from Surface Evolver and the cylindrical interface model are compared at different LAR values. Comparison defines a range of LAR where cylindrical interface assumption is valid. For the defined range of LAR the new analytical beam bending model results (which are easier than Finite Element results; discussed in Chapter 3) are valid. By using the new beam bending model, the effect on the pattern deformation of changing the rinse liquid or adding surfactant to the rinse is observed. For example, using the new beam bending model the state-of-the-art method for resolving the pattern collapse based on

Tanaka's model (see section 1-4.2.2) is checked. The purpose is to determine if the method is always useful to resolve the pattern collapse.

Chapter 3 defines different pattern geometries, rather than a two-line parallel pattern with a large length, where the beam bending model is invalid. These geometries are common in case of microprocessor manufacturing (i.e. two-line parallel patterns with short length, box- and L-shaped patterns). For these complex geometries, the cylindrical model is unable to find the interface curvature value, and/or simulation of the pattern as a beam is invalid.

Curvature values of the rinse liquid interface for these geometries is found using Surface Evolver (curvature value defines the Laplace pressure). The interface shape in general is not cylindrical, and the three-phase line is not necessarily a straight line. Three-phase line defines the area, where Laplace pressure is operative, and the line, where STF is operative (i.e. Laplace pressure is operative on the area underneath the three-phase line and STF operates on the three-phase line). By knowing the pattern geometry and cohesive forces and their location, a model for the pattern will be created in ANSYS, a Finite Element (FE) software, and the pattern deformation will be found. The details of FE method are discussed in Chapter 3. Chapter 4 is the conclusions. In this chapter future possible works are discussed.

Figures

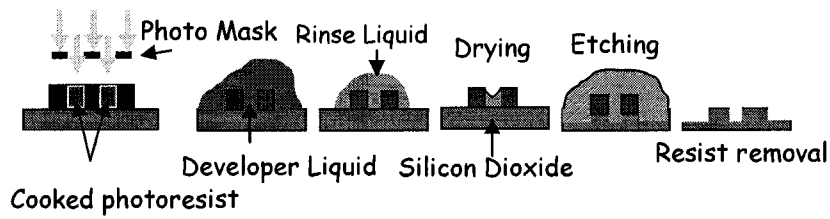


Figure 1-1 Photolithography procedure is shown. One of the obstacles of photolithography process is collapse of photoresists during drying the rinse liquid.

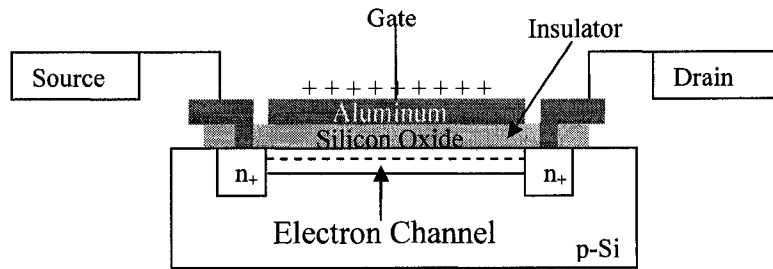


Figure 1-2 Schematic of a MOSFET (Metal-Oxide-Semiconductor Field-Effect-Transistor) is shown.

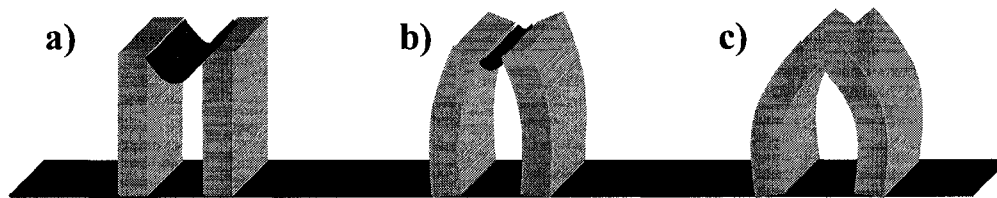


Figure 1-3 Pattern collapse for the case of a two-line parallel pattern is shown. (a) non deformed, (b) deformed and (c) collapsed.

References

- 1 K. Fischer, B. Chadhuri, H. Guckel and C. M. Tang, Proc. SPIE, 4145, 227-234, (2000)
- 2 R. Kupka, F. Bouamrane and S. Megtert, Recent Adv. Prospects Microsys. Technol., 10, 22-28, (2003)
- 3 D. L. Olynick, B. D. Harteneck, E. Veklerov, M. Tendulkar, J. A. Liddle, A. L. D. Kilcoyne and T. Tyliczszak, J. Vac. Sci. Technol. B, 22, 3186-3190, (2004)
- 4 J. Hu, X. Xi, A. Niknejad and Ch. Hu, Solid-State Elect., 50, 1740-1743, (2006)
- 5 W. K. Henson, N. Yang, S. Kubicek, E. M. Vogel, J. J. Wortman, K. De Meyer and A. Naem, IEEE Transaction on Electron Devices, 47, 440-447, (2000)
- 6 K. Deguchi, K. Miyoshi, T. Ishi and T. Matsuda, Jpn. J. Appl. Phys., 31, 2954-8, (1992)
- 7 T. Tanaka, M. Morigami and N. Atoda, Jpn. J. Appl. Phys., 32, 6059-6064, (1993)
- 8 A. Kawai, Proc. SPIE, 3677, 565-573, (1999)
- 9 M. Sanada, O. Tamada, A. Ishikawa, A. Kawai, Proc. SPIE, 5753, 988-994, (2005)
- 10 H. Namatsu, J. Vac. Sci. Technol. B, 19, 2709-2712, (2001)
- 11 Sang-Kon Kim, J. Korean Phys. Society, 42, S371-S375, (2003)
- 12 Y. Inatomi, T. Kawasaki and M. Iwashita, Proc. SPIE 6153, 61533X-1 to 9, (2006)
- 13 S. Mori, T. Morisawa, N. Matsuzawa, Y. Kaimoto, M. Endo, T. Matsuo, K. Kuhara and M. Sasago, J. Vac. Sci. Technol. B, 16, 3744-7, (1998)
- 14 W. P. Lai and W. Fang, J. Vac. Sci. Technol. A, 19, 1224-1228, (2001)
- 15 T. R. Bohme and J. J. de Pablo, J. Chem. Phys., 116, 9939-9951, (2002)
- 16 B. Xu, F. Arias, S. T. Brittain, Xiao-Mei Zhao, B. Grzybowski, S. Torquato and G. M. Whitesides, J. Adv. Mater., 11, 1186-1189, (1999)
- 17 <http://web.mit.edu/6.777/www/matprops/su-8.htm> last accessed on 29 November 2007

-
- 18 K. Yoshimoto, M. P. Stoykovich, H. B. Cao, J. J. de Pablo, P. F. Nealey and W. J. Drugan, *J. Appl. Phys.*, 97, 1857-1865, (2004)
- 19 T. Tanaka, M. Morigami, H. Oizumi, T. Ogawa and Shou-ichi U Chino, *Jpn. J. Appl. Phys.*, 33, L1803-5, (1994)
- 20 Chang-Hwan Choi and Cahng-Jim Kim, *J. Nanotech.*, 17, 5326-5333, (2006)
- 21 K. D. Vora, B. Y. Shew, E. C. Harvey, J. P. Hayes and A. G. Peele, *J. Micromech. Microeng.*, 15, 978-983, (2005)
- 22 T. Shibata, T. Ishii, H. Nozawa and T. Tamamura, *Jpn. J. Appl. Phys.*, 36, 7642-7645, (1997)
- 23 K. Tanaka, R. Naito, T. Kitada, Y. Kiba, Y. Yamada, M. Kobayashi and H. Ichikawa, *Proc. SPIE*, 5039, 1366-1380, (2003)
- 24 I. Junarsa, M. P. Stoykovich, K. Yoshimoto and P. F. Nealey, *Proc. SPIE*, 5376, 842-9, (2004)
- 25 Y. Yamashita, *Jpn. J. Appl. Phys.*, 35, 2385-2386, (1996)
- 26 M. Ohtsu, K. Minami, M. Esashi, *Proc. IEEE Micro Electromech. Sys.*, 228-233, (1996)
- 27 Ki-Soo and G. Lee, *J. Photopolymer Sci. Tech.*, 16, 363-368, (2003)
- 28 J. Reese, *24th Annual Microelect. Eng. Conf.*, 25-29, (2006)
- 29 J. Simons, D. Goldfarb, M. Angelopoulos, S. Messick, W. Moreau, C. Robinson, J. de Pablo and P. Nealey, *Proc. SPIE*, 4345, 19-29 (2001)
- 30 H. Namatsu, *J. Vac. Sci. Technol. B*, 18, 3308-3312, (2000)
- 31 D. L. Goldfarb, J. J. de Pablo, P. F. Nealey, J. P. Simons, W. M. Moreau and M. Angelopoulos, *J. Vac. Sci. Technol. B*, 18, 3313-7, (2000)

-
- 32 N. M. Felix, K. Tsuchiya and C. K. Ober, *J. Adv. Mater.*, 18, 442-446, (2006)
- 33 T. Tanaka, M. Morigami, H. Oizumi and T. Ogawa, *Jpn. J. Appl. Phys.*, 32, 5813-4, (1993)
- 34 H.yung-Joo Lee, Jun-teak Park, Ji-yong Yoo, Ilsin An and Hye-Keun Oh, *Jpn. J. Appl. Phys.*, 42, 3922-3927, (2003)
- 35 A. Drechsler, N. Petong, C. Bellmann, P. Busch, M. Stamm, K. Grundke, O. Wunnicke and J. Reichelt, *J. Progr. Colloid Polym. Sci.*, 132, 82-94, (2006)
- 36 A. Drechsler, C. Bellmann, A. Synytska, N. Petong, K. Grundke, M. Stamm, J. Reichelt and O. Wunnicke, *J. Colloids and Surfaces A Physiochem. Eng.*, 311, 83-92, (2007)
- 37 M. Kotera, N. Ochiai, *J. Microelect. Eng.*, 78-79, 515-520, (2005)
- 38 M. P. Stoykovich, H. B. Cao, K. Yoshimoto, L. E. Ocola and P. F. Nealey, *J. Adv. Mater.*, 15, 1180-1184, (2003)
- 39 A. Kawai and Y. Kaneko, *Jpn. J. Appl. Phys.*, 39, 1426-9, (2000)

Chapter 2 - Analytical Study of the Pattern Collapse in Photolithography Process Using Modified Capillary Forces

2-1 Introduction

One of the problems during manufacturing of micro- and nano-features using photolithography is the collapse of features, colloquially called “pattern collapse”. Pattern collapse is the lasting deformation (any or combination of bending, breaking, tearing or peeling) of features due to unbalanced capillary forces. Pattern collapse is observed in photoresists and substrates. Photoresist collapse mostly happens in microprocessor manufacturing during drying the rinse liquid applied to wash the feature after the development step. Substrate collapse occurs in MEMS and NEMS fabrication process during drying the rinse liquid applied to wash the feature after the etching step. Factors affecting pattern collapse can be categorized into three groups: (i) pattern’s geometry, (ii) pattern’s material, and (iii) rinse liquid and its related capillary forces. Each of these three categories is represented by few parameters in a model (for example, pattern height can be one of the parameters regarding the pattern’s geometry category). A complete pattern deformation model should consider all parameters affecting the pattern deformation. A literature review is performed to find the to-date parameters used in pattern collapse models. As will be shown, the literature models lack two parameters. By including these two parameters a new (more accurate) model to simulate the pattern collapse will be developed.

To date, the basic geometrical parameter, affecting the pattern deformation, has been the pattern's aspect ratio (AR or H/w ; see Fig. 2-1 for definition of H and w). In this study a new geometrical parameter affecting the pattern collapse is defined as the longitudinal aspect ratio (LAR or L/d ; see Fig. 2-1). The need for defining LAR on pattern deformation analysis is shown under the rinse liquid and related capillary forces discussion.

The effect of pattern's material on the pattern deformation has been considered through (i) the interaction of the material and rinse liquid as manifested by contact angle (θ) and, (ii) the modulus of elasticity for the pattern's material (E). However, yield stress [1], adhesion to the substrate [2, 3 and 4], swelling probability [5] are other parameters which are not considered in this study and may be considered in future models for completeness.

Rinsing liquid and its related capillary forces have been studied, to date, by considering only Laplace pressure, ΔP , [1, 6, 7, 8, 9, 10, 11, 12, 13, 14, 15 and 16]. Laplace pressure is the pressure difference across the liquid-air interface, shown in Fig. 2-1, and is a function of rinse liquid surface tension (γ) and rinse interface curvature (Eq. 2-1):

$$\Delta P = \gamma \left(\frac{1}{R_1} + \frac{1}{R_2} \right) \quad (2-1)$$

where R_1 and R_2 are the principal radii of curvature at a point on the interface. To date, for pattern collapse studies the rinse liquid interface is modeled simply with a cylindrical shape, e.g. [1, 7, 8, 9 and 10]; as such, ΔP is described as:

$$\Delta P = \frac{2\gamma \cos\theta}{d} \quad (2-2)$$

Equation 2-2 reveals that Laplace pressure effect can be studied by changing the distance between two adjacent patterns (d , see Fig. 2-1), surface tension of the rinse liquid (γ) and the contact angle (θ). As will be shown, the validity of the cylindrical shape assumption for the rinse interface or validity of Eq. 2-2 depends on the value of LAR . This describes the reason of defining LAR as a new parameter.

In this study another contributor to capillary forces other than Laplace pressure will be introduced. The other capillary force that has been neglected is the surface tension force (STF) which is a concentrated force operating on the three-phase line. Three-phase line is where three bulk phases of solid, liquid and vapor meet. The STF is different from Laplace pressure and should be considered in the pattern collapse analysis. To clarify, consider a flat liquid-air interface where $\Delta P = 0$ (as R_1 and $R_2 \rightarrow \infty$), nonetheless, STF will still exert a force on the pattern (see Fig. 2-2b). For sessile drops on soft flat surfaces Extrand and Kumagai [17] showed that the STF is of such magnitude that it can deform the surface (in the shape of a ridge) at the three-phase line.

In the next sections, first based on literature models for pattern deformation, the effects of geometrical on pattern deformation will be discussed by changing pattern and rinse related parameters. Next, by including the two neglected parameters (LAR and STF) in the pattern deformation models a new model will be developed. Using the new pattern deformation model, adding cationic surfactant approach (see Chapter 1) will be tested to

find whether this approach is always useful *i.e.* whether increasing contact angle by 10 degrees always decreases the pattern deformation.

Literature models have shown that manufacturing of denser features results in a higher AR value, and a higher possibility of collapse, *e.g.* [7]. In most cases, pattern's geometry is dictated by the design limitation. As such, studying pattern's geometry will guide one to determine if for a given geometry there is a need to change other factors such as the rinse liquid or the pattern's material and resolve the pattern collapse.

Based on literature models, a proper material to decrease the pattern deformation is the one with a large modulus of elasticity and contact angle. However, a material with combination of large modulus of elasticity and high contact angle with the ease of process implementation is not readily available or economical [1, 7, 8, 9 and 10]. Instead of changing the pattern's material, one may change the characteristic of the existing pattern. Increasing the contact angle will be studied in the next section. For increasing the stiffness of patterns the following strategies have been used: heating during rinsing, adding nano-particles to form nano-composites [18], flood exposing the patterns [19], using sidewall profiles [20, 21] and buttressed zone plates [22]. Application of the above methods may not be economical for mass production.

Based on literature models, selection of a rinse liquid with a small surface tension and large contact angle, to lower the capillary force, seems useful (d is a fixed design factor). Jincao *et al.* [11] used a rinse liquid with low surface tension to decrease the Laplace

pressure and obtained high ARs without collapse but their experiments had its own limitations (see Chapter 1). Supercritical [12, 13, 23, 24, 25, 26 and 27] and freeze dryings [28] are processes with none or very low surface tension effects, but are costly and have process limitations. Adding surfactant at concentrations near the critical micelle concentration (CMC) is another way of decreasing surface tension to improve pattern collapse [14, 15 and 16]. At these concentrations surface tension is lowered significantly however, some surfactants interact with patterns and melt or cause them to dissolve. Cationic surfactants increase the contact angle with a slight change of surface tension [29]. As will be shown, increasing the contact angle is desired for decreasing the Laplace pressure. Based on literature models for predicting pattern deformation, adding cationic surfactants seems the most proper method for resolving the pattern collapse. This method is easy to apply and proper for mass production. However, as will be discussed later the newly developed model shows that adding cationic surfactants may have an adverse effect on pattern collapse in some cases.

In this study contact angle is assumed constant and equal to the equilibrium contact angle. However, during drying of the rinse liquid, the level of rinse interface in the space between two patterns recedes and receding contact angle [30] (which may not be equal to the equilibrium contact angle) may be a more relevant factor.

In summary, two added parameters in the new model compared to literature models are: (i) STF the second contributor in capillary forces responsible for pattern collapse and (ii)

LAR which defines the region of validity of the cylindrical meniscus assumption (or Eq. 2-2).

The first part of this chapter deals with the effect of adding STF to analyze pattern collapse. A beam bending model will be developed to calculate the pattern deformation for a specific case of a two-line parallel pattern. In the second part, Surface Evolver [31] is applied to find the accuracy of the cylindrical interface model (CIM) for calculating Laplace pressure. LAR is defined as a parameter to show the accuracy and limits for applicability of CIM. It is needed as where interface shape is not cylindrical deformation results from the new model are invalid. In each of the two sections, effects of changing pattern's material, pattern's geometry, and rinse liquid on pattern collapse will be studied.

2-2 Pattern Collapse Modeling

Patterns are assumed as two-line parallel patterns which the space between them is filled with the rinse liquid. To represent the worst case scenario, it is assumed that the described system is surrounded by a gas phase and there is no rinse liquid outside the two-line parallel pattern. Patterns are also modeled as simple clamped cantilever beams and beam sway model of Deguchi *et al.* [32] is applied for pattern deformation analysis (see Fig. 2-3). At this stage cylindrical shape is assumed for the rinse interface shape (similar to other literature e.g. [7]). The next section defines the collapse criterion used in this study.

Lasting deformation is basically the definition of pattern collapse and occurs in two cases: (i) patterns (partly or completely) undergo the plastic deformation (ii) elastic deformation causes sticking of tips of adjacent patterns (elastic deformation before sticking of pattern tips is not generally problematic). For the following reason, in case of studying the collapse of photoresist patterns, the second case is more expected. Complete removal of the residue photoresist from the substrate after acid etching requires weaker bonding between photoresist and substrate (adhesion) compared to the bonding within the photoresist (cohesion). Furthermore, the maximum stress on the photoresist occurs at its base where adhesion force is operative [7]. As a result, in most of the cases, photoresist will be peeled off from the substrate before the base experiences plastic deformation. Therefore, simply here plastic analysis is not performed.

The deformation mechanism of pattern is studied by comparing cohesive and restoring forces (first used by Tanaka *et al.* [7], but consideration of the STF was missing in their model). Simple example of cohesive and restoring forces is a spring being stretched. Cohesive force is the force exerted on the spring and restoring force is its resistance force against stretching. At the equilibrium state both restoring and cohesive forces are equal.

Cohesive force in case of pattern collapse problem is composed of the Laplace pressure (ΔP) and horizontal projection of STF (F_x). By increasing the pattern deformation, ΔP increases and F_x remains almost unchanged. In elastic region, restoring force linearly increases with deformation. At the equilibrium, cohesive and restoring forces cancel each

other. As such, the deformation can be calculated by mathematically setting the cohesive and restoring forces equal to each other.

2-3 Pattern Deformation Model Including STF

The STF can be understood by considering the Young equation (Eq. 2-3) at the three-phase line.

$$\gamma_{SL} - \gamma_{SV} = \gamma_{LV} \cos \theta \quad (2-3)$$

where γ_{SL} , γ_{SV} and γ_{LV} are surface tensions of solid-liquid, solid-vapor and liquid-vapor interfaces, respectively. Considering Fig. 2-2a and Eq. 2-3, the horizontal force resulting from the normal projection of surface tension of the liquid-vapor to the pattern's side wall, acts as a concentrated force along the three-phase line.

The STF is not considered in previous studies and a new term, STF deformation (δ_2), should be added to deformation due to Laplace pressure (δ_1). Also, as will be shown considering the STF causes an indirect increase in Laplace pressure deformation considering Tanaka's model [7], and δ_1 from Tanaka's model needs to be recalculated.

An example is given to show the need for considering the effect of the STF on pattern deformation. For studying pattern collapse problem, Jung *et al.* [15] prepared different pattern dimensions (all line and space shape patterns). They filled the patterns' troughs with water and changed the contact angles and surface tensions by adding different surfactants to the water. In Table 2-1 pressure differences across the rinse liquid interface (Laplace pressure) for three of their solutions are shown. It is observed that Laplace

pressure is higher when liquid is solution-A (compared to solutions B and C). So, based on Tanaka's model, which only considers the Laplace pressure as the cohesive force, maximum deformation should occur in presence of solution-A. The horizontal projection of STF for three different solutions using contact angle and surface tension values in [15] are also shown in Table 2-1. It was observed that the horizontal projection of the STF is very small for solution-A (compared to solutions B and C). From Jung *et al.* [15] experiment, it was observed that the lowest pattern deformation happens in presence of solution-A (compared to solutions B and C) unlike as predicted by model in [7]. This can point to the importance of the effect of STF on pattern deformation.

Regarding Table 2-1, it should be noted that Laplace pressures are normalized by dividing them to Laplace pressures if the rinse liquid was DI-water (because trough width data are missing in [15]). Horizontal projections of the STFs are also normalized by dividing them to the STF if the rinse liquid was DI-water for the same pattern geometry. In the next sections the analytical model for calculations of δ_1 and δ_2 are described.

2-3.1 Analytical Model for Calculation of δ_2

Since the slope of the feature hardly changes as a result of pattern deformation, the cohesive force due to STF (F_x) remains almost constant as:

$$F_x = \gamma L \sin \theta \quad (2-4)$$

Restoring force of a pattern (modeled as a beam) due to any concentrated force (CF) as a function of deformation (δ_{CF}) is [33]:

$$CF = \frac{3\delta_{CF}EI}{H^3} \quad (2-5)$$

where I is the moment of inertia for cross sectional area of the beam/pattern, and is:

$$I = \frac{Lw^3}{12} \quad (2-6)$$

By comparing Eq. 2-4 with Eq. 2-5, deformation due to the STF is calculated as (note that δ_{CF} is replaced by δ_2):

$$\delta_2 = \frac{4\gamma H^3 \sin \theta}{Ew^3} \quad (2-7)$$

To elucidate the importance of STF in the pattern deformation model, consider a simple case of a flat interface introduced in the Introduction. Literatures suggest that collapse would never occur since deformation due to the Laplace pressure (δ_1) is always zero.

However, considering Eq. 2-7, definition of AR ($= \frac{H}{w}$), and the fact that if half of the d value is reached then pattern is considered collapsed (tips of two patterns/beams touch), one can derive Eq. 2-8 to find the maximum AR value for which, if exceeded, collapse will occur.

$$AR = \sqrt[3]{\frac{Ed}{8\gamma \sin \theta}} \quad (2-8)$$

For example, for values of E , d , γ and θ of 4GPa, 65nm, 72mN/m and 60 degrees, respectively, if the AR value becomes greater than 8, pattern will collapse.

2-3.2 Analytical Model for Calculation of δ_1

Considering STF (F_x) in addition to directly changing the total deformation by δ_2 , also indirectly changes the δ_1 through changing the Laplace pressure value. The mechanism is as follows: δ_2 increases the curvature of an already curved interface, and consequently the Laplace pressure, ΔP , will increase (see Eq. 2-9). The ΔP increase, increases the δ_1 . As such, the literature formulation for finding δ_1 (e.g. [7]) needs modifications to account for the indirect effect of STF.

Radii of curvature, in CIM model, by considering the total pattern deformation, δ_T ($= \delta_1 + \delta_2$), are found as:

$$R_1 = \frac{d - 2\delta_T}{2 \cos(\theta - \phi_T)}, R_2 = \infty \quad (2-9)$$

where ϕ_T is the slope of the pattern at the three-phase line (see Fig. 2-3). Laplace pressure (cause of the cohesive force) can be found from Eqs. 2-1 and 2-9 as:

$$\Delta P = \frac{2\gamma \cos(\theta - \phi_T)}{d - 2\delta_T} \quad (2-10)$$

Restoring pressure (conceptually is restoring force but to make the comparison easy and with uniform units, restoring force is divided by the pattern area) of a beam due to any capillary pressure (CP) related to the deformation (δ_{CP}) is [33]:

$$CP = \frac{8EI\delta_{CP}}{LH^4} \quad (2-11)$$

Equations 2-10 and 2-11 should be set equal to one another to find δ_1 (deformation due to Laplace pressure). Therefore the steps in derivation of the model from Tanaka *et al.* [7]

and current one have been similar. However, in the next step, Tanaka's model neglected the effect of the STF on δ_1 (i.e. $\delta_T \approx \delta_1$ and $\phi_T \approx \phi_1$), and used the small deformation assumption (i.e. $\sin \phi \approx \tan \phi \approx \frac{4\delta}{3H}$). As will be shown, the effect of the STF on δ_1 is significant and must therefore be considered. For the cases examined in this study, relaxation of small deformation assumption resulted in a negligible change (less than 1%) in deformation values (see Appendix C). However, for finding a general relation, in this study small deformation assumption is relaxed. The relation for finding the δ_1 is found as (see Appendix D for derivation details):

$$\frac{\gamma \sqrt{\frac{1}{\left(\left(\frac{3\delta_2}{2H}\right)^2 + 1\right)\left(\left(\frac{4\delta_1}{3H}\right)^2 + 1\right)}} \left\{ \cos \theta \left(1 - \frac{4\delta_1}{3H} \times \frac{3\delta_2}{2H}\right) + \sin \theta \left(\frac{3\delta_2}{2H} + \frac{4\delta_1}{3H}\right) \right\}}{(d - 2(\delta_1 + \delta_2))} = \frac{Ew^3}{3H^4} \delta_1 \quad (2-12)$$

Due to its implicit nature, Eq. 2-12 should be solved numerically in conjunction with Eq. 2-7 for δ_2 , to find δ_1 . Figure 2-4 shows cohesive (LHS of Eq. 2-12) and restoring (RHS of Eq. 2-12) pressures on a pattern versus δ_1 . Depending on pattern geometries, pattern materials, and rinse liquids, cohesive and restoring pressure curves may intersect. If cohesive and restoring pressure curves did not intersect it means that the cohesive force is always higher than the restoring force, and collapse will occur. Even where cohesive and restoring pressure curves met, the intersection point does not guarantee that collapse has not occurred as δ_T should always be less than the half pitch, i.e. $\delta_T \leq \frac{d}{2}$ (pattern tips touching).

To demonstrate the effect of the STF on Laplace pressure deformation (δ_1) consider the following example. In Fig. 2-4 cohesive forces due to the Laplace pressure are calculated by (i) Tanaka's model and (ii) current model for δ_1 (small deformation assumption is relaxed and effect of the STF on δ_1 is considered). It is observed that for the specific case presented in Fig. 2-4, Tanaka's model predicts $\delta_1 \approx 32nm$, whereas the current model predicts collapse (cohesive and restoring pressure curves do not intersect). Note that the deformation values in this section and Fig. 2-4 are δ_1 (i.e. deformation caused by Laplace pressure) not δ_T .

During pattern deformation, Laplace pressure and horizontal projection of STF rotate as they remain perpendicular to the pattern. The current analytical beam bending model is unable to consider the force rotation. A Finite Element model is developed in Chapter 3 to calculate the deformation by considering the force rotations. It should also be mentioned that in this study the effect of evaporation on rinse during collapse and receding contact angle discussion are neglected.

By knowing the values for δ_1 (above section) and δ_2 (section 2-3.1), and using superposition principle (superposition principle is valid in elastic region), total deformation (δ_T) of patterns is calculated as the summation of Laplace pressure deformation (δ_1), and STF deformation (δ_2), i.e. $\delta_T = \delta_1 + \delta_2$ (see Fig. 2-3). Results from the developed analytical model are shown in the next section.

2-4 Results From the New Analytical Pattern Deformation Model

From the pattern deformation model with inclusion of the STF, for the cases studied, it is found that for large surface tension (γ), small trough width (d), see Table 2-2, and small elasticity modulus (E), see Table 2-3, pattern deformation increases. Also, by decreasing the pattern height (H) or increasing the pattern width (w), pattern deformation decreases. To meet technological needs (*i.e.* feature size decrease) and keep the AR value constant for proper etching process, pattern width and height should decrease at the same rate. By decreasing the pattern height and width at the same rate (*i.e.* constant AR) for a fixed d pattern deformation decreases (see Fig. 2-5). So, at constant AR and d , the pattern with larger dimensions is more susceptible to collapse (see Table 2-4). However, in most of the cases d is equal to w *i.e.* 1:1 line and space patterns. It is found that decrease of w , d and H at the same rate increases the pattern deformation (see Table 2-5). As such, for 1:1 line and space patterns by shrinking the pattern size maintaining the desired AR becomes challenging.

For the studied cases, for small AR values (see Table 2-6), large contact angles (see Table 2-7), large trough widths (see Table 2-2) and large elastic modulus (see Table 2-3) the error of using Tanaka's model increases, *i.e.* error relative to the new analytical model. It should be mentioned that Tables 2-2 to 2-6 are for $\theta = 45^\circ$, however for $\theta = 5^\circ$ and 85° similar trends for the results were observed.

Literature models, *e.g.* Tanaka's model [7], predicted that by increasing the contact angle pattern deformation decreases. The new analytical model with inclusion of the STF

shows that increase of contact angle in some ranges may increase the pattern deformation and/or cause collapse (see Fig. 2-6). This is important as strategies for decreasing the pattern deformation and avoiding pattern collapse such as adding cationic surfactants may cause a worsening of the pattern collapse. Note that cationic surfactants adsorb to the photoresist surface and increase the contact angle in the order of 10 degrees without significant change of the liquid surface tension [29].

2-5 Non-Cylindrical Rinse Interface Shapes

The purpose of this section is to show the shortcomings of using a cylindrical interface model (CIM). To date CIM is used for calculating interface curvature (consequently ΔP) and predicting pattern collapse. In this section limitations of application of CIM will be presented. As will be shown later, LAR will be used as the primary parameter to quantify the limitation of the CIM.

To investigate the appropriateness of CIM and determine the limits of its applicability, in general, Surface Evolver (SE) is applied. Surface Evolver is a Finite Element based software for calculating the equilibrium shape of interfaces based on total energy (E) minimization for defined surface tensions, interface areas and constraints [31]. Minimization of total energy (E) to find the equilibrium state is done by conjugate gradient method. Knowing that rinse-pattern interface area change is equal to that of air-pattern (*i.e.* $\Delta A_{SV} = -\Delta A_{SL}$) and using Eq. 2-3, energy change (ΔE) as a result of small variation in the system's state can be formulated as:

$$\Delta E = \gamma_{LV}(\Delta A_{LV} - \cos \theta \times \Delta A_{SL}) \quad (2-13)$$

According to Eq. 2-13, initial geometry and θ should be defined as inputs for SE [34] (effect of γ_{LV} is considered in θ). For a given liquid, minimization of ΔE is equivalent to minimizing the value inside the parentheses. At the equilibrium both ΔE and the value inside the parentheses would be zero.

As seen in Fig. 2-7 using SE, curvature values are found for different initial liquid height (ILH) values. ILH is the interface height before initiating minimization or the average interface height, and is an indication of rinse liquid volume (see Fig. 2-7). Volume is a factor to consider as for a very large, and a very small liquid volume, interface shape is influenced by liquid overfilling, and the bottom surface (split the single air-liquid interface into two separate air-liquid interfaces), respectively. To avoid complexities that are out of the scope of this study, very large and small liquid volume cases will not be discussed. As such, moderate ILH values will be used in the rest of our analysis. It should also be mentioned that CIM cannot describe overfill and underfill cases.

Deformation due to Laplace pressure is function of both pressure and area on which Laplace pressure is exerted. The worst case scenario in studying pattern collapse is the condition at which combined pressure and exposed area reach the maximum values. Area exposed to Laplace pressure is limited to area beneath the three-phase line. It can be shown that by increasing ILH from zero to overfill values (i) area exposed to Laplace pressure increases till the three-phase line reaches the pattern edge, then area remains at its maximum possible value which is equal to pattern surface area (ii) Laplace pressure (or curvature value) is constant in a wide region of ILH then starts to decrease for very

large ILH values (see Fig. 2-7). It is observed that for the cases studied in this chapter at the ILH value that Laplace pressure starts to decrease three-phase line is located on the upper edge of the pattern. So the worst case scenario is where exposed area is the entire pattern surface and pressure is equal to its value at the moderate ILH (see Fig. 2-7). It should also be noted that where LAR is very large ($LAR \rightarrow \infty$) pressure at the moderate ILH is equal to CIM pressure (see Fig. 2-7).

In the remainder of this section curvature values will be studied for liquid interface inside two-line parallel and box-shaped patterns using SE and compared with CIM results. A box-shaped geometry has four sides, where a two-line parallel has two walls with open ends. The general shape of rinse interface inside two-line parallel and box-shaped patterns are shown in Fig. 2-8. It should be mentioned that for both cases where pattern length is very large ($L \rightarrow \infty$) the effect of the ends (open or closed) on the interface shape become negligible and interface shape become cylindrical (Fig. 2-8a).

2-5.1 Rinse Interface inside Two-Line Parallel and Box-Shaped Patterns

At finite pattern length values, the interface shape deviates from cylindrical. Using SE, it is found that non-cylindrical interfaces can have curvature values different from CIM curvatures (curvature from CIM remains constant for any L). Beam bending model uses CIM for calculating pattern deformation. So, in the cases that curvature value (and Laplace pressure consequently) from SE is not close to that from CIM, pattern deformation results found from beam bending model are invalid. Note that this is regardless of inclusion or exclusion of STF.

Comparison of SE and CIM curvature values reveals the error in using CIM. This error can quantify the region of validity of beam bending model for finding the pattern deformation. Comparison of SE and CIM curvature values can be done for different contact angle (θ), pattern trough width (d) and pattern length (L). But two of the above three variables (L and d) are combined into a new variable (LAR); because by knowing the value of LAR , independent of d or L the error of using CIM can be defined (see Appendix E).

For the prevalent range of contact angles, i.e. $\theta < 60^\circ$, for both two-line parallel and box-shaped patterns, the error in using CIM compared to SE is almost independent of θ (see Fig. 2-9a). However, for the case of two-line parallel pattern where θ becomes larger than 60° (which rarely happens) the error in using CIM becomes sensitive to θ as well (see Fig. 2-9a). Therefore, in the prevalent range of contact angle for both two-line parallel and box-shaped patterns the error in using CIM compared to SE only depends on LAR value.

For both two-line parallel and box-shaped patterns, the error in using CIM increases by decreasing the LAR value (Fig. 2-9b and Table 2-8). For example, for LAR values smaller than 10 the error of using CIM for calculating Laplace pressure value is larger than 10 percent and increases for further decreasing of LAR value. It should be noted that in some cases only a few percent error in curvature value may lead to incorrect prediction of pattern deformation or collapse. However, in some other cases even 10 percent error is tolerable. Nevertheless, it is suggested that where LAR value is larger than 20, which

means that the error of using CIM to calculate the curvature value is less than 5%, considering the fact that applying CIM to calculate the curvature value is easier than SE, one may apply CIM to calculate the curvature value. Therefore, beam bending results are valid where LAR value is larger than 20. It is highly recommended that for LAR values smaller than 20 curvature of the interface should be calculated from SE model. For the cases that LAR is smaller than 20, Finite Element model discussed in Chapter 3 should be applied to find the pattern deformation (as beam bending results are invalid).

2-5.2 Results From Non-cylindrical Rinse Interface Shape

From SE it is found that in general for two-line parallel patterns, CIM provides larger curvature values (compared to SE) and consequently larger Laplace pressure values (*e.g.* see Fig. 2-10a). So, for a two-line parallel pattern, beam bending model overestimates the pattern deformation. For box-shaped patterns, CIM provides smaller curvature and consequently Laplace pressure values compared to SE (see Fig.2-10b). So, for box-shaped patterns, CIM underestimates the deformation. It should be noted regardless of the value of LAR a box-shaped pattern cannot be modeled as a beam and beam bending model results are invalid for this case. Instead, Finite Element model should be used to find the pattern deformation (the point is addressed in Chapter 3).

It is found that for both two-line parallel and box-shaped patterns, by increasing θ and d , same as for CIM, curvature values and consequently Laplace pressure from SE decrease (*e.g.* Fig. 2-11). Increase of d does not affect the horizontal projection of STF but increase of θ changes the horizontal projection of STF. So, increasing d always

decreases the deformation but for the effect of increasing θ on pattern deformation, each specific case needs to be analyzed.

2-6 Conclusions

Unbalanced capillary force is the main cause of pattern collapse. Laplace pressure is not the only major contributor to the capillary force as it was thought to date. Surface tension force (STF) on three-phase line needs to be considered for an accurate analysis. Based on adding the effect of surface tension force on pattern deformation, a new analytical (beam bending model) is developed for predicting the pattern deformation for a two-line parallel pattern. Based on the new model for large ARs , contact angles (θ), trough widths (d) and small elasticity modulus (E) the importance of considering STF increases. Without considering STF literature models suggested that addition of cationic surfactants to the rinse liquid, resulting in increasing the contact angle, is a proper approach to resolve the collapse problem. However, by considering STF it was found that increasing the contact angle may increase the pattern deformation and worsen the collapse situation.

To date, pattern collapse studies are based on cylindrical shape assumption for the rinse liquid-air interface. Interface curvature value determines the Laplace pressure. Analytical beam bending in this study also uses cylindrical shape assumption for the rinse liquid interface. Cylindrical shape assumption and application of the new beam bending model is valid for very long patterns where end edge effect is negligible. However, the term very long was undefined in literature. In this study, Surface Evolver as an alternative method to find the rinse interface curvature value was applied. Curvature values from

CIM are compared to those from SE at different pattern lengths, trough widths and contact angles. It was found that the error of calculating curvature using CIM is mainly a function of LAR (L/d). For LAR values larger than 20, CIM is accurate enough for developed beam bending model to predict valid deformation results.

From SE results it is found that three-phase line shape and curvature value are functions of rinse liquid volume. The largest pattern deformation occurs at a volume where three-phase line is straight line, area exposed to Laplace pressure is the entire pattern surface, and curvature value is the curvature before decreasing due to the overfilling effect.

Based on calculated Laplace pressures, CIM overestimates the deformation value for two-line parallel patterns and underestimates the deformation value for box-shaped patterns. Regardless of the value of LAR beam bending model is unable to provide the deformation value for closed end patterns.

Tables

Table 2-1 Surface tensions and contact angles of surfactant solutions in Jung *et al.* [15] experiment are presented. Two contributors in capillary force (*i.e.* STF on three phase line and Laplace pressure) are normalized with respect to the values for water, *i.e.* ΔP_{water} and $F_x(water)$.

Surfactant Solution	Surface tension (mN/m)	Contact angle (degree)	$\frac{\Delta P}{\Delta P_{water}}$ (%)	$\frac{F_x}{F_x(water)}$ (%)
A	22	12.5	96	7
B	20	54.7	52	24
C	21	53.5	56	25

Table 2-2 Deformation at three different trough widths values is presented with and without considering surface tension force ($H=250nm$, $E=5Gpa$, $\theta = 45^\circ$, $AR=4$ and $\gamma = 72mN / m$).

$d(nm)$	δ (nm) Tanaka's model	δ_T (nm) new model	Error $\left \frac{\delta_T - \delta}{\delta_T} \right $ (%)
70	10.6	13.2	19.7
104	5.4	8	32.5
150	3.5	6.1	42.6

Table 2-3 Deformation for three different elasticity modulus values is presented with and without considering surface tension force ($H=250nm$, $d=104nm$, $\theta = 45^\circ$, $AR=4.5$ and $\gamma = 72mN / m$).

$E(GPa)$	δ (nm) Tanaka's model	δ_T (nm) new model	Error $\left \frac{\delta_T - \delta}{\delta_T} \right $ (%)
3	20.2	26.4	23.4
4	11.3	16	29.3
5	8.3	12	30.8

Table 2-4 Deformation with and without considering surface tension force at three different pattern widths is presented ($AR=3$, $\gamma = 72mN / m$, $d=100nm$, $E=4Gp$ and $\theta = 45^\circ$).

$w(nm)$	δ (nm) Tanaka's model	δ_T (nm) new model	Error $\left \frac{\delta_T - \delta}{\delta_T} \right $ (%)
50	1.6	2.9	44.8
100	3.3	4.9	32.6
150	5.3	6.8	22

Table 2-5 Deformation with and without considering STF at three different pattern

widths is presented ($AR=3$, $\gamma = 72mN / m$, $E=4Gpa$, $\theta = 45^\circ$ and $d=w$).

$W(nm)$	δ (nm) Tanaka's model	δ_T (nm) new model	Error $\left \frac{\delta_T - \delta}{\delta_T} \right $ (%)
50	3.7	5.5	32.7
100	3.3	4.9	32.6
150	3.2	4.7	31.9

Table 2-6 Deformation with and without considering STF at three different ARs is

presented ($H=250nm$, $d=104nm$, $E=5Gpa$, $\theta = 45^\circ$ and $\gamma = 72mN / m$).

AR	δ (nm) Tanaka's model	δ_T (nm) new model	Error $\left \frac{\delta_T - \delta}{\delta_T} \right $ (%)
4	5.4	8	48
4.5	8.3	12	45
5	13.1	18.2	39

Table 2-7 Deformation with and without considering surface tension force at three different contact angles is presented ($H=250nm$, $d=104nm$, $E=5Gpa$, $AR=4.5$ and $\gamma = 72mN / m$).

θ	δ (nm) Tanaka's model	δ_T (nm) new model	Error $\left \frac{\delta_T - \delta}{\delta_T} \right $ (%)
5	12.5	12.9	4
45	8.3	12	45
85	0.9	6.1	591

Table 2-8 Effect of increasing contact angle and *LAR* on curvature for two-line parallel and box-shaped patterns is summarized. Curvature is calculated form SE.

Pattern Shape	Increasing θ		Increasing <i>LAR</i>	
	Curvature and ΔP	<i>Error</i> of using CIM	Curvature and ΔP	<i>Error</i> of using CIM
Two-line parallel (open-ends)	Decreases	For $\theta < 60^\circ$ unchanged	Increases	Decreases
Box-shaped (close-ends)	Decreases	For all case of θ unchanged	Decreases	Decreases

Figures

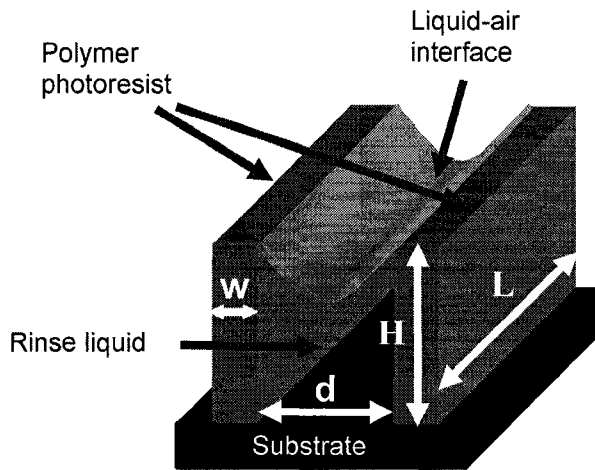


Figure 2-1 Schematic of an isolated two-line parallel pattern, and rinse liquid interface with surrounding air.

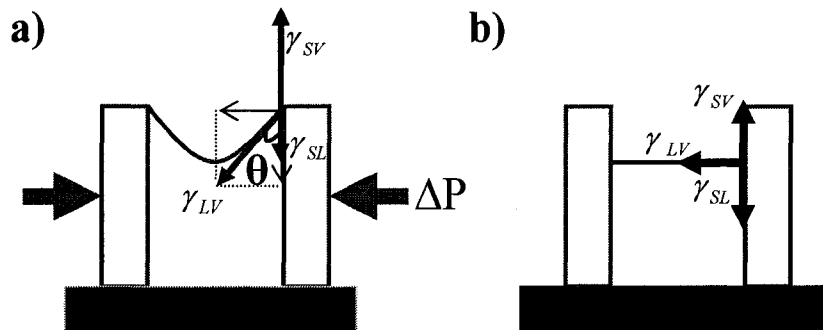


Figure 2-2 (a) Surface tension forces at three phase line are shown. Horizontal projection of liquid-vapor phase surface tension (γ_{LV}) exerts a force on the pattern's side wall. (b) Case of a flat interface ($\Delta P = 0$) where γ_{LV} exerts a force on the pattern's side wall.

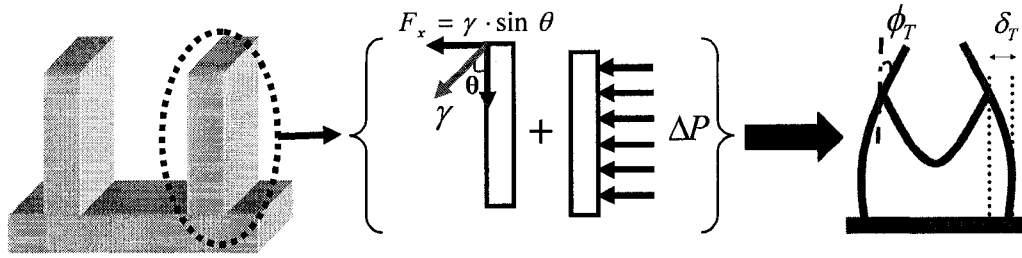


Figure 2-3 Schematic of a beam sway model and additive nature of the STF and Laplace pressure on the pattern. Superposition assumptions are: (i) loads remains horizontal, (ii) elastic deformation (maximum stress is less than yield stress), and (iii) deformation with respect to height is very small [32].

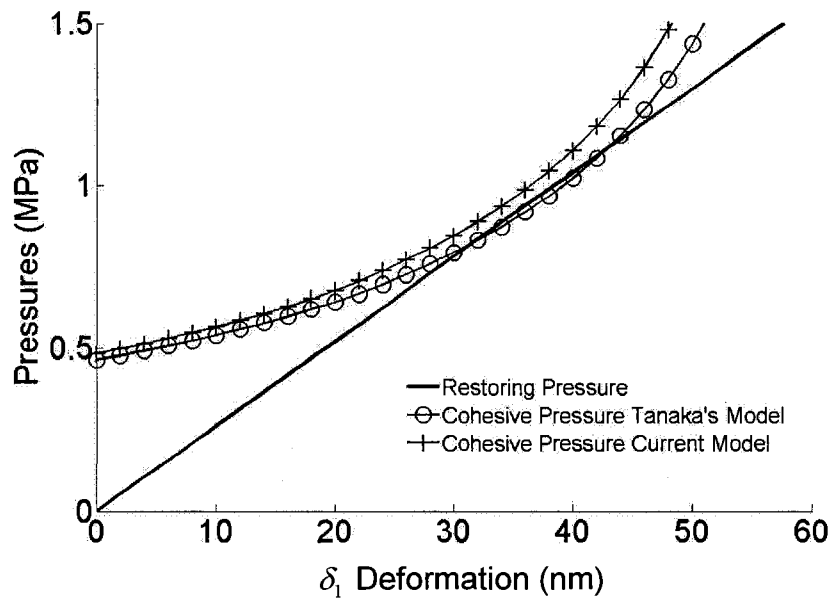


Figure 2-4 Comparing restoring and cohesive pressures due to Laplace pressure by: (i) Tanaka's model, and (ii) current model for δ_1 which considers the effect of STF on Laplace pressure deformation ($AR=6$, $H=350\text{nm}$, $d=150\text{nm}$, $\theta=15^\circ$, $E=5.9\text{GPa}$ and $\gamma=72\text{mN/m}$). Despite Tanaka's model, just by considering δ_1 the new model predicts collapse.

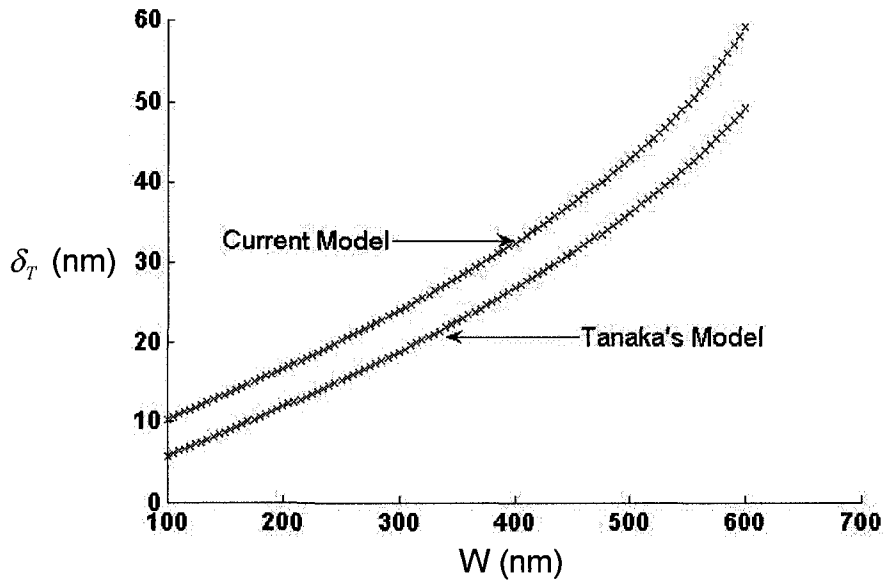


Figure 2-5 At constant AR , pattern deformation increases by increasing w and consequently $H (= AR \times w)$ using both the current model for δ_1 and Tanaka's model ($d=300\text{nm}$, $AR=5$, $E=5.9\text{GPa}$, $\theta = 15^\circ$ and $\gamma = 72\text{mN/m}$).

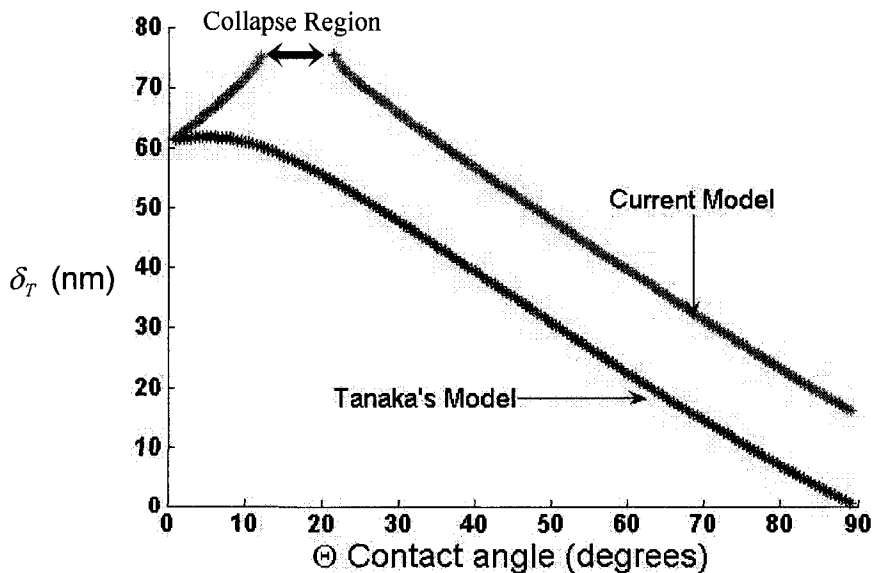


Figure 2-6 The effect of considering STF in predicting deformation value and collapse of features is shown at different contact angles ($H=1000\text{nm}$, $d=300\text{nm}$, $AR=6.67$, $E=5.9\text{GPa}$ and $\gamma = 72\text{mN/m}$).

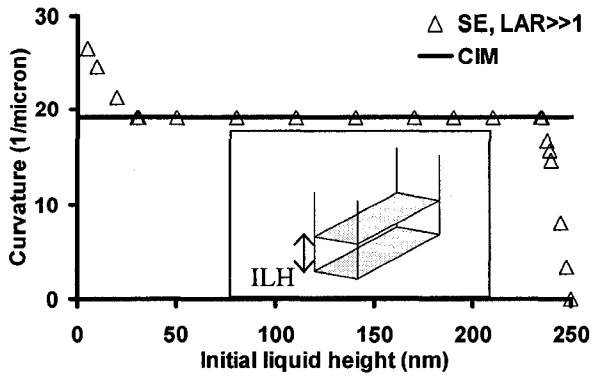


Figure 2-7 Surface Evolver ($LAR \gg 1$) and CIM curvature values are compared at different ILH values ($H=250$ nm, $d=104$ nm, $\theta = 5^\circ$ and water inside a two-line parallel pattern). Overfilling and under filling effects on the interface curvature values are noticeable in SE results.

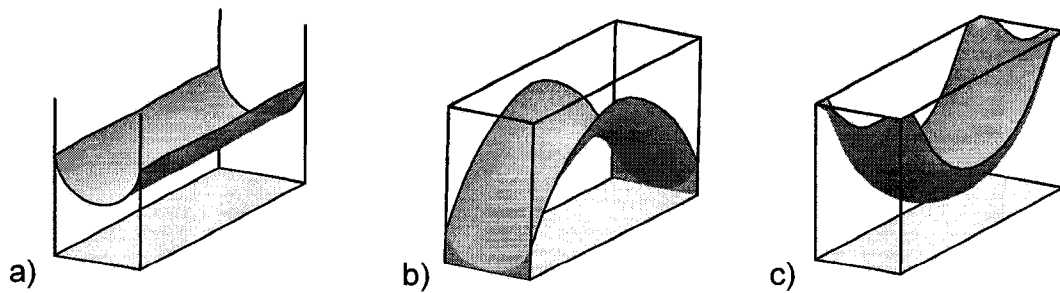


Figure 2-8 Schematic of: (a) cylindrical rinse interface shape for a pattern with very large length ($LAR \gg 1$), (b) rinse interface shape for a case where rinse is between a two-line parallel pattern with small length ($LAR = 5$), and (c) rinse interface shape for a case where rinse is surrounded in a box-shaped pattern with small length ($LAR = 5$). Interface shapes are derived using Surface Evolver.

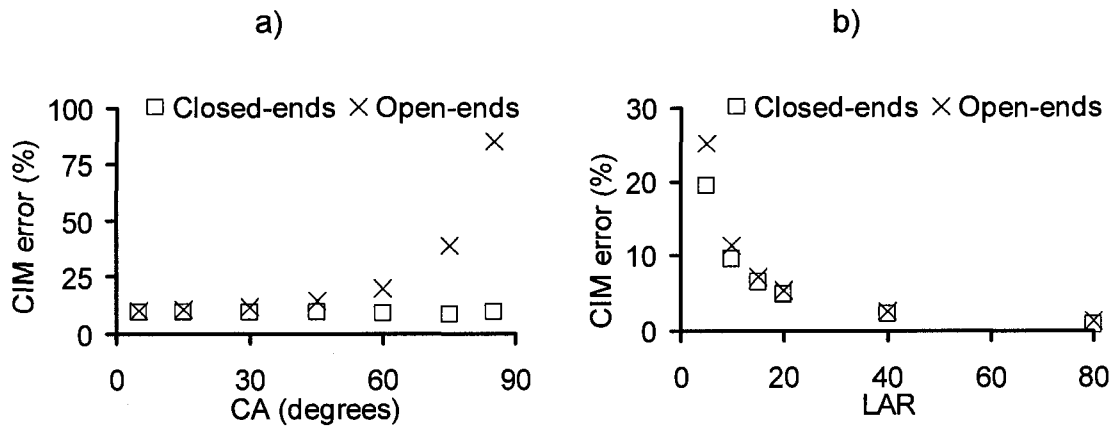


Figure 2-9 Error of using CIM to find interface curvature values, compared to curvature values from SE at (a) different θ values with $LAR=10$, and (b) different LAR values; for two-line parallel (open-ends) and box-shaped (close-ends) patterns ($\theta = 5^\circ$, $H=250$ nm, $ILH=110$ nm and $d=104$ nm).

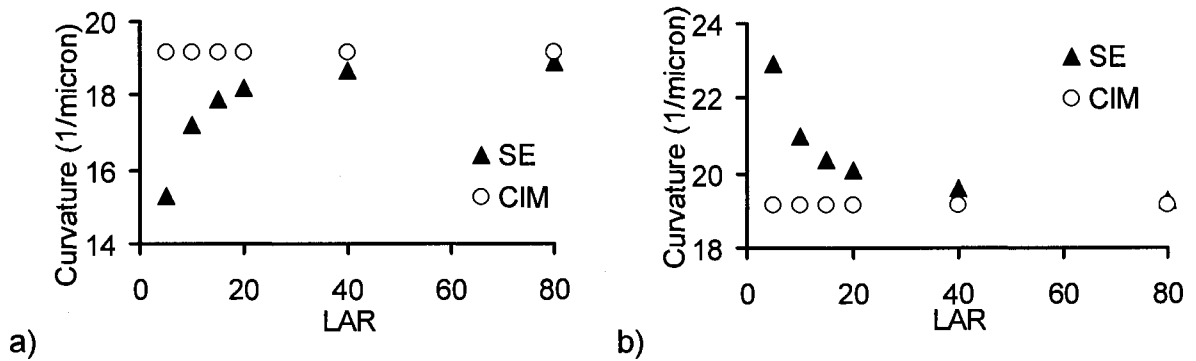


Figure 2-10 SE and CIM curvature values at different LAR values for (a) two-line parallel, and (b) box-shaped patterns ($H=250$ nm, $ILH=110$ nm, $d=104$ nm and $\theta = 5^\circ$).

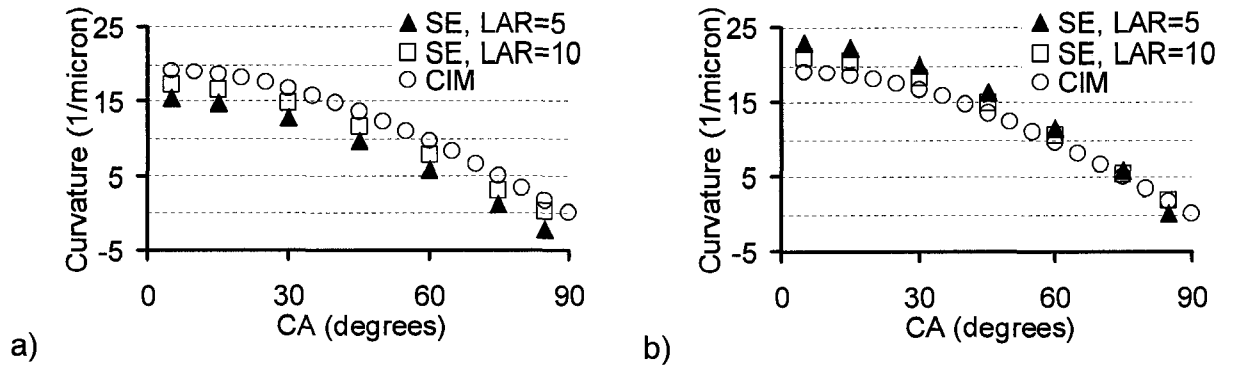


Figure 2-11 SE and CIM curvature values at different contact angles for (a) two-line parallel, and (b) box-shaped patterns are shown ($ILH=110\text{nm}$, $AR=5$, $H=250\text{ nm}$ and $d=104\text{ nm}$). Negative curvature value means that interface curvature is convex and deformation due to the pressure is in outward direction.

References

- 1 K. Yoshimoto, M. P. Stoykovich, H. B. Cao, J. J. de Pablo, P. F. Nealey and W. J. Drugan, *J. Appl. Phys.*, 64, 1857-1865 (2004)
- 2 M. Sanada, O. Tamada, A. Ishikawa and A. Kawai, *Proc. SPIE Conf. on Advances in Resist Technology and Processing XXII*, Bellingham, WA, USA (2005)
- 3 S-K Kim, M-H Jung, H-W Kim, S-G Woo and H. Lee, *J. Nanotech.*, 16, 2227-2232, (2005)
- 4 A. Kawai, *Proc. SPIE Conf. on Metrology, Inspection and Process Control for Microlithography XIII*, Santa Clara, CA, USA (1999)
- 5 S-K Kim, *J. Korean Phys. Soc.*, 42, S371-S375, (2003)
- 6 Y. Yamashita, *Jpn. J. Appl. Phys.*, 35, 2385-2386, (1996)
- 7 T. Tanaka, M. Morigami and N. Atoda, *Jpn. J. Appl. Phys.*, 32, 6059-6064, (1993)
- 8 H. B. Cao and P. F. Nealey, *J. Vac. Sci. Technol. B*, 18, 3303-3307, (2000)
- 9 M. Kortera and N. Ochiai, *J. Microelect. Eng.*, 78-79, 515-520, (2005)
- 10 H-J Lee, J-t Park, J-y Yoo, I. An and H-K Oh, *Jpn. J. Appl. Phys.*, 42, 3922-3927, (2003)
- 11 Y. Jincao, M. A. Matthews and C. H. Darwin, *Ind. Eng. Chem. Res.*, 40, 5858-5860, (2001)
- 12 H. Namutsu, *J. Vac. Sci. Technol. B*, 19, 2709-2712, (2001)
- 13 H. Namatsu, K. Yamazaki, K. Kurihara, *J. Microelect. Eng.*, 46, 129-132, (1999)
- 14 I. Junarsa, M. P. Stoykovich, K. Yoshimoto and P. F. Nealey, *Proc. SPIE Conf. on Advances in Resist Technology and Processing XXI*, Bellingham, WA, USA (2004)

-
- 15 M-H Jung, S-H Lee, H-W Kim, S-G Woo, H-K Cho and W-S Han, Proc. SPIE Conf. on Advances in Resist Technology and Processing XX, Santa Clara, CA, USA (2003)
- 16 K. Tanaka, R. Naito, T. Kitada, Y. Kiba, Y. Yamada, M.Kobayashi and H.Ichikawa, Proc. SPIE Conf. on Advances in Resist Technology and Processing XX, Santa Clara, CA, USA (2003)
- 17 C. W. Extrand and Y. Kumagai, J. Colloid Interface Sci., 184, 191-200, (1996)
- 18 T. Shibata, T. Ishii, H. Nozawa and T. Tamamura, Jpn. J. Appl. Phys., 36, 7642-7645, (1997)
- 19 T. Tanaka, M. Morigami, H. Oizumi, T. Ogawa and Shou-ichi Uchino, Jpn. J. Appl. Phys., 33, L1803-L1805, (1994)
- 20 C-H Choi and C-J Kim, J. Nanotech., 17, 5326-5332 (2006)
- 21 Sh. Fujikawa, R. Takakai and T. Kunitake, J. Langmuir, 22, 9057-9061, (2006)
- 22 D. L. Olynik, B. D. Hartnrck, E. Veklerov, M. Tendulkar, J. Al. Liddle, A. L. D. Kilcoyne and T. Tyliczak, J. Vac. Sci. Technol. B, 22, 3186-3190, (2004)
- 23 D. L. Goldfarb, J. J. De Pablo, P. F. Nealey, J. P. Simons, W. M. Moreau and M. Angelopoulos, J. Vac. Sci. Technol. B, 18, 3313-3317, (2000)
- 24 H. Namutsu, J. Vac. Sci. Technol. B, 18, 3308-3312, (2000)
- 25 N. M. Felix, K. Tsuchiya and C. K. Ober, J. Adv. Mater., 18, 442-446, (2006)
- 26 J. Simons, D. Goldfarb, M. Angelopoulos, S. Messick, W. Moreau, C. Robinson, J. D. Pablo and P. Nealey, Proc. SPIE Conf. on Advances in Resist Technology and Processing XVIII, Santa Clara, CA, USA (2001)
- 27 A. O'Neil and J. J. Watkins, J. MRS Bulletin, 30, 967-975, (2005)

-
- 28 T. Tanaka, M. Morigami, H. Oizumi and T. Ogawa, *Jpn. J. Appl. Phys.*, 32, 5813-5814, (1993)
- 29 A. Drechsler, N. Petong, C. Bellmann, A. Synytska, P. Busch, M. Stamm, K. Grundke, and O. Wunnicke, *Canadian J. Chem. Eng.*, 84, 3-9, (2007)
- 30 H. Y. Erbil, G. McHale, M. I. Newton, *J. Langmuir*, 18, 2636-2641, (2002)
- 31 Brakke K A, *Surface Evolver*, www.susqu.edu/facstaff/b/brakke/evolver last accessed on September 5, 2007
- 32 K. Deguchi, K. Miyoshi, T. Ishii, *Jpn. J. Appl. Phys. Part 1*, 31, 2954-2958, (1992)
- 33 D. R. Cook, W. C. Young, *Advanced Mechanics of Materials* Macmillan Publishing, New York, USA, 70-72, (1985)
- 34 D. Chatain, D. Lewis, J. Baland and W. C. Carter, *J. Langmuir*, 22, 4237-4243, (2006)

Chapter 3 - A Finite Element Model for Predicting Collapse for Different Pattern Shapes During Drying Process in Photolithography

3-1 Introduction

The most widely used method for manufacturing of micro- and nano-scale features is photolithography. In the photolithography process silicon oxide is covered by the photoresist material, and then exposed to the UV (ultra violet) light through a photomask. Depending on the photoresist type, exposed or unexposed parts of the photoresist become dissolvable in the developer which is mainly water. During the acid etching, the remained photoresist acts as a sacrificial layer and keeps the underneath silicon oxide layer intact. By this procedure, pattern on the photomask is replicated into the silicon oxide wafer. One of the main obstacles of photolithography process for producing fine features is collapse of photoresist patterns during drying of the developer (or rinse) liquid [1]. The collapse reason is reported as unbalanced capillary forces during non-uniform drying of the rinse liquid [2, 3 and 4]. The contributors to capillary forces are Laplace pressure and surface tension force [Chapter 2].

Surface tension force (SFT) is a concentrated force on the three-phase line. The value of the SFT is equal to the value of the rinse liquid-air surface tension (γ_{LV}). STF or γ_{LV} is in the direction tangent to the air-liquid interface (Fig. 3-1a). For the purpose of the pattern collapse, the normal projection of the STF to the pattern's side wall is of interest (see Fig. 3-1a). The reason is that the projection of the STF parallel to the pattern's side

wall is cancelled by other interfacial surface tensions according to the Young's equation (see Eq. 3-1).

$$\gamma_{LV} \cos \theta + \gamma_{SL} = \gamma_{SV} \quad (3-1)$$

Extrand and Kumagai [5] showed that the magnitude of the STF is such that it can deform a polymeric substrate at the three-phase line and form a ridge, in case of a sessile drop placed on a soft surface (Fig. 3-1b). Three-phase line is the confluence zone of the liquid, solid and gas phases described by a line.

Laplace pressure (ΔP) is the pressure difference across the interface of the rinse liquid and air. Laplace pressure is a function of the interface curvature (κ) and surface tension of the rinse liquid (γ), as described by Eq. 3-2.

$$\Delta P = \gamma \cdot \kappa \quad (3-2)$$

For the cases that liquid is only present inside the patterns, and interface of the rinse liquid is concave, curvature value and Laplace pressure consequently are negative. Negative Laplace pressure indicates that the pressure inside the rinse liquid is lower than the outside air pressure. So, Laplace pressure causes the patterns to be pushed towards each other. Besides the Laplace pressure value, the area exposed to the Laplace pressure is essential to calculate the pattern deformation. The area is defined and delimited by the three-phase line.

Assuming cylindrical shape for the rinse interface and using trigonometry, Laplace pressure would be [6, 7, 8, 9, 10, 11, 12, 13, 14 and 15]:

$$\Delta P = \frac{2\gamma \cos(\theta - \phi)}{d - 2\delta_r} \quad (3-3)$$

where ϕ is the slope angle of the pattern at its three-phase line, θ is the contact angle (angle of the rinse liquid interface with pattern's side wall) and δ_r is the pattern deformation at the three-phase line (see Fig. 2-3). In Chapter 2 it was shown that the analytical relations for calculating the pattern deformation are Eqs. 3-4 and 3-5.

$$\gamma \frac{\sqrt{\frac{1}{\left(\left(\frac{3\delta_2}{2H}\right)^2 + 1\right)\left(\left(\frac{4\delta_1}{3H}\right)^2 + 1\right)}} \left\{ \cos\theta \left(1 - \frac{4\delta_1}{3H} \times \frac{3\delta_2}{2H}\right) + \sin\theta \left(\frac{3\delta_2}{2H} + \frac{4\delta_1}{3H}\right) \right\}}{(d - 2(\delta_1 + \delta_2))} = \frac{Ew^3}{3H^4} \delta_1 \quad (3-4)$$

$$\delta_2 = \frac{4\gamma H^3 \sin\theta}{Ew^3} \quad (3-5)$$

Equation 3-4 should be solved numerically along with the Eq. 3-5 to calculate the value of δ_1 . δ_1 is the deformation due to Laplace pressure, whereas δ_2 is due to STF. Total deformation of the pattern would be the summation δ_1 and δ_2 assuming superposition assumption can be used.

Above analytical relation is based on assuming cylindrical interface model (CIM) for the rinse liquid interface shape, and modeling the pattern as a beam. Modeling the pattern as a beam is only valid where pattern has a line shape *e.g.* a two-line parallel pattern. In Chapter 2 it was shown that CIM is only valid for two-line parallel patterns with *LAR* larger than 20 (for *LAR* smaller than 20, CIM is inaccurate in predicting the precise interface curvature value and three-phase line shape).

In summary, using beam bending model to predict the pattern deformation becomes invalid for short two-line parallel, box-shaped, open end L-shaped and close end L-shaped patterns (existence of these geometries is shown in [16]).

In the next sections of this chapter a Finite Element model developed to calculate the pattern deformation for various cases, specially the cases that the beam bending results are invalid (*e.g.* short two-line, box- and L-shaped patterns), will be discussed.

The pattern dimensions studied in this chapter are in consideration of international technology roadmap for semiconductors or Moore's law which states that the number of transistors on a chip doubles every 18 months [17]. In 2007 desirable $\frac{1}{2}$ pitch of patterns was 65nm (trough width (d) and pattern width (w) were 65nm) and should shrink to 57nm by the end of 2008 and 40nm by the end of 2011 [18].

3-2 FE Model for Finding Pattern Deformation

In the FE model, pattern geometry is created and loaded by appropriate capillary forces (Laplace pressure and STF). Area exposed to the Laplace pressure is defined by the three-phase line, and STF exerts a force on the three-phase line.

Three-phase line and rinse interface curvature was found using Surface Evolver (SE), a Finite Element software capable of generating accurate interface shapes [19, 20]. Patterns are modeled using ANSYS ver. 10 (computers used: AMD Athlon XP 1800+ 1.54GHz, 1GB RAM and Genuine Intel ® CPU T2300 @ 1.66GHz 980 MHz, 0.99 GB RAM), a

widely known Finite Element package capable of finding deformation due to capillary forces. Pattern deformation is found by solving the cognitive equations generated as a result of using Finite Element approach. As shown in Chapter 2 both the Laplace pressure value and three-phase line locations for a specific geometry are dependent on the rinse liquid volume. The worst case scenario is where the combination of the Laplace pressure and the area exposed to the pressure results in the maximum pattern deformation. In the following sections details of finding appropriate capillary forces (*i.e.* Laplace pressure and STF) and implementing FE approach are provided.

3-2.1 Capillary Forces in FE Model

Deformation due to the Laplace pressure depends on both the Laplace pressure value and pattern area exposed to the Laplace pressure. From SE, it is found that both the Laplace pressure value and area exposed to the pressure change with changing the rinse liquid volume (Figs. 3-2 and 3-3a). Therefore, pattern deformation due to the Laplace pressure (and total pattern deformation consequently) is a function of the rinse liquid volume. It should be noted that from CIM both the Laplace pressure and the area exposed to the pressure were assumed constant with changing the rinse liquid volume. As such, pattern deformation found from beam bending model was independent of the rinse liquid volume, as it was a simplified approach.

Laplace pressure changes by changing the rinse liquid volume (mainly due to overfilling and underfilling effects). To clarify the underfilling effect, consider the concave shape of the rinse interface. For very small rinse volumes, bottom surface influences the rinse

interface shape. To clarify the overfilling effect, consider the rinse liquid inside the free space of a pattern. Top edge of the pattern's side wall acts as an energy barrier for the interface movement. As such, by adding more liquid, concave interface shape may become flat or even convex (curvature of the rinse interface decreases). In a range of rinse liquid volume where interface shape is not influenced by over and underfilling effects, curvature and consequently Laplace pressure is almost constant (ΔP in Figs. 3-2 panel "b" and 3-3).

The area exposed to the Laplace pressure increases by increasing the rinse liquid volume (due to the rise of the rinse interface). Three-phase line rise continues till the three-phase line reaches the top edge of the pattern's side wall. By adding more liquid the area exposed to the Laplace pressure remains constant.

For two-line parallel patterns with $d=w=57, 65$ and 104 nm, it was found that by increasing the liquid volume, first pattern's side wall becomes completely wet. By adding further liquid, Laplace pressure will be influenced by the overfilling effect and decreases (see Fig. 3-2 panel b). As such, for the worst case scenario Laplace pressure is not influenced by the overfilling effect, the area exposed to Laplace pressure is entire pattern's side wall, and the three-phase line is a straight line on the top edge of the pattern's side wall. It is found that the above situations for worst case scenario are almost valid for box-shaped, open end and close end L-shaped patterns. In the next section a Finite Element (FE) method will be developed to find the deformation of a pattern as a result of capillary forces in the worst case scenario, as defined in this section.

3-2.2 Finite Element Method for Finding Pattern Deformation

The procedure of finding the deformation in Finite Element model is as follow (see Fig. 3-4): the geometric model is created in Surface Evolver to find the rinse liquid interface shape and subsequently Laplace pressure value (ΔP in section 3-2.1). By applying the capillary forces (*i.e.* Laplace pressure and STF) to the geometric model created in ANSYS, initial deformed shape of the pattern is found. Pattern deformation changes the initial interface shape. As such, deformed pattern geometry needs to be again imported to the Surface Evolver to find a new interface shape. By knowing the new interface shape and Laplace pressure, pattern deformation will be updated. This procedure continues till the deformation converges within a range of 1%.

The mentioned iterations of coupled ANSYS-Surface Evolver is called FE model. The deformation value from FE may or may not converge. If the deformation from FE model converged to a value smaller than half of the trough width, pattern is not considered collapsed. Non-convergence or convergence to a value larger than half of the trough width signifies the pattern collapse.

Slope angle and deformation of the pattern at the tip are the data used to import the deformed pattern shape into the Surface Evolver. So, Shell43 element (in ANSYS) is selected since it provides both the slope angle and deformation. For the cases selected to study in this chapter (*i.e.* state-of-the-art dimensions for 2007 to 2009) it was observed that slope of the pattern at the tip even at the moment of collapse, or maximum possible deformation, is small (less than 4 degrees). As the value of slope angle is small, to

simplify the complicated simulations, slope angle can be ignored. Therefore, one may choose Solid95 element in ANSYS (which is easier to apply comparing to Shell43) to obtain the pattern deformation with proper accuracy. After development of the FE model, the model needs to be tested with the cases that the pattern deformation value was known.

3-3 Validation of FE Model for Finding Pattern Deformation

To verify the FE model (developed in section 3-2) and see whether for example correct solver method, element and meshing are used, FE and beam bending model (developed in Chapter 2) results are compared for the cases that beam bending model results are valid. The beam bending model is valid for a two-line parallel pattern with LAR value larger than 20.

As seen in Fig. 3-5 for two-line parallel patterns with LAR values larger than 20, beam bending model and FE results are close and the closeness of the results validates the FE results. However, in general, pattern deformation from FE is slightly larger than that from beam bending model. The reason of the slight difference is that beam bending model is based on the small deformation assumption (used for applying superposition principal). At small deformations, pattern's slope angle is small (in the order of few degrees, for example see Fig. 3-6a). Pattern's slope angle is equal to the rotation angle of capillary forces. Therefore, for a small pattern deformation capillary forces remain almost horizontal. However, for a large pattern deformation, capillary forces slightly rotate. In beam bending model, forces are assumed to remain horizontal, but FE model considers

the force rotation. As such, a slight rotation of capillary forces causes a slight difference between FE and beam bending model results.

The deformation value for smaller contact angles is larger. So, for very low contact angles the capillary force rotation and the difference between beam bending and FE results increases (see Fig. 3-5a). Also, decrease of the module of elasticity for the pattern's material (E) increases the pattern deformation and rotation of forces consequently. Due to the larger force rotation at smaller elasticity modulus values, the difference between beam bending and FE increases by decreasing the E (see Fig. 3-5b). Regarding Fig. 3-5 it should be noted that beam bending model is different from Tanaka's beam bending model as Tanaka's beam bending model neglects the STF effect on the pattern deformation. In general, the slight difference between FE and beam bending results increases by changing any factor which leads to increasing the deformation *e.g.* decreasing w or increasing AR and H .

It should be noted that for very large pattern deformations, where rotation of capillary forces is not negligible (more than 5 degrees), beam bending model results are not proper for validation of FE results.

3-4 Pattern Deformation Using FE

FE method is applied to find the deformation of two-line parallel patterns with short length (small LAR value), L-shaped with open ends, L-shaped with close ends, and box-shaped pattern geometries. Beam bending model is unable to predict the deformation for

the mentioned cases. Also, CIM is entirely inappropriate for predicting the interface curvature value and the three-phase line shape of the rinse inside box-shape, open end and close end L-shaped patterns.

3-4.1 Two-Line Parallel Patterns with Short Length

Curvature value and consequently Laplace pressure are functions of LAR value. For the case of two-line parallel patterns with short length, it was found that by decreasing LAR value, pattern deformation decreases (see Fig. 3-6b). This is independent of contact angle. The reason is that for the specific geometry of two-line parallel patterns, by decreasing the LAR value curvature and consequently Laplace pressure values decrease (see Figs. 2-10a and 3-7). Changing LAR also slightly changes the stiffness of the structure (by changing the cross sectional shape of the pattern) which was neglected in beam bending model but this slight change in the pattern stiffness is considered in the FE model.

Further studies showed that for any contact angle there exists an LAR where interface becomes flat or rinse interface curvature becomes zero (see Fig. 3-7). In this study the LAR value at which rinse interface curvature becomes zero is named the transition LAR value. For LAR values lower than the transition LAR , curvature value is positive and Laplace pressure drives out the two adjacent patterns from each other (pressure inside the rinse liquid is higher than the outside air pressure). It is found that for small contact angles the transition LAR value becomes small. For example, transition LAR value is approximately 10 for contact angle of 85 degrees whereas for contact angle of 5 degrees, transition LAR value is about 1. At the transition LAR , Laplace pressure is zero but STF is

still operative on the pattern's side wall. For LAR values smaller than the transition LAR , effects of Laplace pressure and STF are opposite to each other and pattern deformation becomes negligible. For example, for the specific case of line space 1:1 equal to 65nm (state of the art for 2007) with LAR of 5, and contact angle of 85 degrees, where curvature value is positive ($\kappa = 0.8\mu m^{-1}$, interface shape is shown in Fig. 3-7), very small deformation value of 1.176nm was attained (see Fig. 3-7). The ideal case would be where deformation due to the Laplace pressure equalizes the deformation due to the STF.

So, for the cases that design and application limit the change of rinse liquid or photoresist material, change of LAR may be an alternative to resolve the collapse problem for two-line parallel patterns, if functional design of the device being fabricated allows.

3-4.2 Open End L-shaped Patterns

One of the common geometries during manufacturing of micro- and nano-devices is an open end L-shaped pattern (see Fig. 3-3b). Beam bending model is not applicable to L-shaped patterns and as such, there is no analytical model available for this geometry. Furthermore, rinse liquid interface cannot be modeled as a part of a cylinder (SE should be used to find the interface shape and subsequently the Laplace pressure).

From Surface Evolver simulation it is found that independent of legs' length (L_1 and L_2 in Fig. 3-3b) as long as the summation of length of the legs is constant, curvature value will not change noticeably (see Fig. 3-8). Therefore, an equivalent length (L_e) will be defined as given in Eq. 3-8.

$$L_e = L_1 + L_2 + \frac{d_1 + d_2}{2} \quad (3-6)$$

Figure 3-9a also shows the properness of the definition of L_e at different contact angles *i.e.* as long as L_e is constant, change of the length of individual legs does not lead to a significant change in the calculated Laplace pressure.

It is also found that equivalent length defined in Eq. 3-6 can be used to relate the curvature value of an open end L-shaped pattern to the curvature value of a two-line parallel pattern (*e.g.* see Fig. 3-10). Curvature value of an open end L-shaped pattern is equal to curvature value of a two-line parallel pattern with the same LAR (LAR of an L-shaped pattern is defined using L_e instead of L). So, instead of creating a model for an L-shaped pattern in Surface Evolver (which is not easy) one may model a two-line parallel pattern with the same LAR value and find the rinse interface curvature and ΔP . The above finding has been determined for trough widths smaller than 1 micron and contact angles between zero and 90 degrees.

As shown in Fig. 3-11a for L-shaped patterns with open ends by increasing the contact angle and decreasing the LAR value, Laplace pressure on the pattern decreases (similar to a two-line parallel pattern case). It should be mentioned that Laplace pressure is not the only contributor on capillary forces. As mentioned in Chapter 2, increasing the contact angle may have an adverse effect on the pattern deformation by increasing the normal to the pattern's side wall projection of the STF. From Laplace pressure trend it is expected that by decreasing the LAR value pattern deformation to decrease.

FE analysis (mentioned in section 3-2.2) is used to find the deformation of L-shaped patterns with open ends at different LAR values. From comparing two open end L-shaped patterns with similar rinse liquid, trough width and pattern material (same contact angle and STF), it is found that the L-shaped pattern with smaller length deforms less (see Fig. 3-11c). As such, for the cases that pattern material and rinse selection are limited by the manufacturing process, decreasing the LAR value can resolve the collapse problem of L-shaped patterns with open ends.

For a series of patterns which have equal L_e values (but different length for each two legs), capillary force values are equal. However, the stiffness of the pattern may be different. It is found that among many configurations with equal LAR values, the one which has legs with equal lengths has slightly higher stiffness and smaller deformation (see Fig. 3-9c). It is also found that by increasing the difference between the length of the legs, pattern deformation slightly increases (see Fig. 3-9c). The maximum difference in legs length difference, and consequently maximum deformation, is where patterns shape an “LI” configuration (Fig. 3-12a illustrates an “LI” shaped pattern). As, deformation of an “LI” pattern is slightly larger than that for an “LL” pattern (Fig. 3-12b demonstrates an “LL” shaped pattern) with equal LAR value, deformation of an “LI” pattern provides an upper estimate for the deformation value of an “LL” pattern. This is important as for an open end L-shaped pattern with “LI” configuration just the “I” part needs to be modeled and analyzed as the highest deformation occurs in the “I” part. Furthermore, “I” part can be modeled as a beam and for the cases that LAR is larger than 20 interface shape is

cylindrical. So, deformation of the “I” part can be found analytically using the beam bending model developed in Chapter 2.

3-4.3 Box-Shaped and Close End L-Shaped Patterns

It is observed that close end patterns have larger rinse interface curvature and consequently Laplace pressure values compared to open end ones with similar dimensions (*e.g.* compare Figs. 3-9a and 3-9b or compare Figs. 3-11a and 3-11b). On the other hand, ends in close end patterns act as buttresses and stiffen the patterns. From studying the state-of-the-art dimensions of 2007 to 2009 it was found that the effect of ends to stiffen the pattern structure is smaller than the effect of ends on increasing the rinse interface curvature and capillary force, as such, the deformation of a close end pattern is larger than that of an identical open end pattern (*e.g.* compare Figs. 3-9c and 3-9d or compare Figs. 3-11c and 3-11d). So, deformation for an open end pattern provides a lower estimate for the deformation of an identical pattern with close end. For example, deformation of a two-line parallel pattern is slightly smaller than that for a box-shaped pattern. As such, for similar geometries, rinse liquids, and pattern materials, if the open end pattern collapses then identical close end pattern will collapse as well.

For a two-line parallel pattern with LAR larger than 20, pattern deformation can be found analytically. It is important because if the two-line parallel pattern collapsed, then the identical box-shaped pattern will collapse (and no FE modeling is needed). However, if the identical open end pattern did not collapse then the original close end pattern may or

may not collapse and FE modeling is needed. For L-shaped patterns with close ends independent of the value of LAR , FE modeling is needed.

In close end patterns, by decreasing the LAR value, Laplace pressure increases (Fig. 3-11b), so regardless of the LAR value, rinse interface shape remains concave unless the contact angle becomes larger than 90 degrees). From Laplace pressure trend in close end L-shaped patterns, it is expected that by decreasing the LAR value pattern deformation increases. However, it is found that similar to the open end L-shaped cases by decreasing the LAR value pattern deformation decreases. The reason is that by decreasing the LAR value, the effect of ends on pattern stiffness become more significant. So, similar to open end cases for close end cases decreasing the LAR value is useful for decreasing the pattern deformation. The results are tested for elasticity modulus values between 2 and 6 MPa.

3-5 Conclusion

Analytical, beam bending, models developed in the literature for predicting the pattern deformation are limited to a specific case of two-line parallel pattern with LAR larger than 20. The reason is that pattern is modeled as a beam and rinse interface is modeled by CIM. In this chapter four pattern geometries where beam bending model was unable to predict the pattern deformation were studied. These geometries are two-line parallel with short length (LAR smaller than 20), open end L-shaped, close end L-shaped, and box-shaped patterns. For these pattern geometries, pattern cannot be modeled as a beam and/or rinse interface cannot be modeled by CIM. A coupled Finite element model using

Surface Evolver and ANSYS was developed to calculate the pattern deformation value for these cases. The model coupled Surface Evolver- ANSYS in this study is shortly named FE model. FE model was validated by knowing the deformation values for the case of a two-line parallel pattern with LAR larger than 20 using beam bending model. Verification of the FE model showed that for large deformations a slight difference appears between FE and analytical model results. The cause of the slight difference is violation of small deformation assumption used, to apply the superposition principal, in the analytical model.

From studying the interface curvature value of the rinse liquid inside L-shaped patterns an equivalent length was suggested. The equivalent length relates the curvature value of the rinse interface inside an L-shaped pattern to the curvature of the rinse interface inside a two-line parallel pattern. This is important as creating a two-line parallel pattern in Surface Evolver and calculating the curvature value is much easier than that for an L-shaped pattern. From comparing deformations of L-shaped patterns with equal equivalent lengths (and consequently equal capillary forces) it was found that the weakest geometry is the “LI” geometry and at its “I” part. The “I” part deformation provides an upper estimate for the deformation of the original “LL” shaped pattern (with equivalent length or LAR value equal to that of the “LL” shaped pattern). This is important as for open end L-shaped patterns with LAR larger than 20, deformation of the “I” part can be found analytically. If the deformation value of “I” shape part of the “LI” pattern, lead to a non-collapse situation then one may conclude that the “LL” shaped pattern would not collapse (an FE modeling is not needed).

From studying short length two-line parallel, open end L-shaped, close end L-shaped and box-shaped patterns, it was found that the pattern deformation decreases by decreasing the *LAR* value. This is important as for the cases that due to the design specifications, selection of photoresist material and rinse liquid is restricted, by changing the *LAR* value one may resolve the collapse problem.

Figures

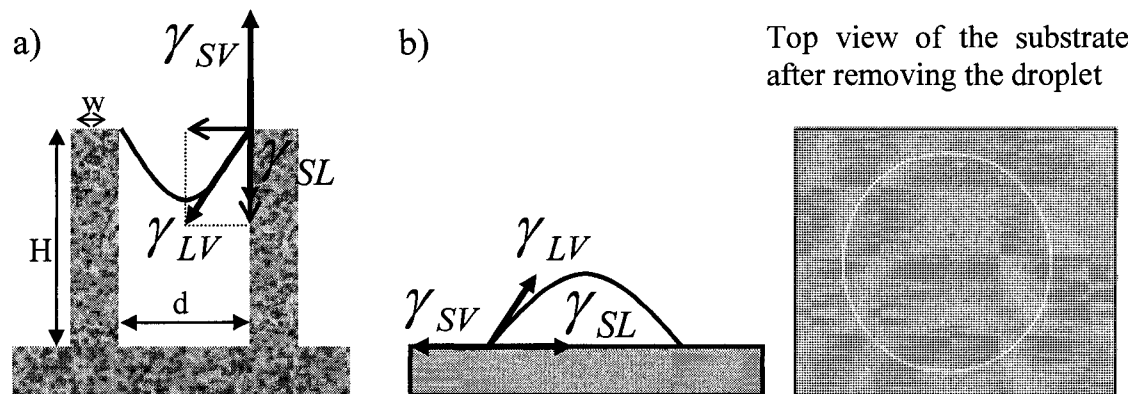


Figure 3-1 (a) Horizontal projection of γ_{LV} is exerting a force on the pattern while its vertical projection, according to Young equation, is canceled by two other interfacial tensions, *i.e.* γ_{SL} and γ_{SV} . (b) Schematic of the experiment done in [5] where a drop was placed on a soft substrate. The normal component of the γ_{LV} to the substrate cause the soft substrate to be deformed at the three-phase line (white circle).

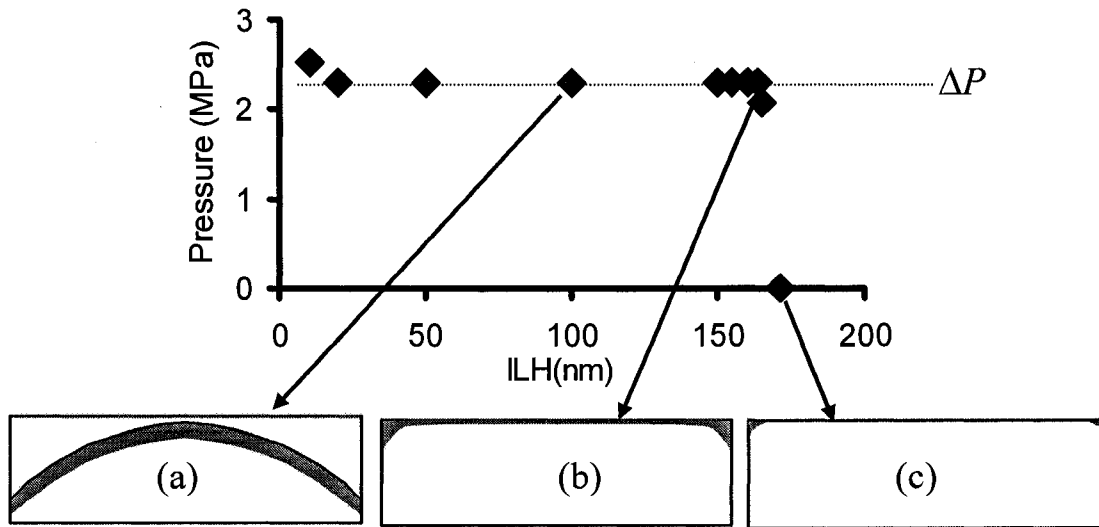


Figure 3-2 Laplace pressure, three-phase line and interface shapes of a two-line parallel pattern at different *ILH* (Initial liquid height) values are shown. For the case “b” which *ILH* is 164nm, three-phase line is mostly a straight line however pressure value is not influenced by the overfilling effect. Note that three-phase lines are the thick black lines in the three panels and gray shades show the interface. $AR (=H/w, \text{ shown in Fig. 3-1}) = 3$, $LAR=10$, $d=w=57\text{nm}$ (state of the art for 2008), $\theta = 5^\circ$, $\gamma = 72.9\text{mN/m}$ and interface shapes shown in the panels are found using Surface Evolver.

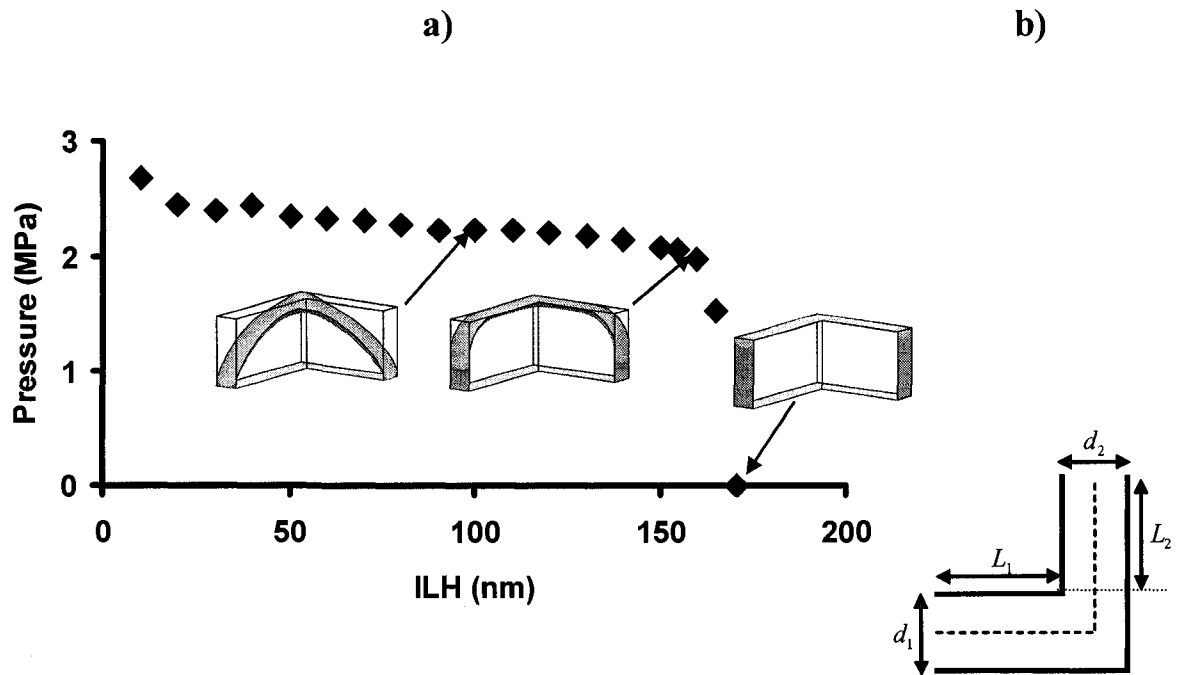


Figure 3-3 (a) Laplace pressure, three-phase line and interface shape of an L-shape pattern as a function of rinse liquid volume is shown. $AR (H/w) = 3$, $LAR=10$, $d=w=57\text{nm}$ (state of the art for 2008), $\theta = 5^\circ$, $\gamma = 72.9\text{mN/m}$ and interface shape is found using Surface Evolver, (b) Top view of an L-shaped pattern is shown. The length of two legs are L_1 and L_2 . Pattern dimensions shown are measured from inside of the pattern wall.

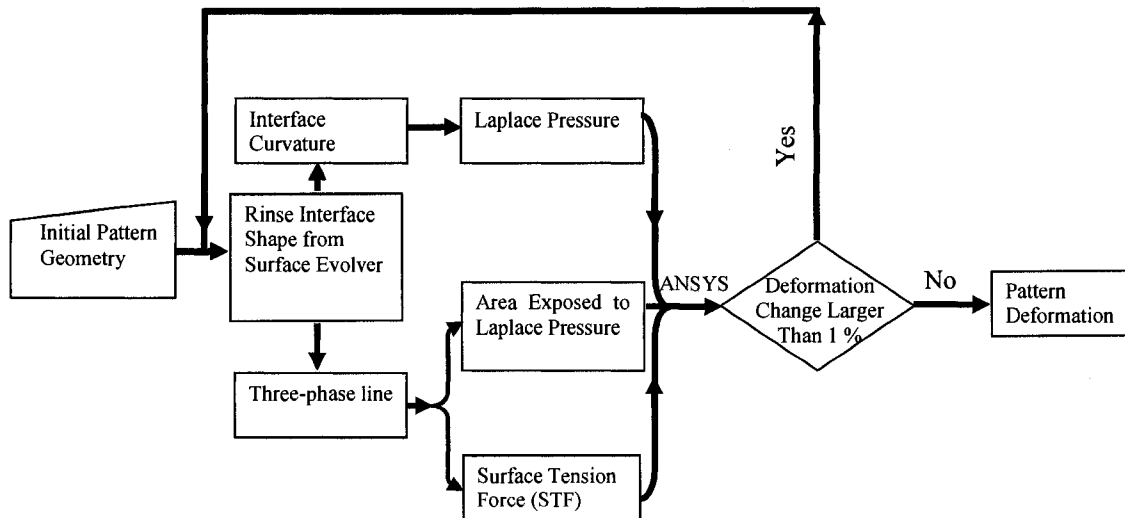


Figure 3-4 Procedure of calculating pattern deformation using FE method is shown.

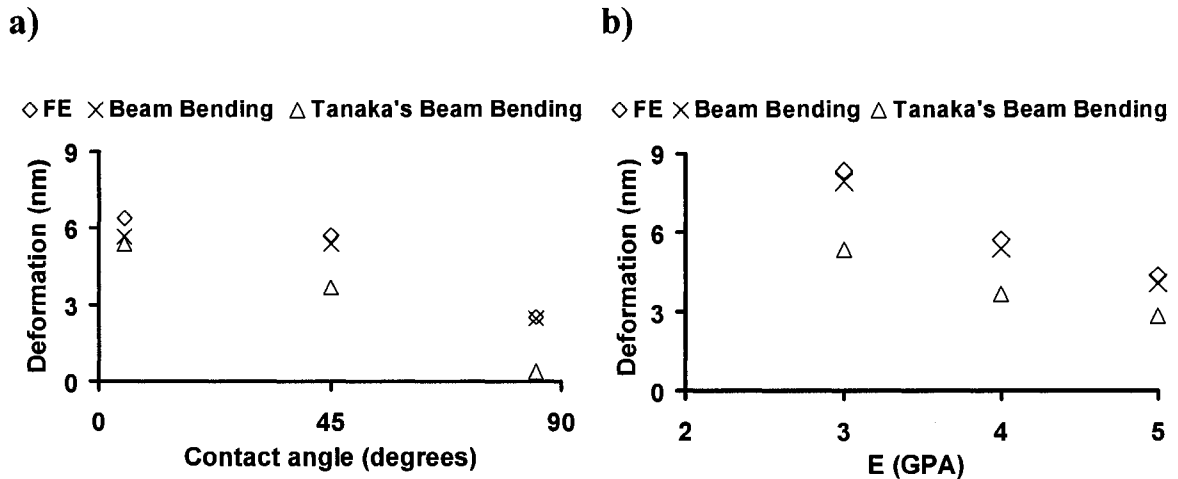


Figure 3-5 Deformations of a two-line parallel pattern from beam bending, Tanaka's beam bending and FE model are compared at (a) different contact angles with $E=4\text{GPa}$, (b) different Elasticity modulus (E) values with $\theta = 45^\circ$. (In both cases $d=w=57\text{nm}$, $AR=3$, $\gamma = 72.9\text{mN/m}$ and $LAR \rightarrow \infty$; see Appendix F for the method of defining an infinite length for the pattern in simulation).

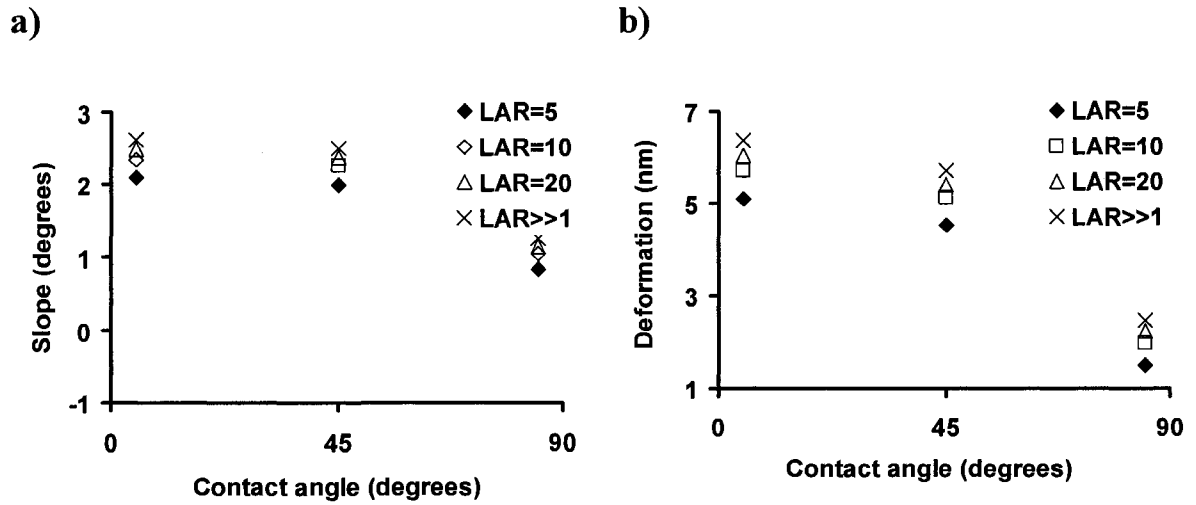


Figure 3-6 (a) Slope of the pattern at its tip, and (b) deformation from FE model at different contact angles is shown for different LAR values ($d=w=57\text{nm}$, $AR=3$, $\gamma = 72.9\text{mN/m}$, $E=4\text{GPa}$ and two-line parallel pattern).

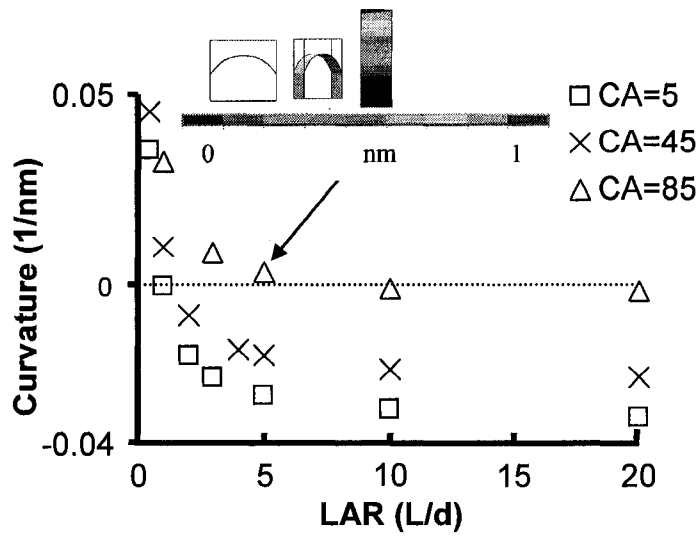


Figure 3-7 Curvature versus LAR values for different contact angles are shown. For small LAR values, curvature is positive. Positive curvature means that Laplace pressure is pushing the patterns outward (against the surface tension force effect). The negative curvature has the opposite meaning ($d=w=57\text{nm}$, $E=5.9\text{GPa}$, $AR=3$ and water inside a two-line parallel pattern).

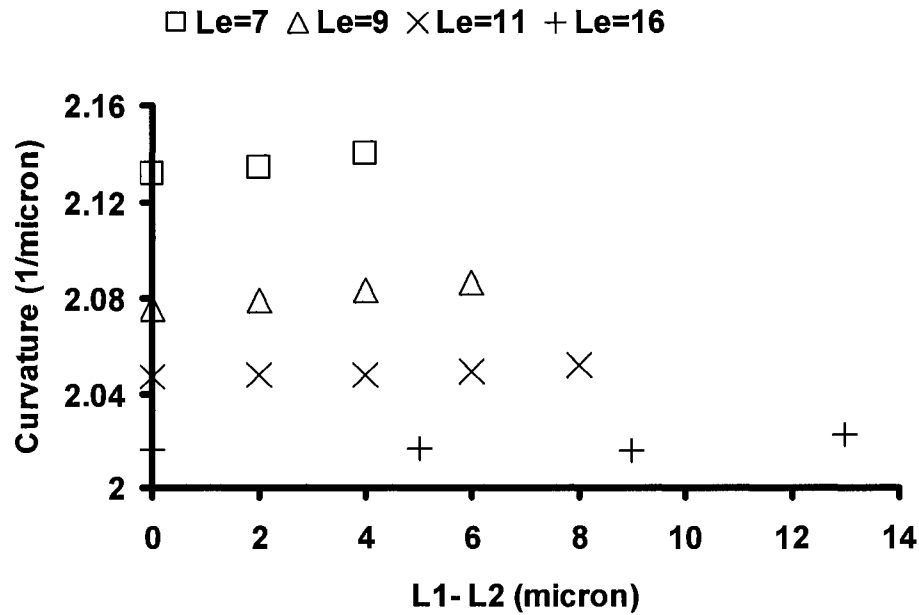


Figure 3-8 Curvature value of open L-shaped patterns. As long as equivalent length (or summation of legs) is constant, curvature value only slightly changes. Although, change of curvature by changing the equivalent length from 7 to 16 is not very much but this amount of change causes a pressure change in the order of 10kPa ($\theta = 5^\circ$ and $d=1$ micron).

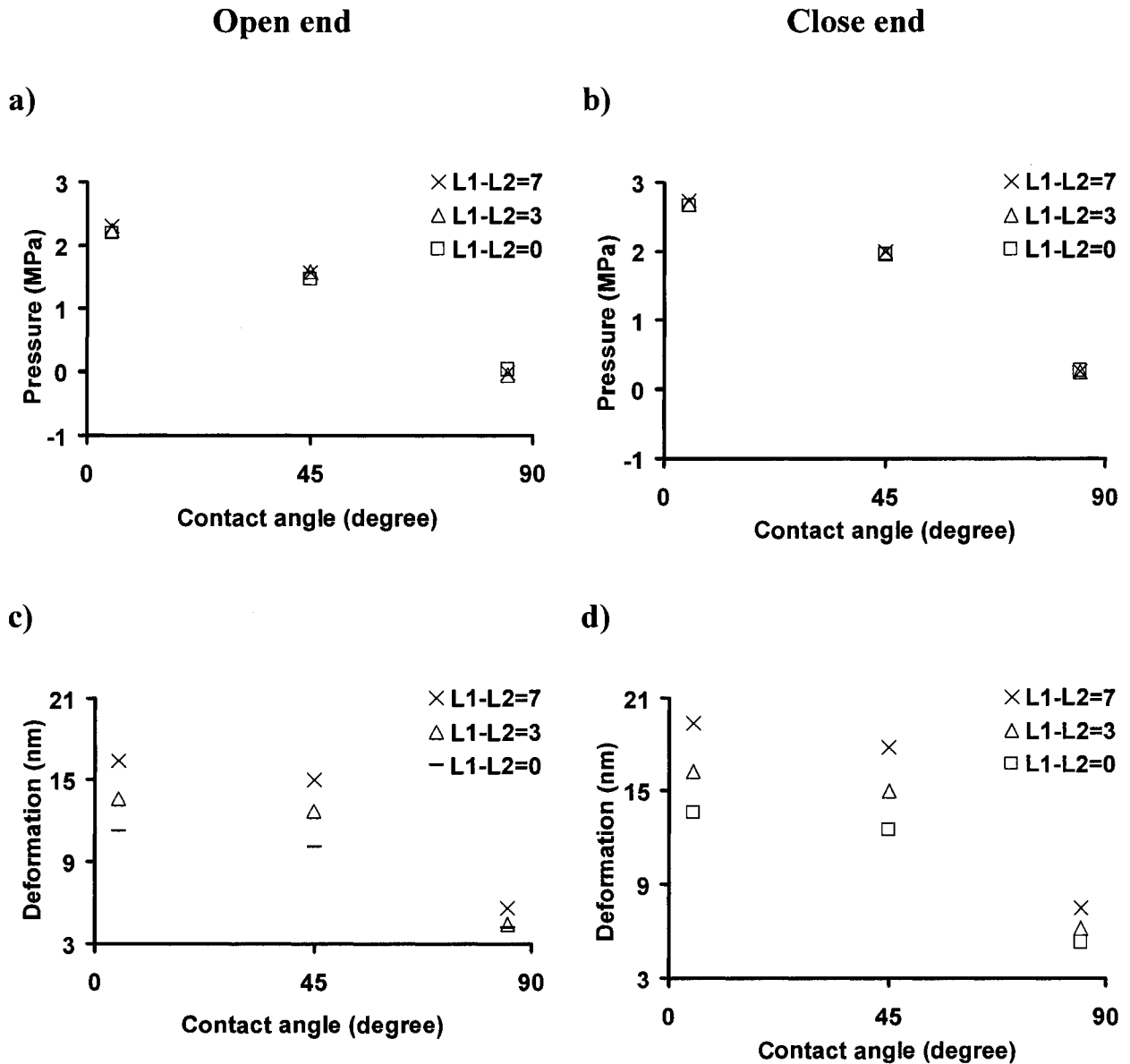


Figure 3-9 (a) Laplace pressure of open end L-shaped patterns, (b) Laplace pressure of close end L-shaped patterns, (c) pattern deformation of open end L-shaped patterns and (d) pattern deformation of close end L-shaped patterns, at different contact angles for different leg's lengths are shown. As long as equivalent length is constant, Laplace pressure is not changing but the deformation may change and minimum deformation is where legs are equal ($d_1 = d_2 = w = 57nm$, $L_e = 531nm$, $\gamma = 72.9mN/m$ and $LAR=10$).

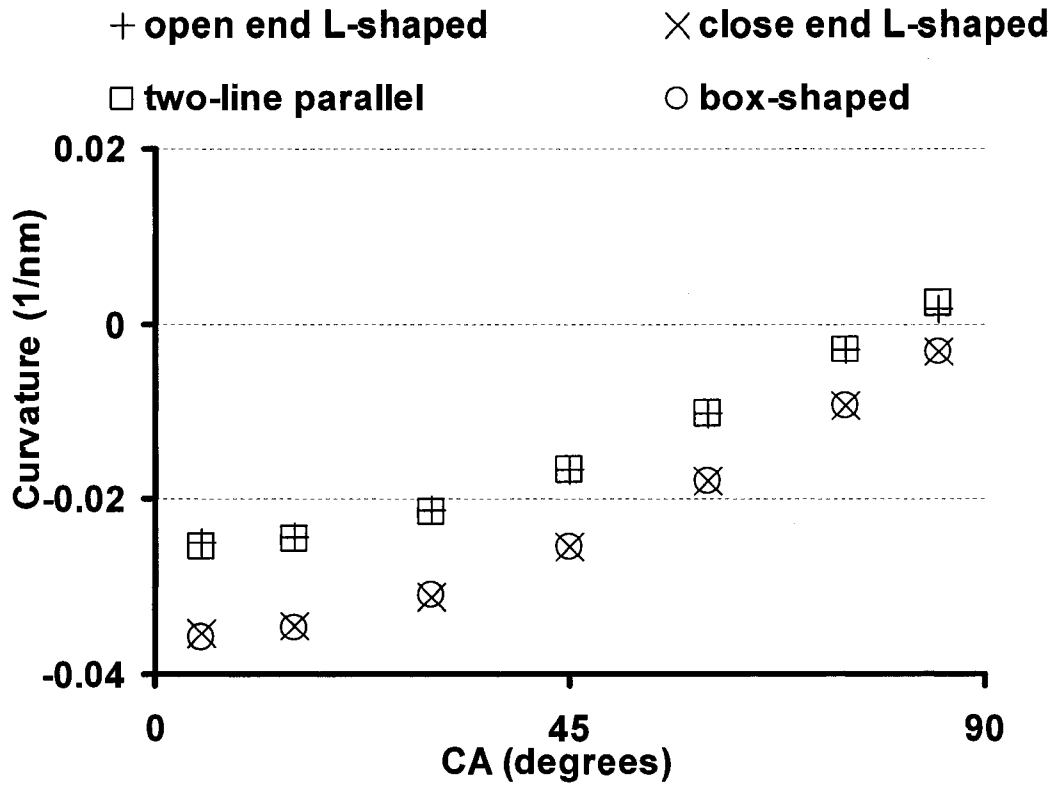


Figure 3-10 Curvature value of a two-parallel line pattern is equal to that of an open end L-shaped pattern with equal LAR value. Curvature value of a box-shaped pattern is equal to that of a close end L-shaped pattern with equal LAR value ($LAR=6$ and $d_1 = d_2 = w = 65nm$).

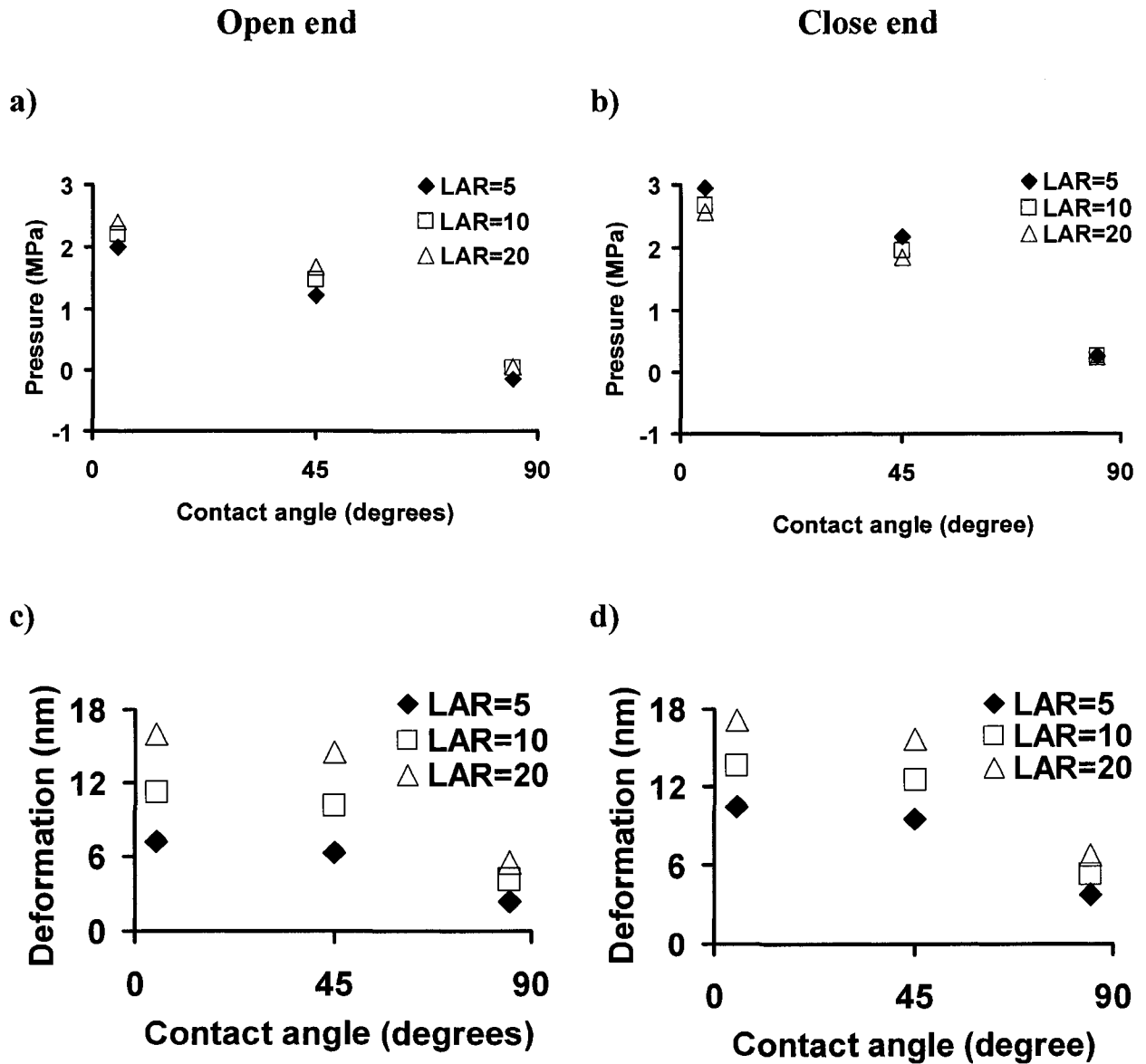
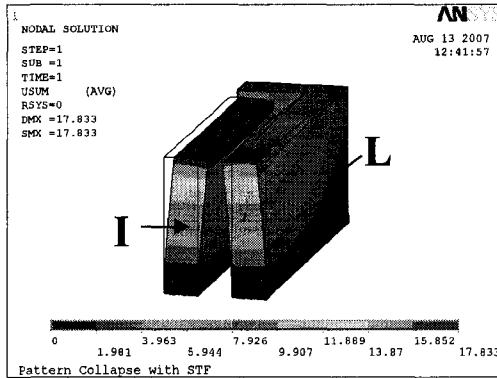


Figure 3-11 (a) Laplace pressure of open end L-shaped patterns, (b) Laplace pressure of close end L-shaped patterns, (c) pattern deformation of open end L-shaped patterns and (d) pattern deformation of close end L-shaped patterns, at different contact angles and LAR values is shown. For large LAR values deformation increases ($L_1 - L_2 = 0$, $d_1 = d_2 = w = 57nm$ and $\gamma = 72.9mN/m$).

a)



b)

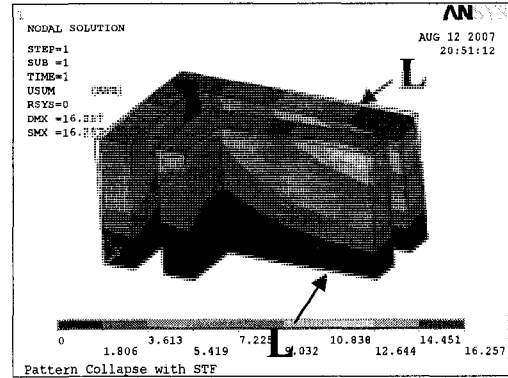


Figure 3-12 (a) “LI” configuration which comprises “I” and “L” shape parts and (b) “LL” configuration which comprises two “L” shape parts are shown. Among geometries with equal *LAR* value “LI” configuration and especially its “I” part has the maximum deformation.

References

- 1 K. Deguchi, K. Miyoshi, T. Ishi and T. Matsuda, *Jpn. J. Appl. Phys.*, 31, 2954-8, (1992)
- 2 T. Tanaka, M. Morigami and N. Atoda, *Jpn. J. Appl. Phys.*, 32, 6059-6064, (1993)
- 3 M. Kotera, N. Ochiai, *J. Microelect. Eng.*, 78-79, 515-520, (2005)
- 4 K. Yoshimoto, M. P. Stoykovich, H. B. Cao, J. J. de Pablo, P. F. Nealey and W. J. Drugan, *J. Appl. Phys.*, 64, 1857-1865, (2004)
- 5 C. W. Extrand and Y. Kumagai, *J. Colloid Interface Sci.*, 184, 191-200, (1996)
- 6 H. B. Cao and P. F. Nealley, *J. Vac. Sci. Technol. B*, 18, 3303-3307, (2000)
- 7 Ki-Soo and G. Lee, *J. Photopolymer Sci. Tech.*, 16, 363-368, (2003)
- 8 M. P. Stoykovich, H. B. Cao, K. Yoshimoto, L. E. Ocola and P. F. Nealey, *Adv. Mater.* 15, 1180-1184, (2003)
- 9 Y. Jincao, M. A. Matthews and C. H. Darvin, *Ind. Eng. Chem. Res.*, 40, 5858-5860, (2001)
- 10 K. D. Vora, B. Y. Shew, E. C. Harvey, J. P. Hayes and A. G. Peele, *J. Micromech. Microeng.*, 15, 978-983, (2005)
- 11 A. Drechsler, C. Bellmann, A. Synytska, N. Petong, K. Grundke, M. Stamm, J. Reichelt and O. Wunnicke, *J. Colloids and Surfaces A Physiochem. Eng.*, 311, 83-92, (2007)
- 12 I. Junarsa, M. P. Stoykovich, K. Yoshimoto and P. F. Nealey, *Proc. SPIE Conf. on Advances in Resist Technology and Processing XXI*, Bellingham, WA, USA, (2004)
- 13 Hyung-Joo Lee, Jun-teak Park, Ji-yong Yoo, Ilsin An and Hye-Keun Oh, *Jpn. J. Appl. Phys.*, 42, 3922-3927, (2003)
- 14 S-K Kim, *J. Korean Phys. Soc.*, 42, S371-S375, (2003)

-
- 15 D. L. Olynick, B. D. Harteneck, E. Veklerov, M. Tendulkar, J. A. Liddle, A. L. D. Kilcoyne and T. Tyliczszak, *J. Vac. Sci. Technol. B*, 22, 3186-3190, (2004)
- 16 T. Ito, K. Kadota, M. Nagao, A. Sugimoto, M. Nozaki and T. Kato, *J. Vac. Sci. Technol. B*, 8, 1080-1086, (1990)
- 17 www.itrs.net/Links/2006Update/FinalToPost/08_Lithography2006Update.pdf, last accessed on 15 December 2007
- 18 www.itrs.net/Links/2006Update/FinalToPost/08_Lithography2006Update.pdf, last accessed on 15 December 2007
- 19 D. Chatain, D. Lewis, J. P. Baland and W. C. Carter, *Langmuir*, 22, 4237-4243, (2006)
- 20 www.susqu.edu/brakke/evolver, last accessed on 15 December 2007

Chapter 4 - Conclusion

4-1 Driving Forces of Pattern Collapse

Pattern collapse is the permanent deformation of photoresist patterns during drying of the rinse liquid in development step of photolithography. To date, unbalanced capillary forces due to the Laplace pressure are identified as the main cause of pattern collapse. In this study it was shown that Laplace pressure was not the only major contributor to the capillary forces. Surface tension force (STF) on the three-phase line needs to be addressed for an accurate analysis.

4-2 Analytical Model to Predict Collapse of Two-Line Parallel Patterns

Based on considering the effect of STF on pattern deformation, a new analytical (beam bending model) was developed for predicting the deformation of a two-line parallel pattern. Beam bending model used small deformation assumption to apply the superposition principal (to add the effects of STF and Laplace pressure). Similar to other analytical models for pattern deformation simulation, analytical model in this study used cylindrical shape assumption for the rinse liquid interface.

The new analytical model showed that for large ARs , contact angles (θ), trough widths (d) and small elasticity modulus of pattern materials (E) the importance of considering the effect of STF increases.

Without considering the effect of STF literature models suggested that adding the cationic surfactants to the rinse liquid is the most proper approach to resolve the collapse

problem (cationic surfactant increasing the contact angle). However, by considering the STF it was found that increasing the contact angle may increase the pattern deformation and worsen the collapse situation.

4-2.1 Bounds of Applicability for Analytical Model for Two-Line Parallel Patterns

Cylindrical shape assumption (CIM) is valid for very long patterns where rinse interface shape is cylindrical. However, the term very long was undefined in literature. In this study, Surface Evolver (SE) as a Finite Element approach was applied to find the rinse interface shape and its curvature value. By comparing rinse interface curvature values from CIM to the curvature values from SE at different pattern lengths, trough widths and contact angles, it was found that the error of calculating the rinse interface curvature using CIM is only a function of LAR (L/d). For LAR values larger than 20, the error of using CIM to calculate the rinse interface curvature is lower than 5%. As such, for LAR values larger than 20 beam bending model results for finding the deformation of a two-line parallel pattern are valid.

From SE results it was found that three-phase line shape and rinse interface curvature value are functions of rinse liquid volume. However, there exist a rinse volume value at which three-phase line is straight line, area exposed to Laplace pressure is the entire pattern surface, and curvature value is nearly at its maximum (*i.e.* the curvature before decreasing due to the overfilling effect). This rinse volume value is called the worst case scenario volume as it produces the maximum pattern deformation. The worst case

scenario volume was assumed in beam bending model. As such, for the cases that volume does not reach the worst case scenario volume, the beam bending model overestimate the deformation value. Also, beam bending model neglects the effect of horizontal force on lateral displacement (the concept of Poisson's ratio). For a more general an accurate evaluation of the pattern deformation a Finite Element (FE) model is developed in this study.

4-3 FE Model to Predict Collapse of Different Pattern Shapes

Other than the shortages for the specific geometry of a two-line parallel pattern, beam bending model is unable to predict the pattern deformation of open end L-shaped, close end L-shaped and box-shaped patterns. A coupled Finite element (FE) model using Surface Evolver and ANSYS is developed to calculate the pattern deformation values for general shape of patterns. The FE model was verified by deformation values of two-line parallel patterns with LAR values greater than 20 using analytical (beam bending) model. Validation process also showed that for large deformations a slight difference appears between Finite Element and beam bending model results. In calculating the pattern deformation, analytical model assumes that capillary forces remain horizontal while the developed FE model considers the force rotations. The cause of the slight difference between FE and analytical results was suggested to be due to the force rotation. The results supported this suggestion as it was seen that for high values of deformation, the difference between FE and analytical results increased. Note that force rotation increases by increasing the pattern deformation.

From studying the interface curvature value of the rinse liquid inside open end and close end L-shaped patterns an equivalent length was suggested. Equivalent length relates the curvature value of the rinse interface inside an open end/close end L-shaped pattern to the curvature of the rinse interface inside a two line-parallel/box-shaped pattern. Defining this equivalent length is important as in Surface Evolver, modeling a two-line parallel and box-shaped pattern and calculating the curvature value are much easier than modeling open end and close end L-shaped patterns.

From studying short length two-line parallel, close end L-shaped, open end L-shaped and box-shaped patterns, it was found that the pattern deformation decreases by decreasing the LAR value. It is important as for the cases that selection of photoresist material, and rinse liquid is restricted due to the design specifications, by changing the LAR value one may resolve the collapse problem.

From comparing deformations of open end L-shaped patterns with equal equivalent lengths (and consequently equal capillary forces) it was found that the weakest geometry is the “LI” geometry and specifically its “I” shape part. As such, deformation of the “I” shape part of an “LI” shape pattern provides an upper estimate for the deformation of the original “LL” shape pattern with equal equivalent length. As a result, if the deformation value of the “I” shape part of an “LI” pattern led to a non-collapse situation then the “LL” shape pattern would not collapse. It is important as for the cases that LAR is larger than 20 the deformation of the “I” part will be found analytically. However, if the deformation

of the “T” shape part led to collapse or LAR was smaller than 20 then FE method should be applied to find the pattern deformation.

4-4 Future Works

In derivation of current beam bending model, Poisson’s ratio is assumed zero. It means that horizontal forces on the pattern (*i.e.* Laplace pressure and STF) do not cause vertical deformation. Current Finite Element model however, considers Poisson’s ratio. As using beam bending model is faster and easier than Finite Element model developing a beam bending model with considering Poisson’s ratio might be a next step.

It should be mentioned that in this study bulk values are used for studying the photoresist material however for example Goldfarb *et al.*[1] stated that elasticity modulus of nano-photoresist deviates from its bulk value. Nevertheless, for improvement of both novel beam bending model and Finite Element results, nano-scale values may be substituted with bulk values in the future.

In both beam bending and Finite Element models pattern deformation is assumed linearly elastic and touching of the tips of two adjacent patterns or the start of plastic deformation are the collapse criteria (whichever occurs first). However, in some cases before pattern tips touch or plastic deformation starts, patterns, at the pattern base, might detach from the substrate and cause collapse. This happens due to the improper pre-baking process. The current model is not able to predict this type of collapse. For improving the model, to

consider the pattern's base detachment from the substrate scenario, maximum tolerable stress of the base should be defined and compared with the stress exerted at the base.

For some applications small plastic deformation of the pattern is permitted. As such, the pattern with that small plastic deformation may not be considered as collapsed. However, both the new beam bending and FE models predict collapse for such a case. The current FE model may be upgraded to account for some specific plastic deformations.

The effect of evaporation of the rinse liquid through changing the rinse liquid volume and contact angle is disregarded in current model. Volume decrease due to the evaporation of rinse liquid changes the contact angle [2] used in beam bending or FE models *i.e.* equilibrium contact angle. In other words, as the level of the rinse liquid inside the pattern goes down, receding contact angle, which is smaller than the equilibrium contact angle, should be used in the model. Contact angle defines the Laplace pressure and horizontal projection of STF.

Due to the rinse liquid penetration into the pattern, contact angle value and pattern stiffness may change (depending on the diffusion amount). Contact angle or stiffness changes due to swelling are disregarded in current simulation model. Forthcoming models may simulate the diffusion into the pattern to find the pattern stiffness as a function of time.

References

- 1 D. L. Goldfarb, M. Angelopoulos, E. K. Lin, R. L. Jones, C. L. Soled, J. L. Lenhart and Wen-li Wu, *J. Vac. Sci. Technol B* 19, 2699-2703 (2001)
- 2 Jung-Hoon Kim, S. I. Ahn, J. H. Kim and Wang-Cheol Zin, *J. Langmuir*, 23, 6163-6169 (2007)

Appendix A – ANSYS codes

This ANSYS code works for two-line parallel, box-shaped open end L-shaped and close end L-shaped patterns. Results of Chapter 3 are derived using this code.

```
FINISH
/CLEAR,NOSTART
/TITLE,
/PREP7
KEYW,PR_STRUC,1
*SET,E,5.9e-9 Elasticity modulus
*SET,v,0.3 Poisson's ratio
*SET,L,2000 Pattern's length
*SET,Teta,85*3.1415/180 Contact angle (rad)
*SET,gama,72 ! for water mN/m Surface Enesion
*SET,H,1500 Pattern height
*SET,w,H/5 Pattern width (H/AR)
*SET,P, 320.52 !KPa Laplace pressure on the pattern (imported from Surface Evolver)
R,1,L,L,L,L,0,
RMORE, ,0,
```

Add these two variables for L-shaped patterns

```
*SET,L1,1 !just coefficient this one is one
*SET,L2,18
```

Selecting Element type

```
ET,1,SHELL43 This element provides both deformation and slope angle. This is the element used
in simulations of this study.
ET,1,SOLID95 This element only provides the deformation value. This element provides results faster.
However, the above element is more accurate as it provides slope angle which is useful to predict more
accurate rinse interface curvature values from SE.
```

```
R,1,1,1,1,1, ,
RMORE, , ,
MPTEMP,,,,,,,,
MPTEMP,1,0
```

Elastic deformation is assumed by changing this part plastic simulation can be achieved as well.

```
MPDATA,EX,1,,E Elasticity modlus is defined.
MPDATA,PRXY,1,,v Poisson's ratio is defined.
```

Creating the model for two-line parallel patterns

```
RECTNG,0,w,0,0.95*H,
RECTNG,0,w,0.95*H,H, The area where STF is operative on it. Three-phase line is assumed as a
narrow area and STF is assumed as Pressure operating on the mentioned area.
```

Creating the model for "LI" shape patterns (open end L-shaped)

```
BLOCK,0,w,0,(L1+1)*w,0,.95*AR*w,
BLOCK,0,(L2+2)*w,(L1+1)*w,(L1+2)*w,0,.95*AR*w,
BLOCK,2*w,3*w,0,L1*w,0,.95*AR*w,
BLOCK,3*w,(L2+2)*w,(L1-1)*w,L1*w,0,.95*AR*w,
BLOCK,0,w,0,(L1+1)*w,.95*AR*w,AR*w,
BLOCK,0,(L2+2)*w,(L1+1)*w,(L1+2)*w,.95*AR*w,AR*w
BLOCK,2*w,3*w,0,L1*w,.95*AR*w,AR*w
BLOCK,3*w,(L2+2)*w,(L1-1)*w,L1*w,.95*AR*w,AR*w
```

Meshing methodology

```
AADD,all
SMRT,3          Fineness of the meshing or mesh coarse which is a number between 1 and 9. From 1
and 9, fineness decreases. The 3 is enough for this study as the results are similar using 3 and 2.
MSHAPE,1,2D
MSHKEY,0
CM,_Y, AREA
VSEL,,, 3
CM,_Y1, AREA
CHKMSH,'AREA'
CMSEL,S,_Y
AMESH,_Y1
CMDELE,_Y
CMDELE,_Y1
CMDELE,_Y2
```

Applying forces and displacement constraints for two-line parallel patterns

```
DL,1, ,ALL,0    !bottom displacement is zero
SFL,2,PRES,-P*1e-15    Defining Laplace pressure on the area
SFL,9,PRES,-P*1e-15-(gama*sin(Teta)*1e-12)/(0.05*H)
```

Applying forces and displacement constraints for “LI” shape patterns

```
DA,1,ALL,0!bottom displacement zero
DA,68,ALL,0    applying deformation constraints
DA,49,ALL,0    applying deformation constraints
DA,13,ALL,0    applying deformation constraints
SFA,6,1,PRES,-P*1e-15    Applying Laplace pressure on pattern areas
SFA,62,1,PRES,-P*1e-15    Applying Laplace pressure on pattern areas
SFA,17,1,PRES,-P*1e-15    Applying Laplace pressure on pattern areas
SFA,16,1,PRES,-P*1e-15    Applying Laplace pressure on pattern areas
SFA,54,1,PRES,-P*1e-15    Applying Laplace pressure on pattern areas
SFA,60,1,PRES,-P*1e-15-(gama*sin(Teta)*1e-12)/(0.05*H) Applying STF on patterns top edge
SFA,66,1,PRES,-P*1e-15-(gama*sin(Teta)*1e-12)/(0.05*H) Applying STF on patterns top edge
SFA,58,1,PRES,-P*1e-15-(gama*sin(Teta)*1e-12)/(0.05*H) Applying STF on patterns top edge
SFA,51,1,PRES,-P*1e-15-(gama*sin(Teta)*1e-12)/(0.05*H) Applying STF on patterns top
SFA,52,1,PRES,-P*1e-15-(gama*sin(Teta)*1e-12)/(0.05*H) Applying STF on patterns top edge
```

FINISH

Solving for finding the pattern deformation and/or slope angle.

```
/SOL
CNVTOL,U, ,0.001,2, ,
ANTYPE,0
NLGEOM,1
ANTYPE,0
NLGEOM,1
/STATUS,SOLU
SOLVE
```

Appendix B – Methodology used in Surface Evolver

The energy in the Surface Evolver can be a combination of surface tension, gravitational energy, squared mean curvature, user-defined surface integrals, or knot energies [1]. Surface Evolver areas are series of attached triangles and refinement produces four triangles inside each single triangle (see Fig. B1). In finding interface shape the exact property function of the system *i.e.* energy or entropy function is unknown. So finding their derivative is impossible. Instead the state of system can be change little by little and it will be checked to see whether the system energy has decreased or not (iterative method). Gradient method, conjugate gradient algorithm and Runge Cutta are iterative minimization methods built in Surface Evolver [1]. Conjugate gradient algorithm is used in this thesis for rinse interface simulation as for cases studied it was the fastest method comparing to the other two methods.

To describe the gradient descent methods (such as conjugate gradient), consider the system as a landscape with mountains and valleys. The gradient of the energy is the steepest uphill direction and the negative of the gradient direction is the steepest downhill direction. The algorithm which seeks the minimum point by gradient is called gradient descent method. The most efficient gradient algorithm is conjugate gradient algorithm. In conjugate gradient method new direction is conjugate to all of the previous ones.

The stopping criteria for minimization in ideal case are either the area meets the constraints, or the derivative of the energy function for the area vanishes. However, these criteria may require an infinite time. As such, checking the energy difference between

two consecutive iterations is used as the stopping criterion in this study. It means that if the difference of energy after the last iteration is less than 1^{-12} , then minimization halts. However, energy difference criterion is not the necessary condition for a point to be a minimum. There are two cases that energy difference is very small but the point is not a minimum.

First, energy minimization is stuck and no movement is observed in the geometry or energy value. In this case step size should be checked and a zero step size shows that a new refinement should be used to resolve the problem. This case mostly happened in L-shaped patterns (especially when the pattern shape was “LI”). Second, saddle point as the value of energy difference is zero at the saddle point. To sort out that the point is a saddle or not its Hessian matrix should be checked. Semi-positive Hessian matrix reveals that the state is not a saddle point. In this study, Hessian matrix and step size are checked to make sure that all the results are at the minimum energy.

As the energy function is in the form shown in Eq. B-1, rather than creating the geometry in Surface evolver, contact angle of the rinse liquid and the pattern’s side wall is needed.

$$E' = \Delta A_{LV} + (-\cos\theta)\Delta A_{SL} \quad (\text{B-1})$$

Surface Evolver codes for finding the rinse interface shape and curvature are provided and described in the next few pages.

Two-Line Parallel and Box-Shaped Patterns

```
PARAMETER angle = 5 //the value of contact angle (degree)
parameter thickofpattern=3*57 //Pattern height (nm)
parameter height= 100 //Average liquid interface height (nm)
parameter troughwidth = 57 The distance between two adjacent patterns
parameter leng=troughwidth*10 //Pattern length (nm)
parameter vol= height*troughwidth*leng
#define T (-cos(angle*pi/180)) The term shown in Eq. B-1
gravity_constant 0 // change the gravity to 9.81e9 for considering the gravity effect
constraint 1 formula: x=0 energy: e1: 0; e2: -T*z; e3: 0
constraint 2 formula: x=troughwidth energy: e1: 0; e2: T*z; e3: 0
constraint 5 nonnegative formula:x
constraint 6 nonpositive formula:-troughwidth+x
constraint 7 nonnegative formula:y
constraint 8 nonpositive formula:y-leng
constraint 9 nonpositive formula: z-thickofpattern
constraint 10 nonnegative formula: z
```

For two line parallel patterns (see Fig. B2a)

```
constraint 3 formula: y=0
constraint 4 formula: y=leng
```

For box-shaped patterns (see Fig. B2b)

```
constraint 3 formula: y=0 energy: e1:T*z ; e2:0; e3:0
constraint 4 formula: y=leng energy: e1:-T*z; e2:0; e3:0
```

vertices

```
1 0 0 0 fixed
2 troughwidth 0 0 fixed
3 troughwidth leng 0 fixed
4 0 leng 0 fixed
5 0 0 height constraints 1,3,9,10
6 troughwidth 0 height constraints 2,3,9,10
7 troughwidth leng height constraints 2,4,9,10
8 0 leng height constraints 1,4,9,10
```

//fixed pattern

```
10 0 0 thickofpattern fixed
11 troughwidth 0 thickofpattern fixed
12 troughwidth leng thickofpattern fixed
13 0 leng thickofpattern fixed
```

edges

//liquid

```
1 1 2 fixed no_refine
2 2 3 fixed no_refine
3 3 4 fixed no_refine
4 4 1 fixed no_refine
5 5 6 constraint 3,9,10
6 6 7 constraint 2,9,10
7 7 8 constraint 4,9,10
8 8 5 constraint 1,9,10
```

// fixed pattern

```
9 10 11 no_refine color red
10 11 12 no_refine color red
```

11 12 13 no_refine color red
12 13 10 no_refine color red
13 1 10 no_refine color black
14 2 11 no_refine color black
15 3 12 no_refine color black
16 4 13 no_refine color black

For two-line parallel patterns

17 1 5 constraints 1,3,9,10
18 2 6 constraints 2,3,9,10
19 3 7 constraints 2,4,9,10
20 4 8 constraints 1,4,9,10

faces

For two-line parallel patterns

1 5 6 7 8 constraints 5,6,7,8,10 color white
2 1 18 -5 -17 constraints 5,6,7,8,10
3 3 20 -7 -19 constraints 5,6,7,8,10
4 -1 -4 -3 -2 fixed no_refine color blue

For box-shaped patterns

1 5 6 7 8 constraints 5,6,7,8,10 color white
2 -1 -4 -3 -2 fixed no_refine color blue

body

1 1 density 1e-24 volume vol //density for water 1e-24 kg/nm³

Closed and Open End L-shaped Patterns

```
PARAMETER angle = 5
// inputs are in nano
parameter d1=57
parameter d2=57
parameter l1=4*57
parameter l2=5*57
parameter Hpattern=3*57
parameter Hwater=130
parameter vol= (d1*l1+d2*l2+d1*d2)*Hwater
#define T (-cos(angle*pi/180))
gravity_constant 0 //just change the gravity to 9.81e9
```

For close end L-shaped patterns

```
constraint 1 formula: y=0 energy: e1: T*z; e2: 0; e3: 0
constraint 5 formula: x=d1+l2 energy: e1: 0; e2: T*z; e3: 0
```

For open end L-shaped patterns

```
constraint 1 formula: y=0
constraint 5 formula: x=d1+l2

constraint 2 formula: y=l1 energy: e1: T*z; e2: 0; e3: 0
constraint 3 formula: y=l1+d2 energy: e1: -T*z; e2: 0; e3: 0
constraint 4 formula: x=0 energy: e1: 0; e2: -T*z; e3: 0
constraint 6 formula: x=d1 energy: e1: 0; e2: T*z; e3: 0
constraint 7 nonpositive formula: z-Hpattern
constraint 8 nonnegative formula: z
//for area 1
constraint 9 nonnegative formula: x
constraint 10 nonpositive formula: x-d1
constraint 11 nonnegative formula: y
constraint 12 nonpositive formula: y-l1-d2
//for area 2
constraint 13 nonnegative formula: x-d1
constraint 14 nonpositive formula: x-d1-l2
constraint 15 nonnegative formula: y-l1
constraint 16 nonpositive formula: y-l1-d2
constraint 17 nonpositive formula: y-l1
constraint 18 formula: x=d1
constraint 19 formula: y=l1
vertices
1 0 0 0 fixed
2 d1 0 0 fixed
3 d1 l1 0 fixed
4 d1+l2 l1 0 fixed
5 d1+l2 l1+d2 0 fixed
6 0 l1+d2 0 fixed
7 0 0 Hwater constraints 1,4,7
8 d1 0 Hwater constraints 1,6,7
9 d1 l1 Hwater constraints 2,6,7
10 d1+l2 l1 Hwater constraints 2,5,7
11 d1+l2 l1+d2 Hwater constraints 3,5,7
12 0 l1+d2 Hwater constraints 3,4,7
13 0 0 Hpattern fixed
```

```

14 d1 0 Hpattern fixed
15 d1 l1 Hpattern fixed
16 d1+l2 l1 Hpattern fixed
17 d1+l2 l1+d2 Hpattern fixed
18 0 l1+d2 Hpattern fixed
19 d1 l1+d2 Hwater constraints 3,7
20 0 l1 Hwater constraint 4,7
21 d1 l1+d2 0 fixed
edges
//liquid
1 1 2 fixed no_refine
2 2 3 fixed no_refine
3 3 4 fixed no_refine
4 4 5 fixed no_refine
5 5 6 fixed no_refine
6 6 1 fixed no_refine
7 7 8 constraint 1,7,8
8 8 9 constraint 6,7,8,17
9 9 10 constraint 2,7,8,13
10 10 11 constraint 5,7,8
// edges 11 and 12 are broken to two
// fixed pattern
11 13 14 no_refine fixed color black
12 14 15 no_refine fixed color black
13 1 13 no_refine fixed color black
14 2 14 no_refine fixed color black
15 3 15 no_refine fixed color black
16 4 16 no_refine fixed color black
17 5 17 no_refine fixed color black
18 6 18 no_refine fixed color black
// for making two areas for interface
19 9 19 constraint 18
20 19 12 constraint 3,7,8
21 11 19 constraint 3,7,8
//for making three areas for interface
22 9 20 constraint 19
23 12 20 constraint 4,7,8
24 20 7 constraint 4,7,8

For open end L-shaped patterns add these
32 1 7 constraint 4,1,7,8
33 2 8 constraint 1,6,7,8
34 4 10 constraint 5,2,7,8
35 5 11 constraint 5,3,7,8

// fixed pattern
25 15 16 no_refine fixed color black
26 16 17 no_refine fixed color black
27 17 18 no_refine fixed color black
28 18 13 no_refine fixed color black
29 3 21 no_refine fixed color black
30 21 6 no_refine fixed color black
31 21 5 no_refine fixed color black
faces
1 7 8 22 24 constraints 7,8,9,10,11,17 color white
2 19 20 23 -22 constraints 7,8,9,10,12,15 color white

```

3 9 10 21 -19 constraints 7,8,13,14,15,16 color white

For close end L-shaped patterns

4 1 2 29 30 6 fixed no_refine color blue

5 3 4 -31 -29 fixed no_refine color blue

For open end L-shaped patterns

4 1 33 -7 -32 constraint 8,9,10,11

5 4 35 -10 -34 constraint 8,14,15,16

6 1 2 29 30 6 fixed no_refine color blue

7 3 4 -31 -29 fixed no_refine color blue

body

For close end L-shaped patterns

1 1 2 3 density 1e-24 volume vol //density for water 1e-24 kg/nm³

For open end L-shaped patterns

1 1 2 3 4 5 density 1e-24 volume vol //density for water 1e-24 kg/nm³

Figure

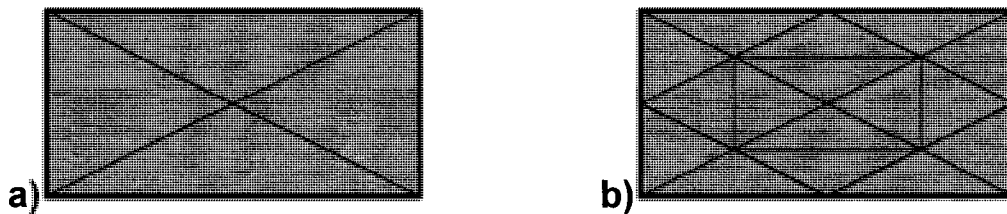


Figure B1 (a) A Surface Evolver area is shown. Area is composed of series of attached triangles. (b) Refinement produces four triangles inside each single triangle.

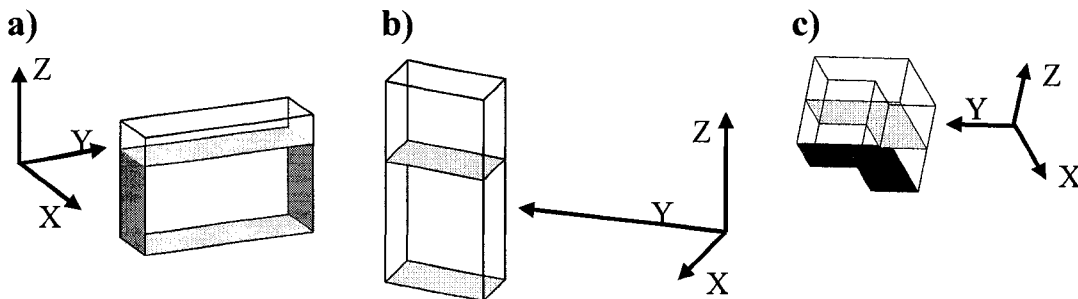


Figure B2 Initial shape of the rinse interface from SE and coordination used in SE for (a) two-line parallel pattern, (b) box-shaped and (c) L-shaped pattern is shown.

References

1. Brakke K A, Surface Evolver, www.susqu.edu/facstaff/b/brakke/evolver last accessed on September 5, 2007

Appendix C - Relaxation of the Small Deformation Assumption Used in Tanaka's model

In this appendix the small deformation assumption used in Tanaka *et al.* [1] model (discussed in Chapter 2) is relaxed. Tanaka's beam bending model with relaxation of small deformation assumption is called improved Tanaka's beam bending model. It should be noted that effect of surface tension force on pattern deformation is not considered in this Appendix. The goal is to show that how accurate small deformation assumption has been for calculating pattern deformation due to only Laplace pressure. The slope of the beam under the capillary pressure (Laplace pressure here) is [2]:

$$\tan \phi = \frac{4\delta}{3H} \quad (\text{C-1})$$

By knowing the slope relation from Eq. C-1 one may have :

$$\sin \phi = \frac{\frac{4\delta}{3H}}{\sqrt{1 + \left(\frac{4\delta}{3H}\right)^2}} \quad (\text{C-2})$$

$$\cos \phi = \frac{1}{\sqrt{1 + \left(\frac{4\delta}{3H}\right)^2}} \quad (\text{C-3})$$

From Eqs. 2-10 and 2-11 (and obviously $\delta_T \approx \delta_1$), from trigonometry one has $\cos(\theta - \phi) = \cos \theta \cdot \cos \phi + \sin \theta \sin \phi$ that will yield:

$$\delta = \frac{3\gamma H^4}{Ew^3(d - 2\delta)} (\cos \theta \cos \phi + \sin \theta \sin \phi) \quad (\text{C-4})$$

By substituting Eqs. C-2 and C-3 into C-4 one may have:

$$\delta(d - 2\delta) = \frac{3\gamma H^4}{Ew^3} \left(\cos\theta \frac{1}{\sqrt{1 + \left(\frac{4\delta}{3H}\right)^2}} + \sin\theta \frac{\frac{4\delta}{3H}}{\sqrt{1 + \left(\frac{4\delta}{3H}\right)^2}} \right) \quad (C-5)$$

After simplification, deformation value without small deformation assumption can be calculated by solving Eq. C-6:

$$\begin{aligned} & \frac{64}{9H^2} \delta^6 - \frac{64d}{9H^2} \delta^5 + \left(\frac{16d^2}{9H^2} + 4 \right) \delta^4 - 4d\delta^3 + \left(d^2 - \frac{16\gamma^2 H^6 \sin^2 \theta}{E^2 w^6} \right) \delta^2 - \\ & \frac{12\gamma^2 H^7 \sin 2\theta}{E^2 w^6} \delta - \frac{9\gamma^2 H^8}{E^2 w^6} \cos^2 \theta = 0 \end{aligned} \quad (C-6)$$

Equation C-6 is the result of equilibrium between restoring and cohesive forces. It should be mentioned that only the real roots of Eq. C-6 should be considered [1].

It can be summarized from Tables C1 to C3 that small deformation used by Tanaka *et al.* [1] is valid as the error of Tanaka's model compared to improved Tanaka's model, for these studied cases and the other studied cases which are not mentioned here is less than 1 percent.

Tables

Table C1 Laplace pressure deformation with and without small deformation

approximation ($H=250nm$, $d=104nm$, $E=5Gpa$, $AR=4$ and $\gamma = 72mN / m$).

θ (degree)	$\delta_1 (\sin \phi \approx \frac{4\delta}{3H})$ nm	δ_1 (without assumption)nm	Error (%)
5	7.822	7.813	0.11
45	5.394	5.392	0.05
85	6.078	6.078	0

Table C2 Laplace pressure deformation with and without small deformation assumption

($H=250nm$, $E=5Gpa$, $\theta = 45^\circ$, $AR=4$ and $\gamma = 72mN / m$).

d (nm)	$\delta_1 (\sin \phi \approx \frac{4\delta}{3H})$ nm	δ_1 (without assumption)nm	Error (%)
70	10.564	10.532	0.31
104	5.394	5.392	0.05
150	3.480	3.480	0.02

Table C3 Laplace pressure deformation with and without small deformation assumption

($H=250\text{nm}$, $d=104\text{nm}$, $E=5\text{Gpa}$, $\theta = 45^\circ$ and $\gamma = 72\text{mN} / \text{m}$).

AR	$\delta_1 (\sin \phi \approx \frac{4\delta}{3H})\text{nm}$	δ_1 (without assumption) nm	Error (%)
4	5.394	5.392	0.05
4.5	8.319	8.309	0.13
5	13.145	13.092	0.406

References

1. T. Tanaka, M. Morigami and N. Atoda, Jpn. J. Appl. Phys., 32, 6059-6064, (1993)
2. Robert D. Cook, Warren C. Young, *Advanced Mechanics of Materials* Macmillan Publishing, New York, USA, 70-72, (1985)

Appendix D - Details of the New Analytical Beam Bending Model

In this Appendix first, an order of magnitude analysis will be performed to compare the magnitude of forces due to Laplace pressure and surface tension force (STF). Then the total deformation of the pattern will be found.

$$\frac{\Delta PHL}{STF} = \frac{2\gamma HL \cos \theta}{d \gamma L \sin \theta} = \frac{2}{\tan \theta} \frac{H}{d} \quad (D-1)$$

H and d are in the same order of magnitude and contact angle is defining the order of magnitude of forces due to the Laplace pressure to that of surface tension force.

In the analytical beam bending model (discussed in Chapter 2), maximum pattern deformation is the summation of capillary pressure (δ_1) and surface tension force (δ_2) deformations. According to Eq. 2-10 deformation due to surface tension affects the deformation due to Laplace pressure (i.e. δ_2 affects δ_1 value). In literature, δ_2 is neglected, it is clear that its effect on δ_1 is not considered as well.

To accurately calculate δ_1 (i.e. considering the effect of surface tension force on δ_1) here we start from the cohesive and restoring forces and setting Eqs. 2-10 and 2-11 equal:

$$\frac{2\gamma.L.\cos(\theta - \phi_r)}{(d - 2(\delta_1 + \delta_2))} = \frac{2ELw^3}{3H^4}\delta_1 \quad (D-2)$$

where left hand side and right hand side of the above equation are cohesive and restoring forces, respectively. If cohesive force is more than the restoring force, collapse will occur. In Eq. D-2, the ϕ_r is the total slope due to all cohesive forces. Using superposition

principle one can write the summation of slope angles due to surface tension force and Laplace pressure as [1]:

$$\phi_r = \tan^{-1}\left(\frac{4\delta_1}{3H}\right) + \tan^{-1}\left(\frac{3\delta_2}{2H}\right) \quad (\text{D-3})$$

Using Eq. D-3 one may write:

$$\cos \phi_r = \cos\left(\tan^{-1}\left(\frac{4\delta_1}{3H}\right)\right) \cdot \cos\left(\tan^{-1}\left(\frac{3\delta_2}{2H}\right)\right) - \sin\left(\tan^{-1}\left(\frac{4\delta_1}{3H}\right)\right) \cdot \sin\left(\tan^{-1}\left(\frac{3\delta_2}{2H}\right)\right) \quad (\text{D-4})$$

and

$$\sin \phi_r = \cos\left(\tan^{-1}\left(\frac{4\delta_1}{3H}\right)\right) \cdot \sin\left(\tan^{-1}\left(\frac{3\delta_2}{2H}\right)\right) + \sin\left(\tan^{-1}\left(\frac{4\delta_1}{3H}\right)\right) \cdot \cos\left(\tan^{-1}\left(\frac{3\delta_2}{2H}\right)\right) \quad (\text{D-5})$$

From trigonometry where $0 < \alpha, \beta < 90^\circ$ one may have:

$$\cos \tan^{-1} \alpha = \chi \Rightarrow \chi = \frac{1}{\sqrt{\alpha^2 + 1}} \quad (\text{D-6})$$

$$\sin \tan^{-1} \beta = Y \Rightarrow Y = \frac{\beta}{\sqrt{\beta^2 + 1}} \quad (\text{D-7})$$

From Eqs. D-6 and D-7, Eq. D-4 can be rewritten as:

$$\cos \phi_r = \frac{1}{\sqrt{\left(\frac{4\delta_1}{3H}\right)^2 + 1}} \times \frac{1}{\sqrt{\left(\frac{3\delta_2}{2H}\right)^2 + 1}} - \frac{\frac{4\delta_1}{3H}}{\sqrt{\left(\frac{4\delta_1}{3H}\right)^2 + 1}} \times \frac{\frac{3\delta_2}{2H}}{\sqrt{\left(\frac{3\delta_2}{2H}\right)^2 + 1}} \quad (\text{D-8})$$

and from Eqs. D-6 and D-7, Eq. D-5 can be expressed as:

$$\sin \phi_r = \frac{1}{\sqrt{\left(\frac{4\delta_1}{3H}\right)^2 + 1}} \times \frac{\frac{3\delta_2}{2H}}{\sqrt{\left(\frac{3\delta_2}{2H}\right)^2 + 1}} + \frac{\frac{4\delta_1}{3H}}{\sqrt{\left(\frac{4\delta_1}{3H}\right)^2 + 1}} \times \frac{1}{\sqrt{\left(\frac{3\delta_2}{2H}\right)^2 + 1}} \quad (\text{D-9})$$

Rearranging the Eq. 2-8 one has:

$$\frac{3\delta_2}{2H} = \frac{6\gamma \cdot AR^2 \sin \theta}{Ew} \quad (D-10)$$

From Eq. D-2 and comparing cohesive and restoring in equilibrium (*i.e.* when cohesive and restoring forces are equal), one has:

$$\frac{\gamma \cos(\theta - \phi_r)}{(d - 2(\delta_1 + \delta_2))} = \frac{Ew^3}{3H^4} \delta_1 \quad (D-11)$$

Left hand side of the Eq. D-12 shows the cohesive force due to Laplace pressure and right hand side is the general form of restoring force due to a distributed load on a beam.

$$\frac{\gamma \{ \cos \theta \cos \phi_r + \sin \theta \sin \phi_r \}}{(d - 2(\delta_1 + \delta_2))} = \frac{Ew^3}{3H^4} \delta_1 \quad (D-12)$$

By substituting Eqs. D-8 and D-9 in Eq. D-12 one may have:

$$\frac{\gamma \sqrt{\frac{1}{((\frac{3\delta_2}{2H})^2 + 1)((\frac{4\delta_1}{3H})^2 + 1)}} \left\{ \cos \theta \left(1 - \frac{4\delta_1}{3H} \times \frac{3\delta_2}{2H} \right) + \sin \theta \left(\frac{3\delta_2}{2H} + \frac{4\delta_1}{3H} \right) \right\}}{(d - 2(\delta_1 + \delta_2))} = \frac{Ew^3}{3H^4} \delta_1 \quad (D-13)$$

The solution of the Eq. D-13 is the deformation due to the Laplace pressure. For total deformation this value should be added to the value from Eq. 2-8. All the results, tables and figures of Chapter 2 which show pattern deformations using “Analytical model” use Eq. D-13 to calculate the deformation due to the Laplace pressure. Here for completeness order of magnitude analysis for comparing capillary and cohesive forces is performed.

$$\frac{STF}{ElasticForce} = \frac{\gamma L \sin \theta}{\delta ELw^3} = \frac{4}{3} \frac{AR^3 \gamma \sin \theta}{E\delta} \quad (D-14)$$

By knowing that $\gamma \approx 10^{-1}$, $E \approx 10^9$ and $\delta \approx 10^{-8}$ then the effect of STF to elastic forces is in order of 0.1 to 1.

$$\frac{\text{Laplace Pressure}}{\text{Elastic Pressure}} = \frac{3AR^3 H \gamma \cos \theta}{dE\delta} \quad (\text{D-15})$$

The order of magnitude of capillary forces to elastic forces due to Laplace pressure is 0.1 to 1.

References

1. Robert D. Cook, Warren C. Young, *Advanced Mechanics of Materials* Macmillan Publishing, New York, USA, 70-72, (1985)

Appendix E - Reason of Defining LAR

In studying rinse curvature with Surface Evolver (in Chapters 2 and 3) three variables affect the curvature value. These three variables are contact angle (θ), pattern trough width (d) and pattern length (L). The two former variables were combined to a newly defined variable *i.e.* LAR (L/d). The reason will be clarified here. In this Appendix, rinse curvature was studied for two types of pattern configurations (*i.e.* two-line parallel and box-shaped patterns). As seen in Fig. E1 for both above mentioned cases by increasing the trough width, rinse interface curvature value decreases. It should be mentioned that trend of decreasing the rinse interface curvature value with increasing the trough width from Surface Evolver is similar to that from cylindrical model (which was independent of pattern length).

By studying the error of using CIM it is found that the error of using CIM for finding the interface curvature is independent of pattern configuration (*i.e.* the defined error is equal for a two-line parallel pattern and an identical box-shaped pattern). For both cases, by increasing the pattern length, the error of using cylindrical model to calculate curvature decreases. Also, increase of the trough width at constant pattern length causes an error increase in application of CIM. Furthermore, by increasing both L and d at the same rate the error in application of CIM remains constant (as an example see Fig. E2). In other words, by knowing LAR (L/d) independent from the values of pattern length and trough width the error of finding curvature value from cylindrical model is understood.

Figures

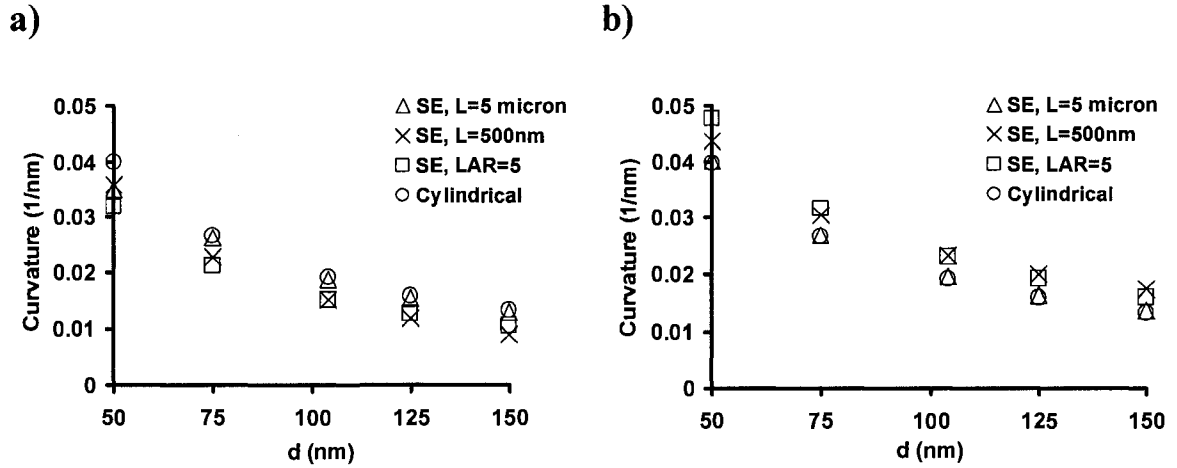


Figure E1 Rinse interface curvature value decreases by increasing the trough width. Rinse has filled the space between (a) a two-line parallel pattern and (b) a box-shaped pattern ($H=250$ nm, $\theta = 5^\circ$ and $ILH=110$ nm).

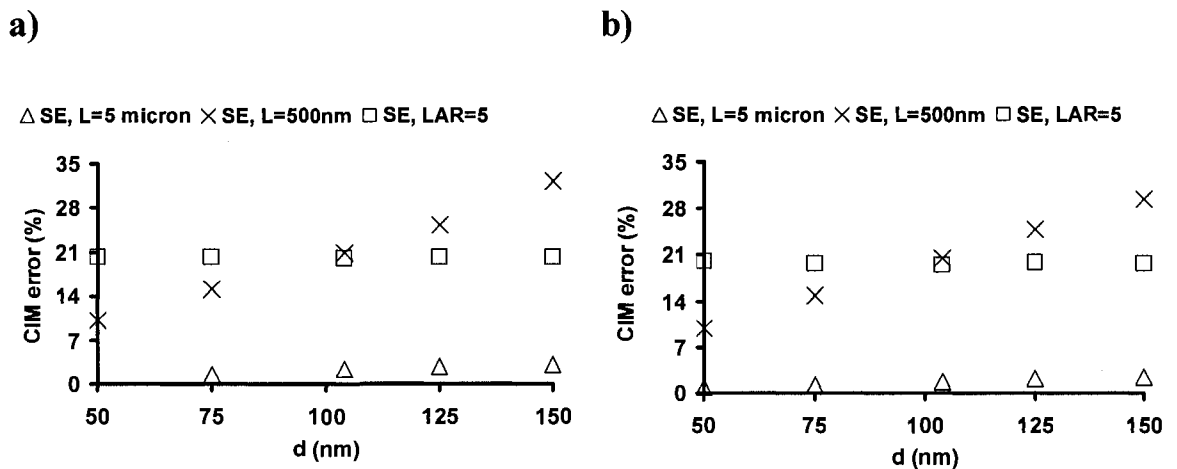


Figure E2 Error of using CIM compared to SE for finding the rinse interface curvature value at different trough width is shown for (a) two-line parallel and (b) box-shaped patterns. Error does not change by increasing d and L at the same rate (or constant LAR).

$H=250$ nm, $\theta = 5^\circ$.

Appendix F –Defining a box-shaped pattern with Infinite length in Surface Evolver

The methodology to define an infinitely large pattern in Surface Evolver (used in Chapter 2) is described in this Appendix. The energy function defined in Surface Evolver in absence of gravity is in the following form.

$$E = \gamma_{LV} A_{LV} + \gamma_{SV} A_{SV} + \gamma_{SL} A_{SL} \quad (F-1)$$

As at the equilibrium state derivative of the energy (Eq. F-1) is zero, by knowing $\Delta A_{SV} = \Delta A_{SL}$ one may change the Eq. F-1 (by using Young Eq. ; see Eq. 1-3) as:

$$\frac{\Delta E}{\gamma_{LV}} = \Delta A_{LV} + \left(\frac{\gamma_{SL} - \gamma_{SV}}{\gamma_{LV}} \right) \Delta A_{SL} \quad (F-2)$$

For the case of box-shaped patterns, rinse liquid is surrounded by four walls. During the energy minimization due to the movement of rinse liquid and air interface (for establishing the equilibrium state) three-phase line on pattern's side walls moves. For the cases that pattern's length is very large (i.e. $L \rightarrow \infty$) the wet area on the pattern's side wall, i.e. A_{SL} , on two smaller walls is negligible with respect to that on two larger walls. As such, ΔA_{SL} on two smaller walls is negligible with respect to ΔA_{SL} on two larger walls as well. In other words, on two smaller walls second part of the right hand side of Eq. F-2 is negligible (with respect to that term for two larger walls). So, energy on two smaller walls is only depends on ΔA_{LV} . From Young equation (see Eq. 1-3) it can be found that $\cos\theta = 0$ or $\theta = 90^\circ$, the second term of the right hand side of Eq. F-2 also vanishes. Therefore, instead of generating a pattern with infinite length, which is equivalent to $\Delta A_{SL} = 0$, one may easily consider $\theta = 90^\circ$ on two small pattern's walls. Curvature values found from Surface Evolver by this method were also verified with

cylindrical model values (as CIM is valid for $L \rightarrow \infty$) and results were exactly similar in the range of SE accuracy *i.e.* 1^{-12} .